Reaction Mechanism of 2-monosubstituted Quinoxalines with Organolithium Compounds: A Theoretical Study

by

Kgotso Herbet Moagi

Supervisor: Prof. Ignacy Cukrowski

Co-supervisor: Dr Darren Riley

Dissertation

Submitted in partial fulfilment of the requirements for the degree of

Master of Science

in

Chemistry

in the

Faculty of Science & Agriculture

University of Pretoria

Pretoria

July 2020

UNIVERSITEIT VAN PRETORIA
UNIVERSITY OF PRETORIA
YUNIBESITHI YA PRETORIA

Declaration

I, Kgotso Herbet Moagi, declare that this dissertation, which I hereby submit for the degree of Master of Science in Chemistry at the University of Pretoria, is my own work and has not previously been submitted by me for a degree at this or any other tertiary institution and that all material contained herein has been duly acknowledged.

Signature: _____

Date: _13/07/2020_

Place: _Soshanguve_

Dedication

This dissertation is dedicated to my young family members: my siblings Karabo, Kegoikantse and Katlego Moagi and cousins Kgaugelo, Lebogang, Lethabo, Boisebo Diago, Ofentse, Dimpho and Thato Moagi. To you guys, I wish you nothing but the best in life and your future endeavours. Whatever journey you may take, always have faith in its success and yourself.

Acknowledgments

First, I would like to thank my Heavenly Father for the good health and well-being that allowed me to complete this project.

I would like to express my sincere gratitude to:

- My supervisor, Prof. Ignacy Cukrowski, for the opportunity, patience, guidance, lunches, and mentoring that you have provided, and most importantly, I would like to thank you for the emotional and financial support.
- My co-supervisor, Dr Darren Riley, for all the kind support and immense contributions you offered during the project.
- My Honours supervisor, Dr Winston Nxumalo, for providing me with information necessary for me to make better decisions.
- Mr Carl van der Westhuizen, Mr George Dhimba and Dr Daniel van Niekerk for all the wonderful discussions and support to make sure that my project is understandable.
- The computational chemistry research group.
- Ms Dineo Baloyi – while words can never be enough, thank you for all the support which you have given throughout this project and the years prior.
- The Department of Chemistry of the University of Pretoria for their warmth and welcoming environment.
- The National Research Foundation for their financial support.

Summary

This dissertation describes the density functional theory (DFT) computational modelling of reactions between organolithium nucleophiles and various substituted quinoxalines. These reactions result in the functionalisation of the C (sp^2)–H bond, thus substituting the α-hydrogen. The reactions are known as nucleophilic substitution of hydrogen (S_NH) and are used by experimental chemists to form new C–C bonds. The S_NH reactions are very important in various industries, e.g. in designing and manufacturing of pharmaceuticals. Quinoxaline is widely used in medicinal chemistry due to its various biological activities; these reactions play a crucial role in the synthesis of new classes of compounds.

The reactions of 2-phenyl- (**A**), 2-butyl- (**B**), and 6-nitro-2-phenyl- (**C**) quinoxaline with lithiofuran (**a**) and lithiothiophene (**b**) involves a direct (**1**) nucleophilic attack on an activated electron-deficient system, leading to the intermediate σ^H-complex. This is followed by hydrolysis (**2**), where an sp^2-type nitrogen is changed to an sp^3 while forming Li$\cdots$OH as a by-product. The presence of Li$\cdots$OH then allows the departure of an α-proton via oxidation reaction, concomitantly forming H_2O_2 as the second by-product. All approaches to functionalise the C(sp^2)–H bond involve elimination of a proton, and an oxidant is needed for the departure of the α-hydrogen. Although the sequence of steps and mechanisms of these C–H transformations are the same, various factors have shown to affect the reactions differently.

The theoretical study of this catalytic-free transformation, shows that the formation of σ^H-adducts is not easily reversible, and that their formation is spontaneous. The reaction does not just require an oxidant to eliminate the α-hydrogen with the pair of electrons, but rather requires the presence of water for hydrolysis prior to oxidation. We must stress the crucial role of the oxidant since the key problem of the S_NH reactions is associated with the elimination of α-hydrogen. However, the main objective of this study is to present a correct and complete mechanistic picture of oxidative nucleophilic substitution of hydrogen (ONSH).

Previous reports indicated that the presence of an electron donating/withdrawing group on the quinoxaline ring had a significant influence on the yield and selectivity. This is between reactions **A**+**a**, **A**+**b**, and **B**+**a**. These experimental observations correlated well with the modelling results when the potential energy surfaces (PES) of the reactions were compared.

Table of contents

List of Figures

Chapter 1

x

List of Schemes

List of Tables

xv

List of Abbreviations

RC   Reactant Complex

GMS   Global Minimum Structures

LMS   Local Minimum Structures

Add.   Adduct

TS   Transition State

Int.   Intermediate

Prod.   Product

R   Reactants

R_1 Phenyl-/n-butyl-

R_2 Nucleophilic reactants

R_X Electrophilic reactants

a   Lithiofuran

a_e Lithiofuran coordinated to 2 explicit THF molecules

b   Lithiothiophene

b_e Lithiothiophene coordinated to 2 explicit THF molecules

A   2-phenylquinoxaline

B   2-n-butylquinoxaline

C   6-nitro-2-phenylquinoxaline

D   5-nitro-2-phenylquinoxaline

1   Nucleophilic addition reaction

1-Aa   Nucleophilic addition of 2-phenylquinoxaline with lithiofuran

1-Ab   Nucleophilic addition of 2-phenylquinoxaline with lithiothiophene

1-Ba   Nucleophilic addition of 2-n-butylquinoxaline with lithiofuran

1-Bb   Nucleophilic addition of 2-n-butylquinoxaline with lithiothiophene

1-Ca   Nucleophilic addition of 6-nitro-2-phenylquinoxaline with lithiofuran

1-Da   Nucleophilic addition of 5-nitro-2-phenylquinoxaline with lithiofuran

2   Hydrolysis reaction

2-Aa   Hydrolysis of Int. **1-Aa**

2-Ab   Hydrolysis of Int. **1-Ab**

2-Ba   Hydrolysis of Int. **1-Ba**

2-Bb   Hydrolysis of Int. **1-Bb**

3   Oxidation reaction

3-Aa   Oxidation of Int. **2-Aa**

2-Ab   Oxidation of Int. **2-Ab**

3-Ba   Oxidation of Int. **2-Ba**

S_N Nucleophilic Substitution

$S_N Ar$ Nucleophilic Aromatic Substitution

$S_N H$ Nucleophilic Substitution of Hydrogen

VNS   Vicarious Nucleophilic Substitution

ANRORC   Addition of the Nucleophile, Ring Opening and Ring Closure

ONSH   Oxidative Nucleophilic Substitution of Hydrogen

RDS   Rate Determining Step

EWG   Electron Withdrawing Groups

LG   Leaving Group

B3LYP   Becke, 3-parameter, Lee-Yang-Parr

DFT   Density Functional Theory

IRC   Intrinsic Reaction Coordinate

DA   Dihedral Angle

TB   Tuberculosis

THF   Tetrahydrofuran

Li···O   Lithium to Oxygen non-covalent bond

HF   Hartree Fock

Chapter 1

INTRODUCTION

1.1. Introduction

The daily work of a computational chemist is to provide insight into how the world works at a molecular level. This knowledge and data can then be used by researchers to assist in the characterisation of novel compounds and materials as well as to facilitate the design of more efficient processes. The purpose of computational modelling is to apply fundamental laws of quantum mechanics and thermodynamics to molecular systems in order to predict the properties of such systems and their related chemical reactions. Extensive research over the last sixty years into the development of advanced integrated software solutions, effective algorithms and computer hardware have matured the field to a point where synthetic chemistry is starting to benefit from computational modelling.[1,2]

Computational chemistry is therefore becoming a crucial tool in which the use of modelling offers a safer, potentially faster and cheaper means to assess chemical processes before resorting to wet chemistry. An important application that has recently seen growth is the identification of plausible synthetic routes to target molecules, the assessment of chemical reactivity and how it varies with changes in substrate and reaction conditions. Critically, although the chemistry of computation has come a long way, more advanced models need to be developed, and computational protocols and the means to interpret growing volumes of data are needed.

1.2   Heterocyclic compounds

There are many organic compounds which contain heteroatoms; these are atoms other than carbon (C) or hydrogen (H). Heterocyclic chemistry deals with heterocyclic organic compounds containing C, H and one or more heteroatoms such as phosphorus (P), sulphur (S), oxygen (O) or nitrogen (N) as part of a ring system.[3]

The importance of heterocyclic compounds comes from their diverse physical, chemical and biological properties.[4] Heterocyclic compounds are widely used as veterinary, agrochemical and pharmaceutical products. However, their applications have also been extended to antioxidants, additives, chemical sensors, corrosion inhibitors, brightening agents, polymer lasers and transistors.[5-7] Among several groups of heterocyclic compounds, quinoxalines of the azine group are crucial constituents of active pharmacological compounds.[8] Quinoxaline is a

2

heterocyclic fused aromatic ring, consisting of a pyrazine (di-azine) and benzene ring. It is commonly referred to as 1,4-benzodiazepine, benzoparadiazine and phenothiazine, and its atomic numbering is shown in **Figure 1.1**. The 2- and 3- positions are equivalent and are designated as α-positions as they chemically act as activated electrophilic sites.[9]
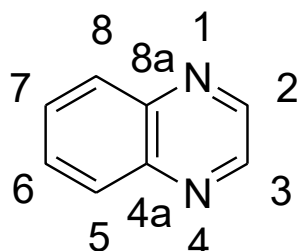
Figure 1.1: Quinoxaline structure

Quinoxalines are regarded as privileged structures due to their reported biological activities against a wide range of targets. The scaffold has therefore been the subject of extensive interest in the medicinal chemistry community,[10,11] with synthesised quinoxalines having been shown to possess activity against HIV, diabetes, fungus, parasites, tuberculosis (TB) and cancer.[12] In addition, the use of quinoxaline derivatives has also been reported in other applications, including organic optoelectronic applications and dye-sensitised solar cells.[13,14] This dissertation will detail the medicinal applications of quinoxaline derivatives in a theoretical context.

1.2.1 Biological activity of quinoxaline

Due to quinoxaline's wide-spread spectrum of biological activity, the molecule acts as a core unit in several biologically active compounds (**Figure 1.2**). The substituents attached to the moiety also play a crucial role in determining the properties of the compound, affecting it biologically, chemically and physically.[9,15,16,20]

Quinoxaline-2-ones and quinoxaline-2,3-diones exhibit anti-microbial, anti-pain and anti-inflammatory activities.[16-19] Ramalingam *et al.*[16] investigated the synthesis of quinoxaline-2,3-diones and evaluated their anti-microbial activity against the Mycobacterium tuberculosis H37Rv strain. The most effective compounds (**2**, **3**, and **4** in **Figure 1.2**) have minimum inhibitory concentrations (MIC99) of 8.01, 8.56 and 8.93 µg/mL, respectively.

© University of Pretoria
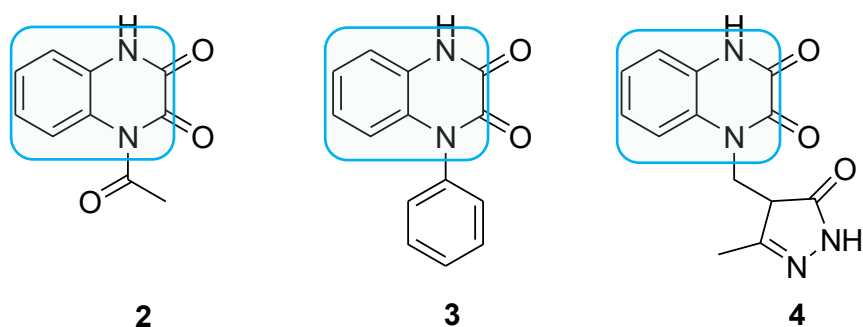
Figure 1.2: Quinoxaline-2,3-diones

Compounds **5** and **6** are quinoxaline derivatives; both have antitumour efficiency and are structurally related.[17] The widespread use of and interest in quinoxalines have led to a need for new and improved synthetic methodologies for their preparation and use.
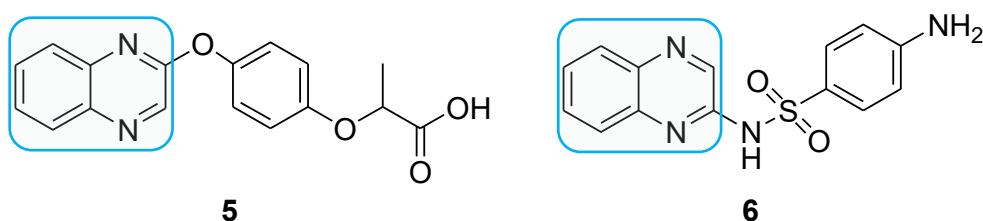
Figure 1.3: Molecular quinoxaline derivatives with antitumour efficiency

1.2.2 Reactivity of substituents on quinoxaline

Current research on nucleophilic substitution (S_N) reactions at the alpha position of the quinoxaline using different nucleophiles (R = alkyl-, aryl-, heteroaryl-, and alkynyl-) has found that reactivity is influenced by different substituents.[9,18-21] However, the influence of substituents at the 2-position of 2-substituted quinoxalines has not been thoroughly studied. Thus, we would like to report on the influence of aryl and alkyl groups at the 2-position in S_N reactions.

Nucleophilic substitution reactions at the 3-position of 2-substituted quinoxalines proceed smoothly with a variety of organolithium/magnesium nucleophiles; 2,3-substituted quinoxalines are obtained when phenyl and butyl substituents are attached at the 2-position (**Table 1.1**). However, yields vary across a wide range of 10 to 70%, and in the former case one can hardly say that the formation of the desired product is a result of a preferential reaction

pathway. The question that then arises is, what is the origin of such variation in the reaction yields?

Table 1.1: Nucleophilic substitution of 2-butyl/phenyl quinoxaline[9]

$$\text{quinoxaline-R}_1 \xrightarrow[\text{THF, RT, 18 hrs}]{\text{R}_2\text{-Li/MgBr}} \text{quinoxaline-R}_1\text{R}_2$$
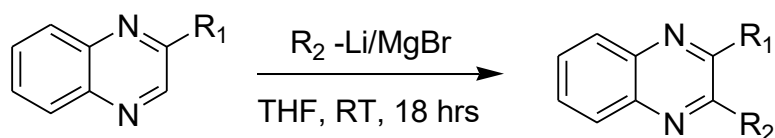
Entry	R₁	R₂-Li/MgBr	R₂	Yield (%)
1	-Phenyl	n-BuLi	-Butyl	66
2		Furan-2-yl-Li	-Furan-2-yl	46
3		Phenyl-MgBr	-Phenyl	22
4	-n-Butyl	Thiophene-2-yl-Li	Thiophene-2-yl	22
5		n-BuLi	-Butyl	97
6		Furan-2-yl-Li	-Furan-2-yl	91

1.3 Nucleophilic substitution

The nucleophilic substitution reactions involve the interaction of an electrophile with a nucleophile and it is one of the most widely studied reactions.[22a] An atom or group called a leaving group (LG) attached to the electrophilic carbon is replaced by a nucleophile through nucleophilic attack. The general reaction mechanism of nucleophilic substitution can proceed either via an S_N1 or S_N2 mechanism where the rate of reaction depends on the concentration of one (S_N1) or both (S_N2) species.

1.3.1 S_N1

The S_N1 reaction (**Scheme 1.1**) allows bond breakage and bond formation as discrete steps.[22b] A carbocation is then formed which is susceptible to nucleophilic attack, either from the back or front-side. The attack results in a racemic mixture.[22b,22c] Among the two processes (the departure of the LG and nucleophilic attack), the former is a slow reaction step (rate-determining step, RDS) while the latter is a fast reaction step.[22d,] For this reason, the rate of reaction is dependent on the concentration of the electrophile alone, hence the 1 in S_N1. This mechanism explains the observed substitution patterns of nucleophilic aromatic reactions.
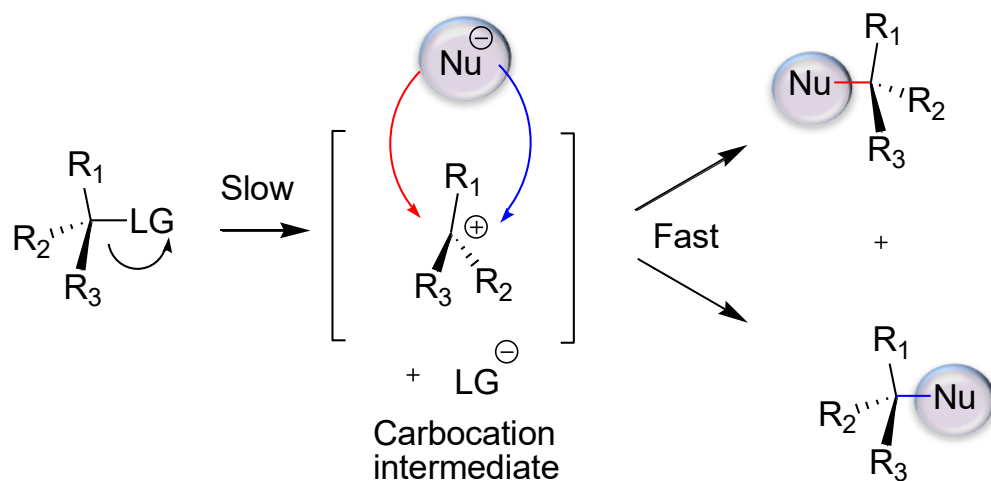
Scheme 1.1: General S_N1 reaction mechanism

1.3.2 S_N2

In an S_N2 reaction (**Scheme 1.2**), nucleophilic attack of the electrophilic carbon leads to a simultaneous bond breakage and bond formation. In other words, the LG departs at the time of the nucleophile-carbon bond formation. The reaction is characterised by back-side nucleophilic attack; this results in the inversion of the stereochemistry. And unlike in S_N1, the reaction is a bimolecular process[22b] where the rate of reaction depends on the concentration of both the electrophile and the nucleophile.
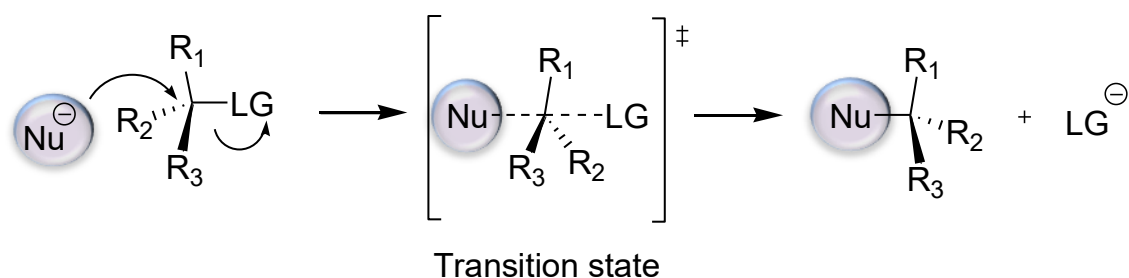
Scheme 1.2: General S_N2 reaction mechanism

1.4 Nucleophilic substitution on aromatic systems, S_NAr

The nucleophilic substitution reaction on aromatic systems is called a nucleophilic aromatic substitution (S_NAr) reaction. It is a process wherein a good leaving group (typically a halide)

is replaced by a nucleophile on an aromatic ring. This is a synthetically and theoretically well-documented process. [23,38,48]

The overall transformation can proceed via several mechanisms: elimination-addition,[24] vicarious nucleophilic substitution (VNS),[25] benzyme (E1cb-Ad$_N$),[26,27] free radical S$_{RN}$1,[28] base-promoted homolytic aromatic substitution (BHAS) couplings,[29] deprotonation of arenes (directed metalations),[30] S$_N$1,[23,31a] and sigmatropic rearrangement.[3b-c,32]

The most common reaction mechanism of S$_N$Ar is the addition-elimination reaction of a multi-step pathway.[24,33] It proceeds through the well-characterised intermediates called the Meisenheimer complex and/or the σ–complex, as shown in **Scheme 1.3**.[34] The intermediate is formed through the addition of the active nucleophile to the electrophilic aromatic system; this then allows for the elimination of the leaving group.

Meisenheimer
intermediate
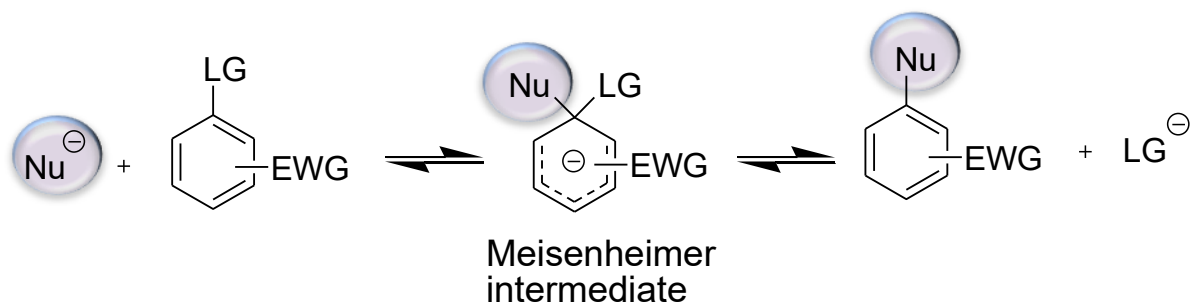
Scheme 1.3: General nucleophilic aromatic substitution reaction

Nucleophilic aromatic substitution proceeds best when arenes possess an electron-withdrawing substituent, such as a nitro group (-NO$_2$) which reduces the electron density of the ring, thus making the ring more electrophilic.[35] The polarising effect of an -NO$_2$ group in nitrobenzene has a comparable effect to systems containing aza groups (-N-), although in principle the nitro group, because it has a stronger polarising effect than the aza group, is still more activating.[36] As a result, aza-activated molecules can also be utilised in nucleophilic aromatic substitution reactions.

As is the case with any chemical conversion, the way in which azines facilitate S$_N$Ar reactions depends on the substituents' steric and electronic effects. Furthermore, as the number of aza groups increases, the electron density of the ring is further decreased, thus increasing the susceptibility of the ring towards nucleophilic substitution.[36]

An overview of the existing literature reveals that the S_NAr process is reasonably well documented for systems such as pyridine, which contain only one aza group. However, similar studies of systems with more than one aza group, such as quinoxalines, have received less attention.

The addition of a nucleophile occurs at the most electron-deficient site/s of the ring, and this holds for all electron-deficient arenes regardless of whether or not these positions are occupied by hydrogen or halogens. In the presence of both halogens or hydrogen, the addition of a nucleophile forms σ^X–adducts (Meisenheimer intermediate) or σ^H–adducts respectively. As illustrated in **Scheme 1.4**, in the case of 4-nitrochlorobenzene, nucleophilic addition to the ring can occur at positions 1 or 3.
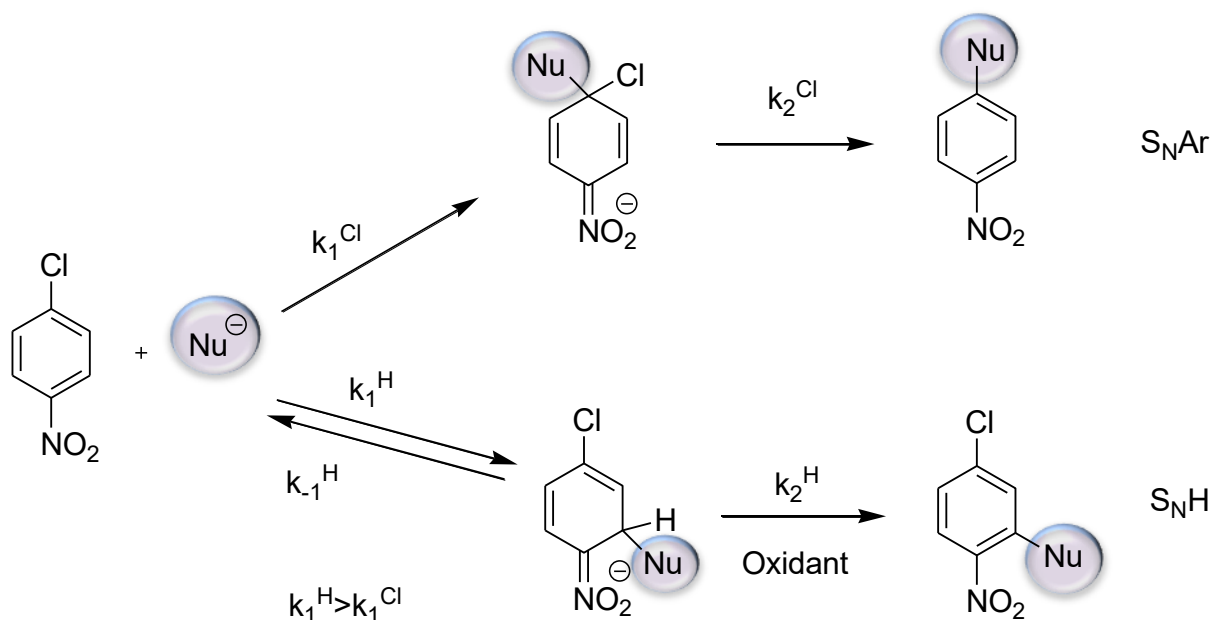
Scheme 1.4: Nucleophilic substitution reaction

The formation of the σ^H–adduct (position 3) proceeds faster than the analogous formation of the Meisenheimer σ^{Cl}–adduct at position 1.[38] In the case of the halide displacement, the elimination of the halogen is faster than the formation of the σ^{Cl}–adduct, and as a result, the latter is the rate-determining step (RDS).[37,38] Conversely, the elimination of the hydride is significantly slower than that of the halide, and in general the reaction is unable to proceed beyond σ^H–adduct formation. The reaction preferably dissociates to reform starting materials. As a result, σ^H–adducts are referred to as "unproductive" intermediates. The classical S_NAr of halogens will not be presented here, but rather the lesser-known nucleophilic substitution of hydrogen (S_NH).

8

1.5 Nucleophilic substitution of hydrogen, S_NH

The formation of σ^H–adduct and the subsequent displacement of the hydrogen atom on aromatic systems, shown in **Scheme 1.5**, is referred to as nucleophilic aromatic substitution of hydrogen. The σ^H–adduct forms through C-H functionalisation. For a successful S_NH reaction, an appropriate auxiliary group (or oxidant) is required to form an S_NH product either through oxidative or eliminative processes.

EWG = Electron withdrawing group
A = Auxiliary group
[O] = Chemical or anodic oxidation

Meisenheimer intermediate
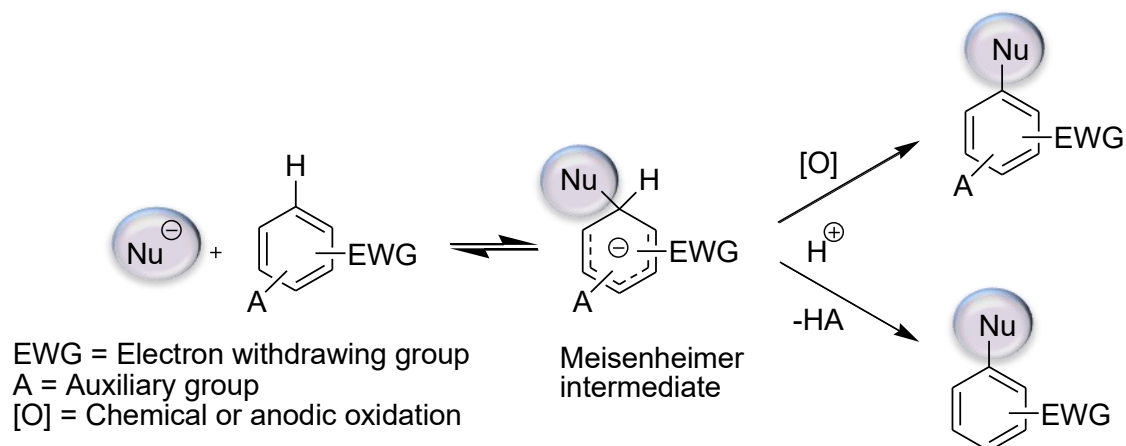
Scheme 1.5: General S_NH reaction

An external reagent is required because the hydrogen atom is a poor leaving group. Furthermore, the conversion is dependent on the nature of the nucleophile used. The latter determines the mechanism of conversion and can proceed in a number of ways: oxidative nucleophilic substitution of hydrogen, ONSH,[39,40] conversion into substituted nitrosoarenes,[41,42] HL elimination (L is a nucleofugal group), vicarious nucleophilic substitution (VNS) of hydrogen,[41,43] ARNRORC,[44,45] and cine-tele substitution.[46]

This dissertation predominantly focuses on the S_NH of 2-monosubstituted quinoxalines treated with organometallic nucleophiles, based on a synthetic study conducted by Nxumalo and Ndlovu.[9] According to the reported study, atmospheric oxygen was used as an oxidative reagent to give the final product 2,3-disubstituted quinoxaline. For this reason, a more detailed description of ONSH will be reported rather than other S_NH reaction mechanisms.

1.5.1 Oxidative nucleophilic substitution of hydrogen – ONSH

The formation of a σ^H–adduct through the addition of a neutrally charged nucleophile (e.g. ROH, NH_3, RNH_2) will result in ONSH. Dating back to as early as 1930,[47] the organolithium-mediated nucleophilic addition of carbon fragments to pyridine was shown to occur at the α-position. In the process, an intermediate σ^H–adduct (**8**) in

Scheme 1.6 is formed with the newly formed C–C bond, facilitating the establishment of a Li–N bond.

Chupakin *et al.*[48] reported that the formation of **8** occurs at 0 °C, and by increasing the system's temperature to 100 °C, **8** transforms into the desired ONSH end-product **10** (

Scheme 1.6). This process is equivalent to the hydrolysis of **8** resulting in the formation of **9** which, with the addition of an oxidant, also results in the ONSH product **10**. To the best of our knowledge, no method has been reported detailing the explicit introduction of water into such systems in order to study the viability of the hydrolysis pathway. In a number of reactions, σ^H–adducts have been identified by ^1H and ^{13}C NMR spectroscopic analysis.[49-52]
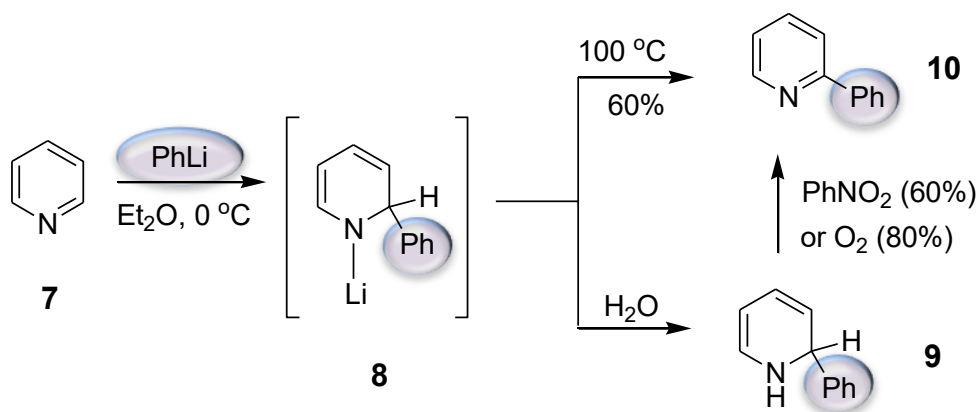
Scheme 1.6: Reactions of organolithium compounds with pyridines that result in ONSH

According to experimental chemistry, unless a system is carefully sealed, increasing the temperature in the absence of a blanketing inert gas will inevitably result in moisture entering into the system with atmospheric gases. A study conducted by Nxumalo and Ndlovu[9] involved synthesising 2,3-R_1R_2-quinoxaline by adding Li–R_2 to 2-R_1-quinoxaline at –78 °C; the reaction was then warmed up to 25 °C while stirring for 18 hours and the final product was obtained simply through the system's exposure to atmospheric oxygen (external reagent). This then

10

paved the way for us to conduct computational studies based on experimental conditions reported by Nxumalo and Ndlovu.[9]

When using external oxidants in ONSH, it is critical to choose the appropriate oxidant as nucleophilic species are vulnerable to oxidative processes. Atmospheric oxygen is a possible oxidant, its involvement in the facilitation of reactions is considered a special reaction as it provides an environmentally friendly process in which no harmful by-products are produced.[53-55] It was found that potassium permanganate in liquid ammonia works efficiently in the oxidation of σ^H–adducts of some anionic nucleophiles and Grignard reagents oxidised to nitroarenes.[56a] Other oxidants that may be used include bromine,[56b] 2,3-dichloro-5,6-dicyano-1,4-benzoquinone (DDQ)[56d] and dimethyldioxirane (DMD).[56c] In some cases, metals and salts have been used on carbon nucleophiles, but in most instances were less efficient.[56e-f] Overall, a C-H metal-free functionalisation process avoids the production of metal impurities; such reactions are considered ideal for industrial and academic chemists. Considering that the oxidation of σ^H-adducts can be exercised in several different paths depending on the oxidising agent, one can propose that a common reaction mechanism for ONSH with various oxidants is lacking.

Hydrolysis and oxidation reaction steps (

Scheme 1.6) involved in the reaction of ONSH are poorly documented, and thus the mechanism can be considered incomplete, unlike the nucleophilic addition step that involves σ^H–adduct formation. The ONSH reaction in

Scheme 1.6 was hypothesised to proceed via lithium hydride formation.[57,58] It was, however, later revealed that the process of α-hydrogen atom substitution proceeds through an intermediate adduct, **11a** (

Scheme 1.7), when treated with 4 equivalences of pyridine.[48] It was also reported by Chupakin *et al.*[48] that lithium hydride (a by-product) is involved in the reduction of pyridine in

11

the reaction with **11a**; however, the "by-product" was not detected in the crude product. The reaction results in 2-n-butyl-pyridine and an air-stable dimer.
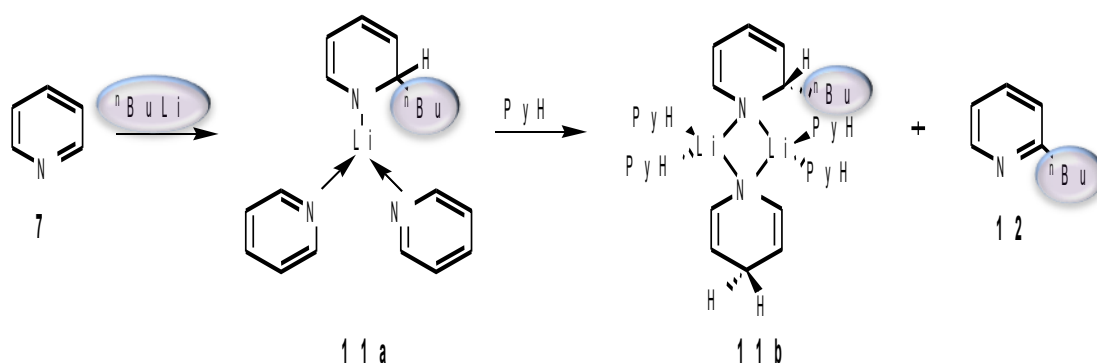
Scheme 1.7: Treatment of adduct **11a** with pyridine (4 equiv.) to give a dimer and 2-n-butylpyridine (**12**)

1.5.2 Conversion of σ^H-adducts into nitroso compounds

The conversion of σ^H-adducts into replaced nitroso arenes proceeds through the protonation of the -NO$_2$ group of the intermediate in a protic solvent. The reaction via σ^H-adduct formation releases a hydroxide anion. Water is subsequently eliminated to form the nitroso arene compound; however, the product is often further rearranged, see **Scheme 1.8**.[59,60] Due to the stoichiometry of the reaction, it is referred to as an intramolecular redox process.
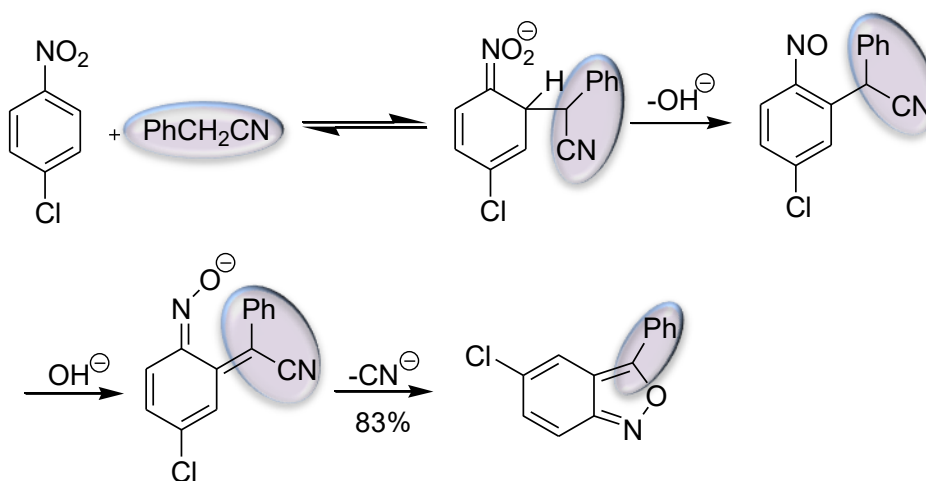
Scheme 1.8: The conversion of σ^H-adducts into nitroso arenes

This mechanism produces nitroso arenes which are more active than nitro-arenes and because of this they can undergo transformation reactions that depend on the reaction conditions, nitro-arene and nucleophile. Only in a few cases are nitro-arenes reported to be isolated.[60-62] As

12

exemplified in **Scheme 1.8**, often under reaction conditions the nitroso arenes undergo multiple-step transformations to heterocyclic systems, and thus these processes are often not predictable.

1.5.3 Cine- and tele-substitution

For an auxiliary group present in a substrate, the nucleophilic aromatic substitution reaction would follow the cine-tele substitution reaction mechanism.[44,63] After the addition of the nucleophile to the electron-deficient arene, the leaving group (LG) departs. A cine-substitution occurs when a LG departs from a vicinal position to the nucleophilic addition site. However, if the LG departs from a position of at least one atom away from the nucleophilic addition site, then it is termed tele-substitution reaction.

The reaction of 2,3-dinitronaphthalene with ethyl cyanoacetate in dimethylformamide (DMF) solvent is an example of a cine-substitution reaction. In the process, a nitrous acid is eliminated by base-induction to form a cine-substitution product [ethyl cyano-2-(3-nitronaphth-1-yl) acetate], **Scheme 1.9**.[64]
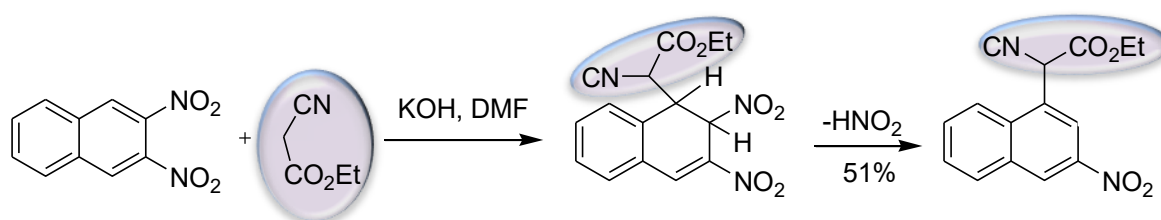
Scheme 1.9: 2,3-Dinitronaphthalene undergoing cine-substitution reaction

The tele-substitution is evident in the reaction of 3-(trichloromethyl) nitrobenzene with a Grignard reagent (**Scheme 1.10**).[65] The reaction shows the conversion of the σ^H-adduct through the departure of a chlorine ion four carbon atoms away from the nucleophilic addition site.
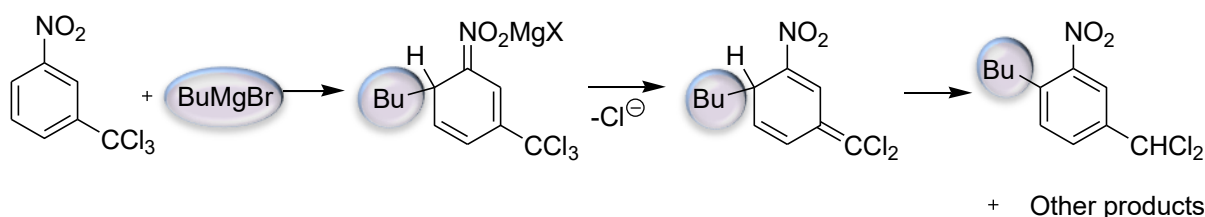
Scheme 1.10: Reaction of tele-substitution as an eliminative option for S_NH reactions

1.5.4 ANRORC

ANRORC is an acronym for "addition of the nucleophile, ring opening and ring closure". **Scheme 1.11** shows an example of ANRORC, in which a halogen-substituted heterocyclic compound is treated with a strong nucleophilic agent, e.g. amide anion. The reaction involves bromopyrimidine with potassium amide. It proceeds via a multi-step pathway, with the initial step forming the σ^H-adduct rather than the σ^{Br}-adduct through nucleophilic addition. The adduct subsequently undergoes ring opening and ring closure to form the final product (**Scheme 1.11**).[66]

A closer investigation of the reaction shows that the leaving group (Br^-) departs from a carbon atom that is more than one atom away from the nucleophilic addition site, thus this reaction can also be considered a tele-substitution.
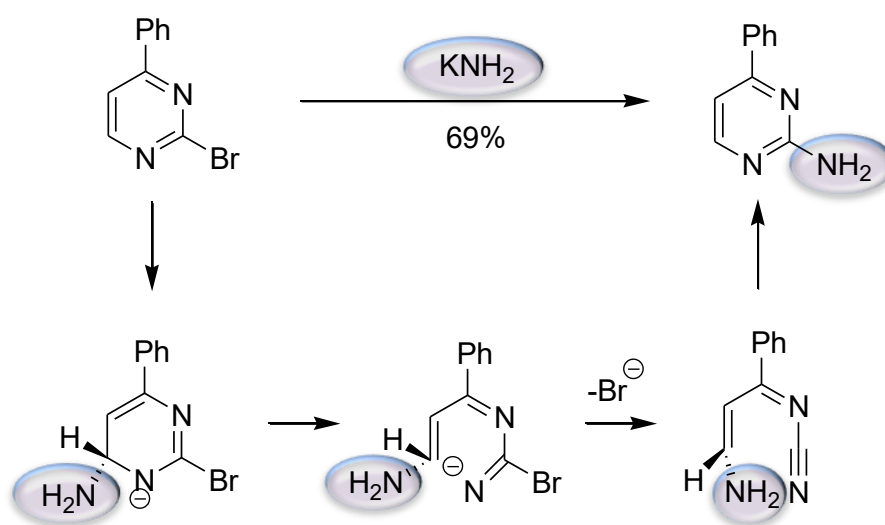
Scheme 1.11: ANRORC reaction mechanism

1.5.5 Vicarious nucleophilic substitution

The conversion of a σ^H-adduct by eliminating hydrogen via vicarious nucleophilic substitution (VNS) requires that the nucleophile carry one auxiliary group at its centre. Such nucleophiles are added to nitro-arene, forming a σ^H-adduct which is treated with a base that induces β-elimination of HX to form anionic products. The anionic products are then

14

protonated to give VNS products.[41,67] **Scheme 1.12** is an example of a general VNS reaction with a carbanion as the nucleophile. In order for this reaction to succeed, the hydrogen atom should occupy at least one position either *ortho-* or *para-* to the nitro group.[66a-b, 68]
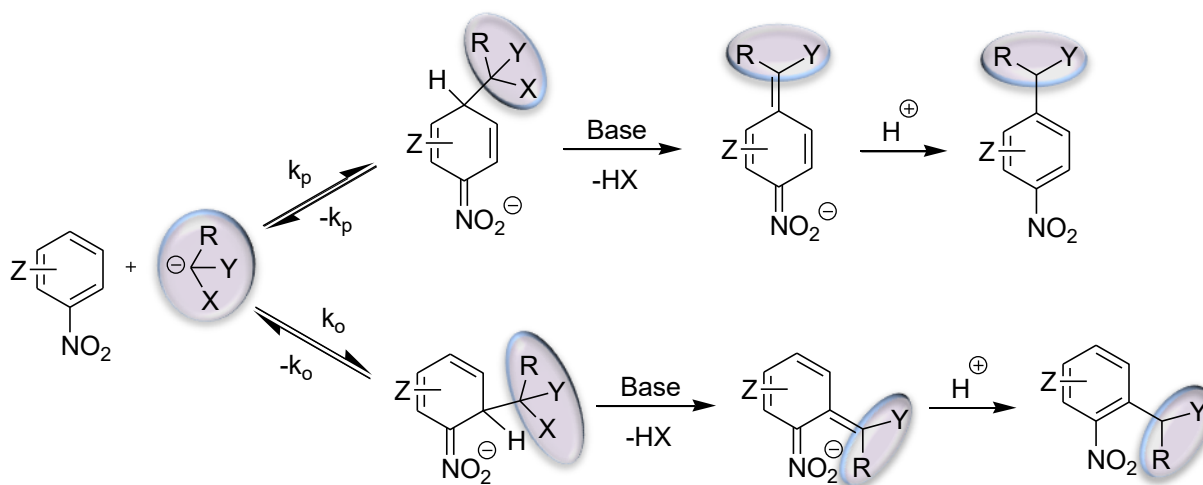
Scheme 1.12: Vicarious nucleophilic substitution of hydrogen

The reaction of VNS is a common process for the conversion of σ^H-adduct complexes in electron-poor aromatic systems containing carbon substituents. Due to this commonality, VNS is applied in the introduction of amino and hydroxy-substituents into arenes,[69] electron-poor alkenes,[70] and cyclisation to form three-membered rings.[71.] A detailed description of the scope of VNS has been reported by Makosza and Winiarski.[41]

The short description given is evidence of how versatile VNS is in the conversion of σ^H-adduct complexes in electron-deficient aromatic rings. Hence it is considered an effective tool for the functionalisation of electron-deficient systems in the field of synthetic chemistry.

1.6   Conclusions

Heterocyclic compounds play an important role in the manufacturing of industrial products due to their wide spectrum of properties and have been applied in a number of fields. These heterocyclic compounds are mostly used in the synthesis of pharmaceutical products and are functionalised through nucleophilic aromatic substitution reactions for the synthesis of new products with pharmaceutical importance.[58]

The S$_N$Ar reaction has fascinating mechanistic attributes and substantial practical value. Due to this, since the early days of computational chemistry, several quantum chemical calculations have investigated the interactions of electron-deficient arenes with nucleophiles. The analysis has been largely limited to reporting calculations of nucleophilic additions involving simple nucleophiles displacing halogens in haloarenes, halonitroarenes, and halodinitroarenes. The arene mostly consists of a benzene ring and halogens, typically chlorine, bromine and fluorine.

Although azine rings are largely overlooked due to their weaker polarising activation effect, quinoxalines, contrary to nitroarenes and azines of one aza group, have two aza groups that improve the activation effect of the ring. As a result, the addition-elimination reaction can also be applied to the quinoxaline system, and because these reactions require no transition metal as a catalyst, continued study of these compounds and reactions is an attractive proposition, particularly in the field of drug discovery and design.

There is evidence that the σ^H–adducts can be isolated.[49-52] Even so, over the years the reported computational modelling calculations have ignored the alternative reaction pathways where additions occur on positions occupied by hydrogen (S$_N$H). This may be due to the spontaneous inability to depart from the initial σ^H–adducts. Several experimental and theoretical studies have explicitly shown that the σ^H–adducts are formed faster than the σ^X–adducts. The σ^X–adducts, due to their ability to depart from this initial adduct, result in S$_N$Ar, hence the formation of σ^H–adduct(s) is ignored.

The reaction mechanism of the formation of σ^H–adducts that give biologically active quinoxaline-substituted products using organolithium nucleophiles is not well known. To the best of our knowledge, the reaction of 2,3-disubstitued quinoxaline with organolithium compounds undergoes nucleophilic substitution via the oxidative nucleophilic substitution of hydrogen (ONSH). Chupakin et al.[48] hypothesised that LiH reduces pyridine in a reaction of ONSH; however, the LiH was not detected in the crude product. It is therefore apparent that the reaction mechanism of ONSH is incomplete, and thus further investigation should be conducted.

Several publications on ONSH have focused on nitroarenes, with very few on azine groups (e.g. quinoxaline). That being said, in the case of 2,3-disubstituted quinoxalines, which have high medicinal relevance with the products showing activity against tuberculosis,[9] no theoretical work or in-depth understanding has yet been published that has characterised the

16

mechanism by which these substitutions occur. Nor has the influence of hydrolysis, oxidation, the effect of the directing group (on the C–H functionalisation) and the substituent effect on the yield of the products been described.

In aromatic chemistry, the direct C–H functionalisation has now become a topic of interest for several journals. C–H functionalisation consists of several features, which include the metal-free hydrogen displacement reaction that proceeds in various pathways. The S_NAr of hydrogen has been explained primarily as C–H functionalisation of π-deficient aromatic compounds.[43,72]

1.7 Purpose of the study

The importance of the S_NAr reaction is evident in synthetic chemistry as it opens up a wide range of paths for the synthesis of new molecules through the C-C bond formation. As mentioned, the well-known, very useful classical S_NAr of halogens will not be presented here, but rather the lesser known nucleophilic substitution of hydrogen (S_NH). It is worth noting that the reaction(s) presented here proceed in the absence of catalysts (transition metals), and thus are well suited for the synthesis of pharmaceuticals.[58]

A more in-depth study of the reaction will not only help in the understanding of why the reaction prefers one route over another, but will allow the overall control of the commercially important reaction. In this way, a correlation between reacting species that are crucial for synthesis can be found, thereby making it feasible for designing new synthetic routes.

1.8 Aims and objectives

Previous work discussed evidences the insufficient understanding of reaction mechanisms and substituent selectivity in nucleophilic substitution of hydrogen (S_NH) reactions. This project therefore aims to model the S_NH reactions conducted by Nxumalo and Ndlovu[9] with different substrates and nucleophiles to investigate their influence on reactivity.

Current research will apply/modify nucleophilic substitution reactions on the alpha-position of quinoxaline treated with organolithium nucleophiles in tetrahydrofuran solvent, as

17

synthesised by Nxumalo.[9] Due to the vast difference in product yields, a density functional theory (DFT) study will be conducted to explore the origin of such variation in reaction yields.

The current study is based on investigating the reaction route of the hydrogen displacement of 2-phenyl-quinoxaline and 2-butyl quinoxaline, and the effects of the electron withdrawing group and substituents on quinoxaline derivatives. This will help to identify the influence of substituents at the 2-position.

The DFT will be used to study the transition state structures, intermediates, products, regio-selectivity and mechanism of the reaction, taking into consideration factors such as steric hindrance, stereochemistry, substitution, temperature, and solvent effect. Understanding the reactivity of quinoxaline derivatives at a molecular level will help to predict which reactions are likely to work. This will help in the planning and design of new reactions, leading to the synthesis of novel quinoxaline derivatives having either medicinal or industrial applications.

1.9   References

1. The Nobel Prize in Chemistry, 1998: Walter Kohn, John Pople, www.nobelprise.org/nobel_prises/chemistry/laureates/1998/; Google ScholarCheck for full text via OCLC.

2. The Nobel Prize in Chemistry, 2013: Martin Karplus, Michael Levitt, Arieh Warshel, www.nobelprise.org/nobel_prises/chemistry/laureates/2013/. Google ScholarCheck for full text via OCLC.

3. R. Dhivare, P. Chaudhari, S. Rajput, *Am. J. Het. Chem.*, 2018, **4**(1), 26-29.

4. A. Al-Mulla, *Der Pharma Chemica.*, 2017, **9**(13), 141-147.

5. A.R. Katritzky and C.W. Rees, 1984. *Comprehensive heterocyclic chemistry*. Pergamon Press.

6. W. Czarnik, Special Issue on Combinatorial Chemistry, *Acc. Chem. Res.*, 1996, **29**(3), 112-113.

7. G. Anilkumar, K. K. Krishan and A. P. Thankachan, *Tetrahedron*, 2015, **16**(71), 2333-2347.

8. (a) S. A. Kotharkar, D. B. Shinde, *Bioorg. Med. Chem. Lett.*, 2006, **16**(24), 6181-6184.
   (b) A. Dell, D.H. William, H.R. Morris, G.A. Smith, J. Feeney, G.C.K.J. Roberts, *Am.*

Chem. Soc., 1975, **97**(9), 2497-2502. (c) C. Bailly, S. Echepare, F. Gago and M.J. Waring, *Anti-Cancer Drug Des.*, 1999, **14**(3), 291-303.

9. N.T. Ndlovu and W. Nxumalo, *Molecules*, 2016, **21**(10), 1304.

10. D.P. Singh, S.K. Deivedi, S.R. Hashim, R.G. Singhal, *Pharmaceuticals*, 2010, **3**(8), 2416–2425.

11. P. Selvam, M. Chandramohan, C. Pannecouque, and E. de Clercq, *Int. J. Pharm Ind. Res.*, 2011, **1**(2), 138–140.

12. (a) P. Ramalingam, S. Ganapaty and C.B. Rao, *Biorg. Med. Chem. Lett.*, 2010, **20**(1), 406–408. (b) S. Balasubramanian, P. Sasikumar and D. Velmurugan, *Int. J. Pharm. Sci. Drug Res.*, 2014, **6**, 60–66. (c) L.C. Potey, S.B. Kosalge and M.A. Hadke, *Int. J. Adv. Sci. Technol.*, 2013, **2**, 126–134. (d) A. Agboke, A. Attama, C. Qkoye and C. Jackson, *Innov. J. Med. Health. Sci.*, 2014, **4**, 93–98. (e) G. Le Douaron, L. Ferrié, J.E. Sepulveda-Dias, M. Amar, A. Harfouche, B. Séon-Méniel, and R. Raisman-Vosari, *J. Med. Chem.*, 2016, **59**(13), 6169–6186. (f) G. Le Douaron, F. Schmidt, M. Amar, H. Kadar, L. Debortoli, A. Latini, B. Séon-Méniel, L. Ferrié, P.P. Michel, D. Touboul, et al. *Eur. J. Med. Chem.*, 2015, 89, 467–479.

13. R. M. Kamble, B. K. Sharma, A. M. Shaikh and S. Chacko, *J. Chem. Sci.*, 2017, 129(4), 483–494.

14. J.A. Pereira et al. *Eur. J. Med. Chem.*, 2015, 97, 664-672.

15. https://www.researchgate.net/publication/51029429_Quinoxaline_14-di-N-oxide_and_the_potential_for_treating_tuberculosis [accessed Sep 4, 2017].

16. Ramalingam, P., Ganapaty, S. and Rao C.B., In vitro antitubercular and antimicrobial activities of 1-substituted quinoxaline-2,3(1H,4H)-diones, *Bio. Org. Med. Chem. Lett.*, 2010, 20, 406-408.

17. H. Gao, E. F. Yamasaki, K. K. Chan, L. L. Shen and R. M. Snapka, DNA sequence specificity for topoisomerase II poisoning by the quinoxaline anticancer drugs XK469 and CQS, *Mol. Pharmacol*. 63 (2003) 1382–1388.

18. Zhuo, F.; Xie, W.; Yang, Y.; Zhang, L.; Wang, P.; Yuan, R.; Da, C. TMEDA-assisted effective direct ortho arylation of electron-deficient N-heteroarenes with aromatic Grignard reagents. *J. Org. Chem*. 2013, **78**, 3243–3249.

19. Prokhorov, A.M.; Makosza, M.; Chupakhin, O.N. Direct introduction of acetylene moieties into azines by $S_N H$ methodology. *Tetrahedron Lett.* 2009, **50**, 1444–1446.

20. Zhuo, F.; Xie, W.; Yang, Y.; Zhang, L.; Wang, P.; Yuan, R.; Da, C. TMEDA-assisted effective direct ortho arylation of electron-deficient N-heteroarenes with aromatic Grignard reagents. *J. Org. Chem.* 2013, **78**, 3243–3249.

21. Prokhorov, A.M.; Makosza, M.; Chupakhin, O.N. Direct introduction of acetylene moieties into azines by S_NH methodology. *Tetrahedron Lett.* 2009, **50**, 1444–1446.

22. a) Sason, S.; H. Bernhard, S.; Wolfe, S. Theoretical aspects of physical organic chemistry: the S_N2 mechanism; *Wiley: New York*, 1992. b) Lim C, Kim SH, Yoh SD, Fujio M, Tsuno Y. The Menschutkin reaction of 1-arylethyl bromides with pyridine: Evidence for the duality of clean S_N1 and S_N2 mechanisms. *Tetrahedron letters.* 1997 May 5; **38**(18):3243-6. c) Xu, Z.B. and Qu, J., Hot water-promoted sn1 solvolysis reactions of allylic and benzylic alcohols. *Chemistry–A European Journal*, 2013, **19**(1), 314-323. d) Okamoto, K., Takeuchi, K.I. and Shingu, H., Kinetic Studies on Solvolysis. VIII. Phenolysis of Optically Active α-Phenethyl Chloride in Phenol-Benzene Solven— Three-stage Mechanism in the SN1-Type Solvolysis. *Bulletin of the Chemical Society of Japan*, 1962, **35**(4), 525-531.

23. a) D. Kikelj, *Synthesis*, 2006, **14**, 2271−2285. b) 58. K. Błasiak, W. Danikiewics, and M. Mąkossa, *J. Am. Chem. Soc.*, 2016, **138**(23), 7276−7281. c) 59. M. Liljenberg, T. Brinck, B. Herschend, T. Rein, S. Tomasi, and M. Svensson, *J. Org. Chem.*, 2012, 77(7), 3262−3269.

24. Hoffman, R. W., 1967, Dehydrobenzene and Cycloalkynes, *Academic Press: New York*.

25. K. Błaziak, W. Danikiewicz, M. Makosza, *J. Am. Chem. Soc*. 2016, **138**, 7276 – 7281.

26. H. Takikawa, A. Nishii, T. Sakai, K. Suzuki, *Chem. Soc. Rev*. 2018, **47**, 8030 – 8056.

27. J. A. Garcia-Lopez, M. F. Greaney, *Chem. Soc. Rev*. 2016, **45**, 6766 – 6798.

28. R. A. Rossi, A. B. Pierini, A. B. PeÇeÇory, *Chem. Rev.* 2003, **103**, 71 – 168.

29. A. Studer, D. P. Curran, *Nat. Chem.* 2014, **6**, 765 – 773.

30. V. Snieckus, *Chem. Rev.* 1990, **90**, 879 – 933.

31. a) S. Crespi, S. Protti, M. Fagnoni, *J. Org. Chem*. 2016, **81**, 9612 –9619 b) Wojciechowski, K. *Tetrahedron*, 1993, **49**, 10017. c) Wojciechowski, K. *Synth. Commun.* 1993, **23**, 2415.

32. Kosinski, S.; Wojciechowski, K. *Eur. J. Org. Chem*. 2000, **7**, 1263-70.

33. (a) J.F. Bunnett and R.E. Zahler, Chem. Rev., 1951, **49**(2), 293–412 (b) J. Miller, 1968, Aromatic Nucleophilic Substitution, Elsevier, Amsterdam.

34. (a) F. Terrier, Chem. Rev., 1982, **82**(2), 78–152. (b) G.A. Artamkina, M.P. Egorov and I.P. Beletskaya, *Chem. Rev.*, 1982, **82**(4), 427–459.

35. A.F. Pozharskii, 1985. Theoretical Basis of the Chemistry of Heterocycles. Khimia, Moscov.

36. O.N. Chupakhin, V.N. Charushin, and H.C Van der Plas, *Tetrahedron*, 1988, **44**(1), 1-34.

37. M. Makosza, W. Danikiewics and K. Blasiak, *J. Am. Chem. Soc.*, 2016, **138**(23), 7276-7281.

38. (a) M. Makosza, *Org. & Med. Chem. Int. J.*, 2017, **2**(2); (b) M. Mąkosza, *Chem.-A. Eur. J.*, 2014, **20**(19), 5536-5545.

39. M. Mąkosza, K. Kamieńska-Trela, M. Passewski and M. Bechcicka, *Tetrahedron*, 2005, **61**(50), 11952 11964.

40. D. Sulikowski and M. Mąkosza, *Eur J Org Chem.*, 2010, **22**, 4218-4226.

41. M. Makosza and J. Winiarski, *Acc. Chem Res.*, 1987, **20**(8), 282-289.

42. Z. Wróbel and A. Kwast, *Synthesis*, 2010, **22**, 3865-3872.

43. a) Makosza, M.; Wojciechowski, K. *Chem. Heterocycl. Compd.* 2015, **51**, 210. b) Makosza, M. *Heterocycles*, 2014, **88**, 75. c) Makosza, M., *Synthesis,* 2011, **15**, 2341.

44. a) H. C. van der Plas, *Tetrahedron*, 1985, **41**, 237. b) H. C. van der Plas, *Acc. Chem Res.*, 1978, **11**, 462-488

45. H. C. van der Plas, "Ring Transformations of Three·, Four-Five-, Six- and Seven-membered Heterocycles", Vol. I and II, Academic Press, New York and London, 1973.

46. Epishina, M. A.; Kulikov, A. S.; Ignat'ev, N. V.; Schulte, M.; Makhova, N. N. Mendeleev Commun. 2015, **25**, 41. b) Charushin, V. N.; Chupakhin, O. N., Eds. Metal Free C-H Functionalization of Aromatics. Nucleophilic Displacement of Hydrogen. In Top Heterocyclic Chemistry, Maes, B. U. W., Cossy, J., Poland, S., Series Eds.; Springer: Heidelberg, New York, Dordrecht, London, 2014; **37**. c) Makosza, M. *Chem. Soc. Rev.* 2010, **39**, 2855.

47. K. Ziegler and H. Zeiser, Ber. Dtsch. *Chem. Ges. B*, 1930, **63**(7), 1847-1851.

48. I. S Kovalev, O.N. Chupakhin, D.S. Kopchuk, G.V. Syryanov, V.L. Rusinov and V.N. Charushin, *Russ. Chem. Rev.*, 2015, **84**(12), 1191-1225.

49. G. Fraenkel and J.C. Cooper, *Tetrahedron Lett.*, 1968, **9**(15), 1825-1830.

50. C. S. Giam and J.L. Stout, *Chem. Soc. Chem. Commun,* 1969, 142.

51. W. Clegg, L. Dunbar, L. Horsburgh, R.E. Mulway, Angew. *Chem., Int. Ed. Engl.*, 1996, **35**(7) 753-755.

52. Y.N. Bubnov, E.V. Klimkina, S.A Starikova and A.V. Ignatenko, *Russ. Chem. Bull., Int. Ed.*, 2001, **50**(6), 1078-1084.

53. V.N. Charushin, and O.N. Chupakhin, eds., 2014, Metal Free C-H Functionalisation of Aromatics. Nucleophilic Displacement of Hydrogen, Springer, 37, p. 283.

54. Q. Chen, T. León and P. Knochel, Angew. *Chem. Int. Ed.*, 2014, **53**(33), 8746-8750.

55. (a) O.N. Chupakhin, I.A. Utepova, I.S. Kovalev, V.L. Rusinov and S.A. Starikova, *Eur. J. Org. Chem.*, 2007, **5**, 857-862; (b) I.A. Utepova, A.A. Musikhina, O.N. Chupakhin, and P.A. Slepukhin, *Organometallics*, 2011, **30**(11), 3047-3053; (c) M.V. Varaksin, I.A. Utepova, O.N. Chupakhin, and V.N. Charushin, *J. Org. Chem.*, 2012, **77**, 9087-9093; (d) P.S. Fier and J.F. Hartwig*, Science*, 2013, **342**(6161), 956-960.

56. (a) M. Makosza and K. Stalinski, *Pol. J. Chem.*, 1999, **73**(1), 151-161. (b) G. Bartoli, *Acc. Chem. Res.*, 1984, **17**(3), 109-115. (c) M. Makosza, W. Adam, C.G. Shao, and M. Surowiec, *J. Org. Chem.*, 2001, **66**(15), 5022-5026. (d) T.V. RajanBabu, B.L. Chenard and M.A. Petti, *J. Org. Chem.*, 1986, **51**, 1704-1712. (e) Y. Tagawa, M. Nomura, H. Yamashita, Y. Goto and M. Hamana, Heterocycles, 1999, **51**(10), 2385-2397. (f) T. Itoh, Y. Matsuya, H. Hasegawa, K. Nagata, M. Okada, and A. Ohsawa, *Chem. Pharm. Bull.* 1995, **45**, 881883.

57. T.A. Geissman, M.J. Schlatter, I.D. Webb and J.D. Roberts, *J. Org. Chem.*, 1946, **11**(6) 741-750.

58. H. Gilman and J.T. Edward, *Can. J. Chem.*, 1953, **31**(4), 457-468.

59. Davis, R. B.; Pizzini, L. C.; Benigni, J. D. *J. Am. Chem. Soc.*, 1960, **82**, 2913.

60. Davis, R. B.; Pizzini, L. C.; Bara, E. J. *J. Org. Chem.*, 1961, **26**, 4270.

61. Bartoli, G.; Rosini, G. **Synthesis** 1976, 270.

62. Bartoli, G.; Leardini, R.; Medici, A.; Rosini, G. *J. Chem. Soc.*, *Perkin Trans.* 1978, **1**, 692.

63. Chupakhin, O. N.; Charushin, V. N.; van der Plas, H. C. Nucleophilic Aromatic Substitution of Hydrogen; *Academic Press: New York*, 1994.

64. Tomioka, Y.; Miyake, J.; Yamazaki, M. *Chem. Pharm. Bull.*, 1982, **30**, 851.

65. Makosza, M.; Varvounis, G.; Surowiec, M.; Giannopoulos, T. *Eur. J. Org. Chem.*, 2003, 3791.

66. (a) Kroon, A. P.; van der Plas, H. C. Recl. Trav. Chim. 1973, **92**, 1020. (b) Kroon, A. P.; van der Plas, H. C. *Recl. Trav. Chem.* 1974, **93**, 111.

67. (a) Makosza, M.; Kwast, A. *J. Phys. Org. Chem.*, 1998, **11**, 341. (b) Glinka, T.; Makosza, M. *J. Org. Chem.*, 1983, **48**, 3860.

68. Makosza, M.; Wojciechowski, K. Liebigs *Ann./Recueil,* 1997, 1805.

69. (a) Makosza, M.; Sienkiewicz, K. *J. Org. Chem*. 1990, **55**, 4979. (b) Makosza, M.; Sienkiewicz, K. *J. Org. Chem*. 1998, **63**, 4199. (c) Brose, T.; Holzscheiter, F.; Mattersteig, G.; Pritzkow, W.; Voerckel, V. J. *Prakt. Chem*. 1992, 334,

70. (a) Makosza, M.; Kwast, A. J. Chem. *Soc., Chem. Commun*. 1984, 1195. (b) Makosza, M.; Kwast, A. *Tetrahedron* 1991, **47**, 5001. 71.

71. a) Bachowska, B.; Zujewska, T. *Monatsh. Chem*. 2001, **132**, 849. b) Bachowska, B. *Monatsh. Chem*. 2002, **133**, 1071.

72. O. N. Chupakhin, and V. N. Charushin, *Tetrahedron*, 2016, **57**, 2665-2672.

Chapter 2

THEORETICAL BACKGROUND

Chemistry is the study of the properties of molecules and their reactivity; it is the branch of science that deals with the construction of molecules from substances which make up matter. A subfield of this is a combination of mathematical methods and basic laws of physics (statistical mechanics and dynamics) that are applied to review the procedures of chemical importance. This concept is known as theoretical chemistry.

In the growing field of theoretical chemistry, a dominant subfield called computational chemistry has suddenly begun to surface. It uses computer simulations to solve chemical problems, and new theoretical methods are being developed all the time. There are indeed problems with the current theoretical methods, such as problems relating to accuracy and system size. Although information on a system of thousands of particles can be obtained, the larger the system the less accurate the results. Among other reasons for computational modelling, the purpose is to apply fundamental laws of quantum mechanics and thermodynamics to study the predicted properties of molecular systems and chemical reactions.

The interested reader looking for a more thorough description of mathematical details on the theoretical work presented in this chapter can refer to any of the following three books: *Essentials of Computational Chemistry, Theories and Models* by Christopher J. Cramer. Wiley: Chichester, England. 2002;[1] *Computational chemistry: a practical guide for applying techniques to real world problems* by D. Young, John Wiley & Sons, (2004);[2] and. *Computational organic chemistry* by S.M. Bachrach, Wiley-Interscience, 2007.[3]

2.1　Quantum chemistry

Electrons are fast-moving particles, and due to their light weight characteristic, this makes it impossible to provide a description using classical mechanics. They are found in close proximity to the nucleus, which is made up of protons and neutrons. These electrons and nuclei are what constitutes an atom, and when atoms are held together by chemical bonds due to intramolecular forces, they make up a molecule whose properties can be investigated. Electrons have a two-sided characteristic known as the wave-particle duality, which must be described using wave functions, ψ. A description of how the wave function of a system gradually develops over time is given by Newton's second law of motion, known as the Schrödinger

equation (see equation 2.1). The Schrödinger equation is a linear partial differential equation that describes the wave function or state function of a quantum-mechanical system.

$$\boldsymbol{H}\psi = i\hbar\frac{\partial \psi}{\partial t}$$ 2.1

If the Hamilton operator, $\boldsymbol{H}$, does not depend on time (equation 2.2), then:

$$\boldsymbol{H}(\mathbf{r})\psi(\mathbf{r}) = E\psi(\mathbf{r})$$ 2.2

E in equation 2.2 expresses the system's electronic energy. Finding the position of a particle is made possible by the associated wave function. The time-dependent Schrödinger equation, equation 2.1, which describes the wave-like properties of matter, is used for quantum mechanical systems to find their allowed energy levels. To find this information in molecular systems, the time-independent Schrödinger equation must be solved, and solving this equation is not feasible for molecular systems which are generally of interest to organic chemists. Thus, a few approximations are acquired to make the mathematics easy to deal with. The goal is to find suitable functions with the correct magnitude to be summed and this would essentially result in the preferred solution.

2.1.1   The Born-Oppenheimer approximation

For any system with n number of particles, the Hamiltonian operator, Ĥ, contains the potential and kinetic energy for all particles, while the total wave function is dependent on both the positions of the electrons and the nuclei. For any changes relative to the position of the nuclei, the electrons respond in an instant to the traverse.[4] This is due to the lightness of the electrons relative to that of the nuclei, and thus their velocities are much greater. For this reason, the separation of the total wave function into two parts is now feasible: (i) the electronic wave function for a fixed nuclear geometry and (ii) the nuclear wave function.

The movement of nuclei creates a potential energy surface (PES) through the determination of molecular electronic energy. This means that for fixed nuclei, the Schrödinger equation can be solved to a good approximation only for the electronic part. This approximation is called the adiabatic or Born-Oppenheimer approximation.[5,6–8] After its application, ignoring relativity, the Hamiltonian, Ĥ, results in equation 2.3:

$$\hat{H} = -\sum_i^e \frac{\hbar^2}{2m_e} \nabla_e^2 - \sum_I^n \frac{\hbar^2}{2M_I} \nabla_n^2 - \sum_I^n \sum_i^e \frac{Z_I e'^2}{r_{Ii}} \nabla_e^2 - \sum_{i<j}^n \frac{Z_I Z_J e'^2}{r_{IJ}} + \sum_{i<j}^e \frac{e'^2}{r_{ij}} \qquad 2.3$$

The first and second term in equation 2.3 represent the kinetic energy of electrons and nuclei respectively, the third term represents electron-nuclear attraction, and the last two terms represent the repulsion of nuclei and electrons respectively. The Laplacian operator, ∇_i^2, acts on particle i/I, r_{ij}/r_{IJ} is the distance between the particles, $\hbar = h/2\pi$ (Planck's constant divided by 2π), m is the mass of the particle and $e' = e/4\pi\varepsilon_o$, where e is charge and ε_o is vacuum permittivity.

2.1.2 Linear combination of atomic orbitals (LCAO) approximation

The wave function of an electron in a molecule is referred to as a molecular orbital (MO). Molecular orbitals are calculated through a technique called the linear combination of atomic orbitals (LCAO) approximation.[3] Molecular orbitals extend to all regions within the molecule, i.e., MOs are not localised but are polycentric. The atomic orbitals (AOs) in the molecule which are nearly of equal energy and orthonormal symmetry, combine to give an equal number of MOs. The electronic wave functions are MOs that are responsible for the traverse of the whole molecule, while the MOs are constructed by the LCAO method, χ_μ.

$$\emptyset_i = \sum_\mu^k c_{i\mu} \chi_\mu \qquad 2.4$$

$c_{i\mu}$ is the expansion coefficient of atomic orbitals (χ_μ) in molecular orbitals ($\emptyset_i$), and the index μ spans the AO of every atom in the molecule.

2.1.3   Variational principle

The principle of variation is defined as any wave function built from the linear combination of orthonormal functions is bound to result in an energy that is either equal to or more than the system's lowest energy value.[3] The principle provides an easy path for assessing the quality of various expansions; a better wave function results from low energy supply. The principle, however, is not an approximation to solve the Schrödinger equation, but it preferably enables

the best possible solution to the Schrödinger equation through a practical approach (equation 2.5).

$$\frac{\langle \phi | \hat{H} | \phi \rangle}{\langle \phi | \phi | \rangle} \geq E_o \qquad 2.5$$

From the definition of the variational principle, the quality of various truncated expansions such as trial wave function, can be measured as electronic energy (equation 2.5). Thus, the energy can be minimised through the adjustments of certain parameters within the wave function to obtain an almost exact solution.

An approximate wave function can be found through the use of equation 2.5, the better the choice of ϕ (trial functions) and the number of parameters, the better the accuracy.

2.1.4   Basis set

A basis set is a mathematical set of N functions utilised to produce molecular orbitals within a system.[2] These basis sets are mostly pre-optimised to reduce the number of functions required. The functions resemble the atomic orbitals due to their usual placement at the centre of the atomic nuclei, but functions centred in lone pairs or bonds can also be used. The functions in turn add up to form an approximate of the total wave function.

There are so many basis sets currently available that a researcher may not need to modify a basis set again. The set of functions of a basis set are linearly combined (equation 2.6); these functions are dependent on all n electrons:

$$\emptyset_i = \sum_{i=1}^{N} c_i, x_i. \qquad 2.6$$

In equation 2.6, $\emptyset_i$ represents the molecular orbital and c_i is referred to as the molecular orbital expansion coefficients. The coefficients c_i in an electronic structure calculation are changed to minimise the energy with the characteristics of each basis function remaining constant. For a summation that is above the set of infinite N functions, x_i, an exact energy, is obtained.

However, according to the variational principle, for a finite set of functions the computed energy should be above the exact energy.[3]

2.2   Density functional theory, DFT

The principle behind density functional theory (DFT) is that the energy of a molecule can be measured from the electron density rather than a wave function.[2] It is an *ab initio* method, an approximate quantum mechanical calculation).[2] The wave function depends on coordinates x, y and z of each electron.[3] As a result, the function is complex and difficult to easily interpret.

The goal is to develop DFT functionals that connect the correlation energy with the electron density.[6–8] Hohenberg-Kohn[9] proved the functional's existence relating the electron density to the energy (see equation 2.7). However, Hohenberg-Kohn's theorem does not provide any guidance to the form of the functional.

$$E[\rho(\boldsymbol{r})] = E_{elec},$$
<div align="right">2.7</div>

E_{elec}, equation 2.7, is the exact electronic energy. From this, the theory was then proven to follow the variational principle. This then means that for a given electron density, the resultant energy will be equal to or greater than the system's lowest energy. The idea is that equation 2.7 could be easier to evaluate than the conventional ab-initio approaches due to the simpler variable dependency.

The practical application of the theory was laid by Kohn and Sham, a method structurally similar to the Hartree-Fock (HF) method, which is a common type of *ab initio* calculation.[5,2] Using DFT to solve for the energy, Kohn and Sham[5] suggested that the form of the functional is:

$$E[\rho(\boldsymbol{r})] = T_{\acute{e}}[\rho(\boldsymbol{r})] + V_{ne}[\rho(\boldsymbol{r})] + V_{ee}[\rho(\boldsymbol{r})] + E_{XC}[\rho(\boldsymbol{r})],$$
<div align="right">2.8</div>

and V_{ee}, the electron-electron repulsion, (equation 2.9)

$$V_{ee}[\rho(\boldsymbol{r})] = 0.5 \int \int \frac{\rho(\boldsymbol{r_1})\rho(\boldsymbol{r_2})}{|\boldsymbol{r_1} - \boldsymbol{r_2}|} d\boldsymbol{r_1} d\boldsymbol{r_2}.$$
<div align="right">2.9</div>

29

The nuclear-electron attraction equation, V_{ne}, is given by equation 2.10:

$$V_{ne}[\rho(\boldsymbol{r})] = \sum_{j}^{nuclei} \int \frac{Z_j}{|r - r_k|} \rho(\boldsymbol{r}) d\boldsymbol{r}, \qquad 2.10$$

E_{XC} is known as the exchange-correlation functional and $T_{é}[\rho(\mathbf{r})]$ is the kinetic energy functional. If the exchange-correlation functional had been known, the energy $E[\rho(\mathbf{r})]$ in equation 2.8 would have been solved. Unfortunately, the term is not known and there is no known method of deriving it, thus a sequence of component functionals leading to the existence of E_{XC} have been proposed. The proposed solution, however, results in a number of various DFT methods.

Although the DFT and the HF of the wave mechanics are similar in structure, an important difference separates the DFT from other traditional *ab initio* methods. The DFT method produces molecular energy, including the electron correlation, and therefore provides the correlation energy which is difficult to compute in wave mechanics and which it does at a similar computational cost. Paraphrasing Cramer's[1] differential description between the DFT and the HF, the different post-HF electron correlation and HF methods give a precise solution to an estimated theory; however, a precise theory with an estimated solution is provided by the DFT. Furthermore, the DFT predicts electronic structures and allows the calculation of total energies and forces – it can be used for the study of thermodynamics and kinetics. Due to its independence from the number of electrons, it enables calculations with several numbers of electrons and is overall a well-established technique. Setbacks associated with the DFT method is the limitation in accuracy with the calculation of electronically excited states.

2.2.1 Exchange-correlation functional

The definite form of the exchange-correlation (XC) functional responsible for the improvement of accuracy is not really known, but its existence is assured by the Hohenberg-Kohn theorem.[3] Generally, the exchange-correlation functional is separated into two components, a correlation part, E_C, and a pure exchange part, E_X.[10] This is an assumption, and there is no way of validating it. These component functionals are mostly written in terms of

30

energy density, ε (energy per particle), and depend only on the electron density, $\rho(\mathbf{r})$ (equation 2.11).[10]

$$E_{XC}[\rho(\mathbf{r})] = E_X[\rho(\mathbf{r})] + E_C[\rho(\mathbf{r})] = \int \rho(\mathbf{r})\varepsilon_X[\rho(\mathbf{r})]d\mathbf{r} + \int \rho(\mathbf{r})\varepsilon_C[\rho(\mathbf{r})]d\mathbf{r}. \quad 2.11$$

The major contributor to the E_{XC} is the exchange energy, and the value of ε_X is assumed by the local density approximation (LDA) to be determined from the density. The use of only the electron density approximation to define the XC functional is known as the LDA – the Kohn-Sham equation can only be defined through the LDA. The second class of functional, known as the generalised gradient approximation (GGA), depends on the gradient of the local electron density and the density itself. Although the LDA involves less physical information than the GGA, the latter is not always accurate.

The mostly popular functional is the hybrid method, which is a combination of XC functionals with the HF exchange term, both of which components can be LDA or GGA. The inaccuracy built into the XC functionals and the lack of correlation in HF induces errors which can be cancelled using the hybrid functionals. The Becke 3-parameter, Lee-Yang-Parr (B3LYP) functional (equation 2.12) which we have used in this study, consists of Becke's exchange functional and the Lee-Yang-Parr (LYP) correlation functional. B3LYP is a widely used hybrid functional due to its high accuracy and relatively low computational cost.[11,12]

$$E_{XC}^{B3LYP} = (1-a)E_X^{LSDA} + aE_X^{HF} + b\Delta E_X^B + (1-c)E_C^{LSDA} + cE_C^{LYP} \quad 2.12$$

The coefficients a, b and c represent the "3" in the acronym B3LYP. The first three terms, E_X^{LSDA}, E_X^{HF} and E_X^B, are exchange energies from using local spin density approximation (LSDA), the HF scheme and Becke's 1988 exchange functional respectively. The last two terms and E_C^{LSDA} and E_C^{LYP} are the correlation energies from using the LSDA and GGA of Lee, Yang and Parr respectively.[13]

All hybrid methods have a portion which is semi-empirical in nature, including B3LYP. Among several correlation functionals, the Perdew and Wang (PW91)[14] and LYP[13] functionals are two of the most widely used. LYP computes the full correlation energy, which is not common for PW91 in B3PW91 as it computes the correction to LSDA.

31

Kinetic energy density was recently included in the hybrid meta functionals. In situations such as transition metal-transition bonds, including π-π stacking, and non-covalent interactions, where certain DFT methods were having problems, these meta-functionals were successful.[15]

There are more complicated functionals that often do not perform as well as B3LYP, although it is difficult to explain the lack of success of these functionals.

2.3   Calculations
2.3.1   Geometry optimisation

Geometry optimisations usually attempt to find the geometry of the input molecular structure specified, which minimises the total energy of the molecule to locate minima. From the input, the algorithm is set to adjust its geometry along the potential surface until a stationary point (local minimum) is found. A good estimate of the initial structure in terms of atomic coordinates greatly influences the computational time, and most times determines the convergence to an energy minimum. Only when the forces (root mean square and maximum) are zero is the structure converged – the structure will then be successfully optimised according to a set of specified convergence criteria.[16]

2.3.2   Potential energy surface (PES)

The potential energy surface (PES) is a surface consisting of distant atoms that produce a sequence of single-point energy calculations which sample up to form a surface region of potential energy PES. The surface can be explored and analysed to obtain information on the chemical system. The computed PES is characterised by various optimised structures at every point. All geometric points along the reaction coordinate are simultaneously optimised; for this reason, the molecule may have different symmetry, but the use of symmetry can be turned off.

The potential energy surface gives a description of conformers, isomers and energies of various structures of a system.[2] The PES calculation reliably locates transition structures, namely saddle points which are found between the products and the reactants of a reaction on this surface. For all optimised structures on the topology the minima are located (i.e.,

intermediates, reactants and products). The initial input structure determines which minimum can be found. Due to the competing forces within bonds to determine the lowest energy conformer, there are several local minima. The lowest energy minimum is referred to as the global minimum structure (GMS).

The method of computing a PES for a reaction using G09 is developed by decreasing (or increasing) the distance between atoms of the same (or separate) molecule at an infinite or known distance apart. They approach (or separate) each other at intervals of small-distance steps (e.g. 0.01 Å). For intervals of large-distance steps (~0.5 Å), the resultant structures and energy values will not be a true reflection of the PES, as crucial steps might go unnoticed.

2.3.3 Frequency

Frequency calculation is a keyword type of calculation that computes force constants and the resulting vibrational frequencies.[17] Regarding the Cartesian nuclear coordinates, a process of determining the energy's second derivatives computes the vibrational frequencies; the coordinates then change to mass weighted.[17,18] However, this change is not valid at any geometry other than the stationary point. Thus, it is only practical to submit a frequency calculation at a stationary point.

Frequency calculations start by computing the energies of the input structure before computing the frequencies at that structure. The calculation requires the second derivative for (a) locating a minimum, (b) identifying the stationary point, (c) calculating the vibrational frequencies, and (d) computing the zero-point vibration energy and thermochemical data terms. This then limits the input structure(s) to be a stationary point on the PES for a successful frequency calculation. For this reason, it is necessary to submit a geometry optimisation to locate a minimum (stationary point) prior to a frequency calculation.

Secondly, the validity of the frequency is dependent on the basis set and theoretical model of the resultant optimised structure. Both the optimisation and frequency calculations must be performed at the same level of theory.

Frequency calculations can be used to distinguish between minima. A minimum with zero imaginary frequencies is either a relative minimum or an absolute global minimum, and

33

energies must be used in comparison with other isomers for differentiation. A maximum with 1-imaginary frequency is referred to as a transition state.

2.3.4 Transition state (TS)

A first-order saddle point which is a maximum at a minimum energy path is known as a transition state. This saddle point is a maximum in one dimension and a minimum in all other dimensions. The transition state is a reflection of bond formation and/or cleavage that corresponds to the vibrational frequency mode between atoms. This is characterised by the presence of one imaginary frequency (negative force constant). At this point of the path the molecule is highly unstable and reactive and proceeds to form the desired products, and in some instances, due to the loss of excess vibrational energy, reactants may be formed again instead of products.

Transition structures are an important point along a reaction path, and it is crucial to obtain them when modelling a chemical reaction. This is due to their relationship with the reactants and products, which gives information on the rate (the height of the barrier) and reactivity of the reaction.

A PES scan can be done or a reasonable guess can be made in the search for the transition state structure. If several TSs of different functional groups are to be investigated, a certain TS of the simplest case can be found and used as a template and added to it, and this would be the various functional group moieties. Finding the "correct" TS is not guaranteed, and therefore many attempts are often required to determine the TSs. Once the "correct" TS has been successfully located, an Internal Reaction Coordinate (IRC) calculation can be conducted in order to verify it.

2.3.5 Intrinsic reaction coordination (IRC)

Intrinsic reaction coordinate (IRC) data permit the theoretical investigation of chemical reactions – how reactants and products are connected with or related to each other through a temporary transition state. It is important to note that a chemical reaction may have more than

one reaction path connecting the products and the reactants on a PES, which correspond to different transition structures.

Gaussian 09 software can calculate a reaction path when an IRC keyword is requested in the route section. This calculation starts at the transition structure and proceeds down the trajectory several times (default is 6) in mass-weighted coordinates, in both directions, optimising each point that represents the geometric structure of the molecular system along the energy surface. Consequently, an IRC definitively joins two minima through a transition state on the PES by a single reaction path.[19] However, most often, once the calculation is complete the output will not be a true reflection of the minimum on either side of the reaction path, due to the calculation not stepping all the way to the minimum. Although the calculation can be continued by using the IRC=RESTART keyword on the route, each output structure will have to be subjected to a single-point geometry optimisation calculation.

2.3.6   Solvation model

The presence of a solvent in any reaction system can significantly affect the molecular system being studied. Due to the interaction between the solvent and the solute, the energy-dependent properties of the solute such as electronic spectrum, vibrational frequency, geometry and total energy depend on the solvent. This may result in an altercation of the reactivity, molecular orientation and energy of the system. Hence it is imperative to take into consideration the effect of solvation when modelling a system in solution.

A widely used method of solvation modelling is implicit, where the continuum of a uniform dielectric constant mimics the effect of the solvent. A solute lies in a cavity of solvent, and the cavity can be distinctively defined by several methods.

A dipole in the field of the solvent is induced by the dipole of the molecule, which will interact with the dipole of the solvent. As a result, a net stabilisation is reached. A more recent method is Tomasi's Polarised Continuum Model (PCM),[20] where the multiple interlocking atomic spheres define the cavity. Another widely used method is the explicit solvation model, which includes the presence of explicit solvent molecules surrounding the solute.

The implicit solvent models take into consideration the equilibrium interactions with the solvent, while the explicit solvent approach is unable to do that due to the need to account for many degrees of freedom of the solvent. In most cases, the combination of both methods (explicit and implicit) known as the hybrid solvation model (HSM) are used. This provides better results, but demands a lot of computational time. In this study, two THF solvent molecules were used to study the effect of explicit solvation, combined with implicit solvation with THF.

By minimising the computational time by as much as the computational time is reduced, the accuracy of the results can be affected. The solvent with the lowest energy configuration is sufficient for the prediction of the solvent effects in cases where the effect relies on the coordination of the solvent molecules with the solute. This coordination can result in a slight change in the geometry of the transition structure and thus affect its energy and reaction rate. The coordination of the solvent molecules with the solute does not in any way alter the method in which transition states are found, but may rather alter the results.

2.4 Conclusion

Chemistry can be described mathematically through theoretical chemistry. Computer programs and algorithms are developed on the basis of theoretical chemistry, which can be used to predict chemical properties. This then allows computational chemistry to be applied to specific chemical problems.

Computational chemistry helps with the understanding of experimental data, and most importantly it provides a starting point for laboratory synthesis. It can be used to investigate reaction mechanisms that are not easily understood through experimental studies or to predict unknown molecules. Furthermore, the application of computational chemistry can help the experimental chemist, or it can intrigue curiosity to find new chemical objects.

2.5 References

1.   Horn, A. H. C. Essentials of Computational Chemistry, Theories and Models By Christopher J. Cramer. Wiley: Chichester, England. 2002. 562 pp. ISBN 0-471-48551-

9 (hardcover). $110. ISBN 0-471-48552-7 (paperback). $45. *J. Chem. Inf. Comput. Sci.* **43**, 1720–1720 (2003).

2. Young, D. *Computational chemistry: a practical guide for applying techniques to real world problems*. (John Wiley & Sons, 2004).

3. Bachrach, S. M. *Computational organic chemistry.* (Wiley-Interscience, 2007).

4. Born, M. & Oppenheimer, R. J. On the quantum theory of molecules (English translation). *Ann. Phys.* **457**, 1–32 (1927).

5. Kohn, W. & Sham, L. J. Self-consistent equations including exchange and correlation effects. *Phys. Rev.* **140**, A1133 (1965).

6. Baerends, E. J. & Gritsenko, O. V. Quantum chemical view of density functional theory. *J. Phys. Chem. A* **101**, 5383–5403 (1997).

7. Ziegler, T. Approximate Density Functional Theory as a Practical Tool in Molecular Energetics and Dynamics. *Chem. Rev.* **91**, 651–667 (1991).

8. St-Amant, A. Density Functional Methods in Biornolecular Modelling. *Keviews Comput.* 217 (1996).

9. Hohenberg, P. & Kohn, W. Inhomogeneous electron gas. *Phys. Rev.* **136**, B864 (1964).

10. Loftsdóttir, K., Jensen, L., Jensen, L. & Loftsdóttir, K. *Introduction to comp. Crisis in the Nordic Nations and Beyond* (2018). doi:10.4324/9781315574882-1.

11. Stephens, P. J., Devlin, F. J., Chabalowski, C. F. & Frisch, M. J. Ab Initio calculation of vibrational absorption and circular dichroism spectra using density functional force fields. *J. Phys. Chem.* **98**, 11623–11627 (1994).

12. Becke, A. D. Density-functional thermochemistry. III. The role of exact exchange. *J. Chem. Phys.* **98**, 5648–5652 (1993).

13. Lee, C., Yang, W. & Parr, R. G. Development of the Colle-Salvetti correlation-energy formula into a functional of the electron density. *Phys. Rev. B* **37**, 785 (1988).

14. Perdew, J. P. & Wang, Y. Accurate and simple analytic representation of the electron-gas correlation energy. *Phys. Rev. B* **98**, 244–249 (2018).

15. Zhao, Y., Schultz, N. E. & Truhlar, D. G. Design of density functionals by combining the method of constraint satisfaction with parametrization for thermochemistry,

thermochemical kinetics, and noncovalent interactions. *J. Chem. Theory Comput.* **2**, 364–382 (2006).

16. Schlegel, H. B. Exploring potential energy surfaces for chemical reactions: An overview of some practical methods. *J. Comput. Chem.* **24**, 1514–1527 (2003).

17. Freq | Gaussian.com. https://gaussian.com/freq/.

18. Baboul, A. G. & Schlegel, H. B. Improved method for calculating projected frequencies along a reaction path. *J. Chem. Phys.* **107**, 9413–9417 (1997).

19. Das, A., Majumdar, L., Chakrabarti, S. K., Saha, R. & Chakrabarti, S. Formation of cyanoformaldehyde in the interstellar space. *Mon. Not. R. Astron. Soc.* **433**, 3152–3164 (2013).

20. Cossi, M. Continuum solvation model for infinite periodic systems. *Chem. Phys. Lett.* **384**, 179–184 (2004).

Chapter 3

INVESTIGATING THE S_NH REACTION MECHANISM OF 2-MONOSUBSTITUTED QUINOXALINE WITH LITHIOFURAN USING DFT

3.1 Introduction and aim

Azine rings are heterocyclic compounds that contain at least one nitrogen atom in their ring system. They belong to the electron-deficient heteroaromatics due to the electron withdrawing effect of the aza group (R–N=R). Quinoxaline is one example of an azine ring, and unlike most aromatic imines, it has two electron-accepting sp^2 sites at positions 2 and 3 (see **Figure 3.1**). Because of this, the molecule is susceptible towards nucleophilic attack.
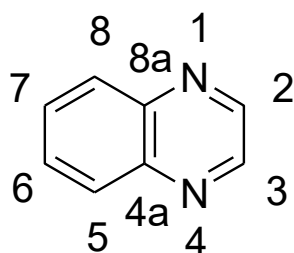
Figure 3.1: Quinoxaline structure

In this chapter we focus on a study conducted by Nxumalo and Ndlovu,[1] which shows the nucleophilic substitution of 2-phenylquinoxaline (**A**) and 2-*n*-butylquinoxaline (**B**) when treated with lithiofuran (**a**) in tetrahydrofuran (THF) solvent (see **Scheme 3.1**). As mentioned in Section 1.2.2 of Chapter 1, these reactions give products of vastly different yields, and this presumably distinguishes the influence of the substituents on reactivity.
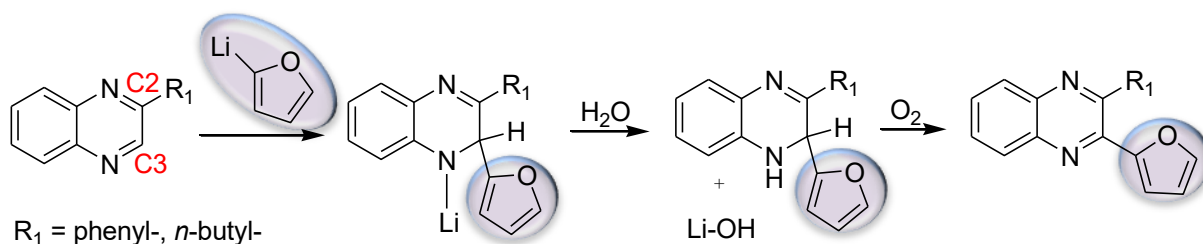
Scheme 3.1: Oxidative nucleophilic substitution of hydrogen (ONSH) of 2-phenylquinoxaline (**A**) and 2-*n*-butylquinoxaline (**B**) treated with lithiofuran to obtain 2,3-disubstituted quinoxalines of 46% and 91% yields respectively

A density functional theory (DFT) study to investigate the origin of such variation in reaction yields is reported; however, in the case in hand, no specific reaction mechanism of the nucleophilic substitution (S_N) was reported by Nxumalo and Ndlovu[1]. However, it should be mentioned that they did make use of atmospheric oxygen to obtain their final product. The reaction correlates well with the requirements of a method suggested by Chupakhin[2] called

"oxidative nucleophilic substitution of hydrogen" (ONSH). However, the method itself, as discussed in Section 1.5.1 of Chapter 1, is still not fully understood. It was hypothesised that the reaction proceeds with the formation of LiH as the by-product, but its presence could not be detected in the crude product.[3,4] Therefore there appears to be a general lack of in-depth understanding of the reaction mechanisms and selectivity of substituents in nucleophilic substitution of hydrogen (S_NH) reactions, which prompted this study.

The reactions were modelled using the ONSH mechanism (**Scheme 3.1**) in order to establish (i) the reaction pathway of the α-hydrogen (at the C3-position) displacement in **A** and **B** and the by-products that are formed, (ii) the influence of phenyl- and *n*-butyl-substituents at the C2-position, and (iii) the factors that affect the reaction yield.

3.2 Results and discussion

3.2.1 Nucleophilic addition reaction (σ^H-complex formation)

The quinoxaline molecule contains electrophilic reactive sites on carbon C2 and the hydrocarbon skeleton C3 - **Figure 3.2**. The carbon (C3) and nitrogen (N4) atoms of the N4=C3 bond present a large electronegative area that is susceptible to nucleophilic attack at the carbon atom.
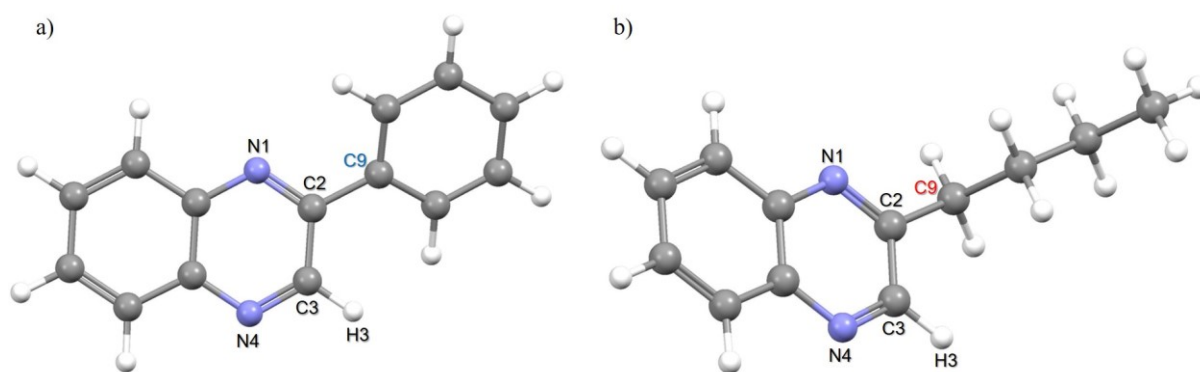
Figure 3.2: Global minimum structures: a) 2-phenyl quinoxaline (**A**) and b) 2-*n*-butyl quinoxaline (**B**)

2-*n*-butylquinoxaline (**B**) was submitted for a conformational search due to the flexibility of the butyl chain. The resultant conformers had a flexible chain resembling a chair- and boat-like conformation (see Appendix A: **Table 0.1**). The "chair" is 0.53 kcal/mol more stable than the "boat" structure; however, this energy difference is negligible. Thus, either conformer is likely

to be present in the reaction vessel. In this study the boat conformer was used. No conformers were found for 2-phenylquinoxaline (**A**).

A and **B** were each optimised in the presence of a nucleophile lithiofuran (**a**). The optimisation of **A** with **a** formed adduct (Add.) **1-Aa**, and **B** with **a** formed adduct (Add.) **1-Ba**, **Figure 3.3**. The **1-Aa** and **1-Ba** notations differ only in the electrophile **A/B** used. The notation stands for: nucleophilic addition reaction (step-**1**) of 2-phenylquinoxaline (**A**)/2-*n*-butylquinoxaline (**B**) with lithiofuran (**a**). The number changes with the change in the reaction step.
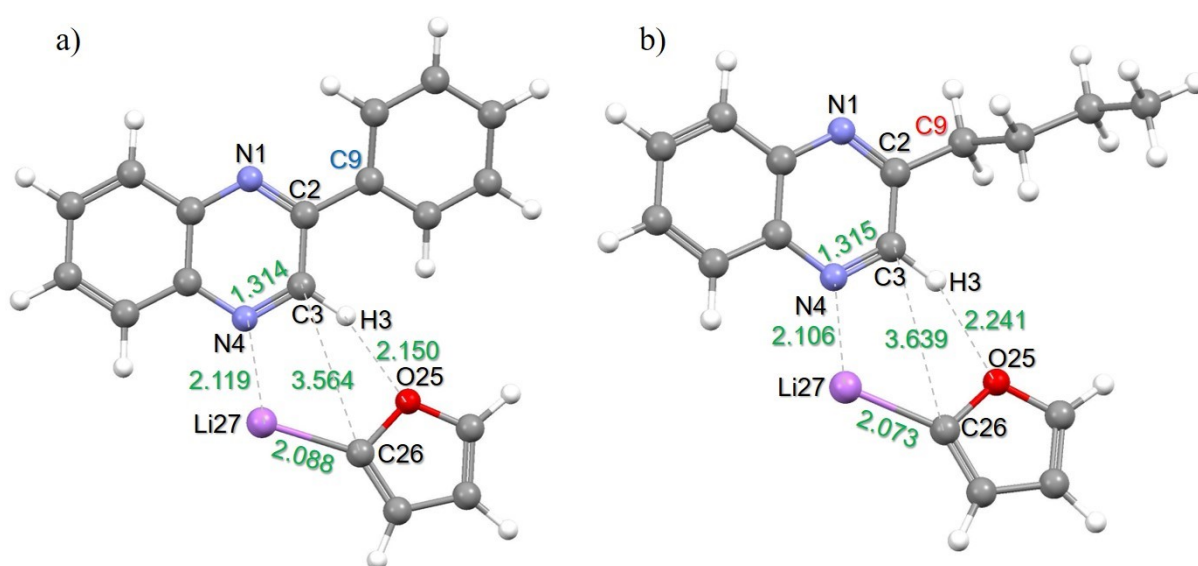
Figure 3.3: Geometry optimisation of quinoxaline derivatives with nucleophile lithiofuran (**a**) led to the formation of adduct a) **1-Aa** and b) **1-Ba**

Both quinoxaline derivatives (R_x = **A**, **B**) interact similarly with **a**, showing similar atomic affinities, atomic distances and structural geometry to form Add. **1-Aa** and **1-Ba**. The two adducts are global minimum structures (GMSs) at $\Delta G_{1\text{-Aa}}$ = –13.99 kcal/mol and $\Delta G_{1\text{-Ba}}$ = –13.56 kcal/mol; the energies are measured relative to the sum of separate reactants. In both cases, the inter-atomic distance d(Li27, N4) is 2.111 ± 0.015 Å, and this is the shortest inter-molecular distance in the adducts. The N4 atom has a lone pair of electrons that are sp^2-hybridised; this part of the ring qualifies the quinoxaline derivative as a Lewis base and thus a ligand that is susceptible to coordinate with metal ions such as Li27. Thus it is as if the reaction is facilitated by the Li27 and N4 atoms due to their strong affinity towards one another. Although, Li27·N4 interact strongly, other non-covalent interactions between the rest of the atoms also contribute to the stability of the structures.

Nxumalo and Ndlovu[1] showed that these reactions form a C-C bond through nucleophilic substitution reaction at the C3 position, thus a reaction coordinate scan between the C3 and C26 bond was performed. The reactants ($\mathbf{R_x}$ and $\mathbf{a}$) from each Add. were initially placed at d(C3,C26) ~3.564 Å apart from each other, the coordinate was then scanned in decreasing 0.01 Å steps until the formation of a C3–C26 bond.

A C3–C26 bond formation led to a nucleophilic addition reaction, **Figure 3.4**. Through bond cleavage and bond formation, adducts **1-$\mathbf{R_x}$a** formed transition states (TSs) **1-Aa** and **1-Ba** with ΔG = 1.4 kcal/mol and 2.7 kcal/mol, respectively. Furthermore, the energy difference between the transition state (TS) and Add. reveals an activation energy barrier $\Delta G^{\ddagger}$ of 15.43 kcal/mol and 16.21 kcal/mol for the reaction involving **1-Aa** and **1-Ba** respectively. The energy barrier difference between the two reactions (0.78 kcal/mol) is negligible; thus, the substituents R_1 (n-butyl-, phenyl-) at position C2 of $\mathbf{R_X}$ have no significant steric-effect on the nucleophilic addition of $\mathbf{a}$ to the quinoxaline analogues.
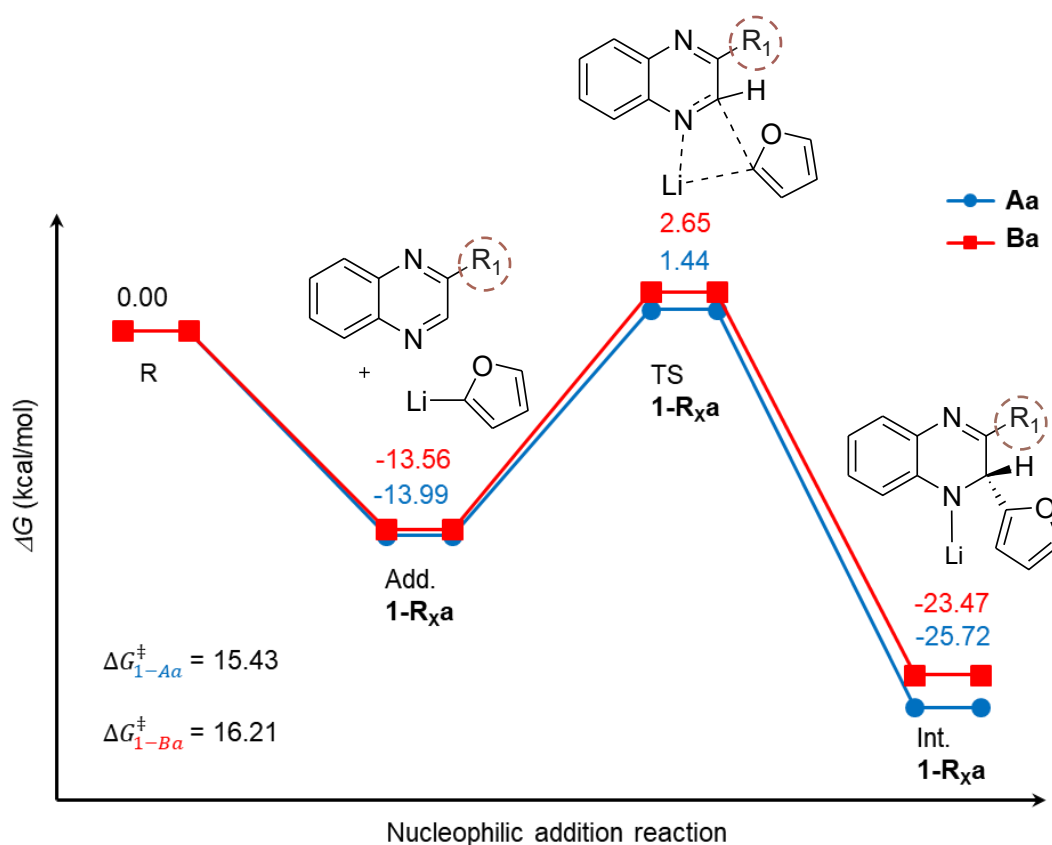
Figure 3.4: Nucleophilic addition reaction profiles of lithiofuran (**a**) with a) 2-phenylquinoxaline (**A**) and b) 2-n-butyl quinoxaline (**B**). Energies are measured relative to the reactants (R) and the activation energies are measured relative to the adducts (Add.)

In nucleophilic addition reaction, the TS has a central atom vibrating between the leaving group (LG) and the nucleophile. It was expected that α-H3 would be the leaving group and form LiH with Li27. Unexpectedly, however, the vibrational frequencies show that the central atom C26 of the nucleophile, vibrates between the leaving group Li27 and the electrophile, **Figure 3.5**. Li27 is the only leaving group in the reaction while α-H3 remains bonded to C3. No by-product was formed during the reaction step.
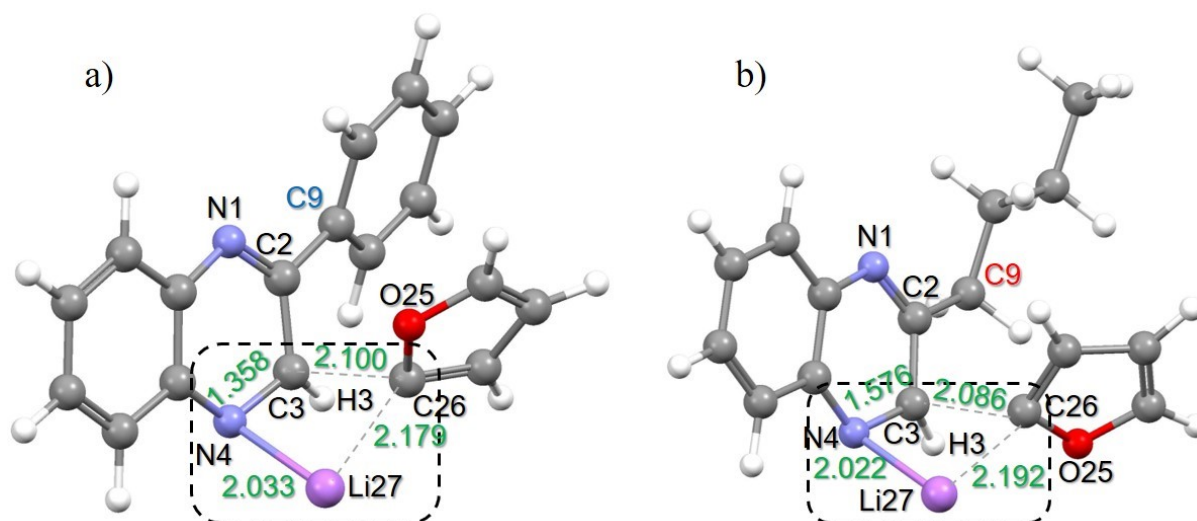
Figure 3.5: Transition states of the nucleophilic addition reaction of a) 2-phenylquinoxaline (TS **1-Aa**) and b) 2-butylquinoxaline (TS **1-Ba**) molecules with lithiofuran. The grey dashed lines show the bond cleavage of C26–Li27 and bond formation of Li27–N4 and C26–C3

The single negative vibrational frequency obtained from both transition states denotes the simultaneous bond cleavage of Li27–C26; and the bond formations of Li27–N4 and C3–C26. The vibrational movements of these coordinates are included in the attached CD. The vibrational frequencies for TS **1-Aa** and **1-Ba** are –300.07 cm^{-1} and –291.65 cm^{-1}, respectively. These frequencies signify that the potential energy surface (PES) is moderately curved at the region of the TSs of the nucleophilic addition reaction.

As the energy of the system stabilises from the TS **1-Rxa**, intermediates (Int.) shown in **Figure 3.6** (Int. **1-Rxa**, σ^H-adduct) are formed. The formation of the stable σ^H-adduct complex incited structural changes from planar (aromatic) to bridge-headed geometry around N4=C3–C2. This is concomitant with the saturation of N4=C3 π-bond (1.308 Å) to single bond N4–C3 (1.470 Å), and consequently the ring loses its aromaticity.
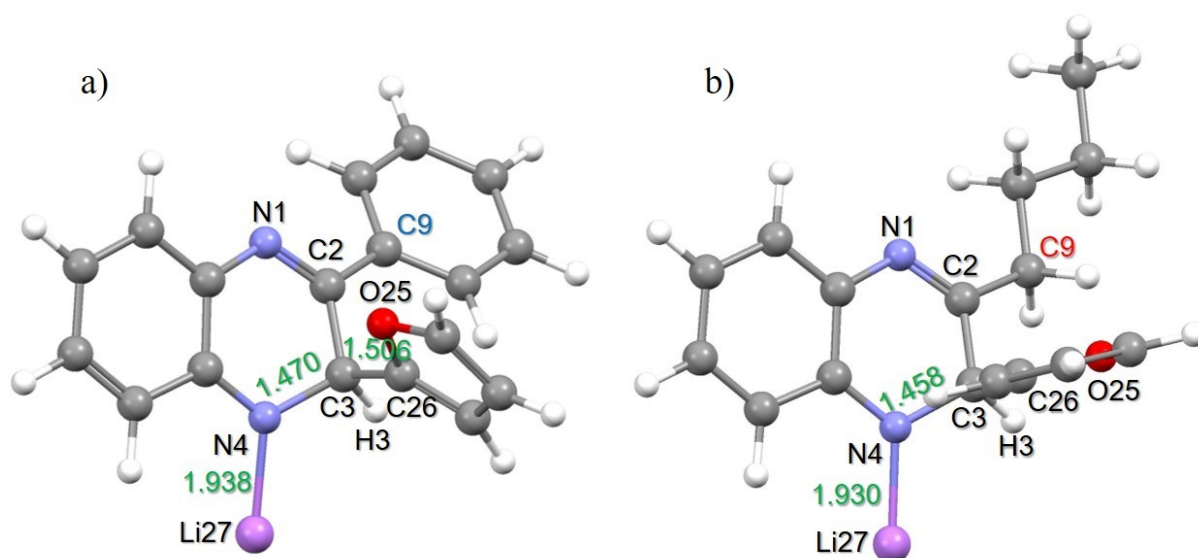
Figure 3.6: Local minimum structures (LMS) of σ^H-adducts a) Int. **1-Aa** and b) Int. **1-Ba**

The subsequent C3–C26 bond formation and the presence of the C3–H3 bond caused crimping of the **R$_x$** ring to the discontinued conjugation ring system, leading to a pseudo-tetrahedral geometry around the C3 position. Geometry changes through the formation of σ^H-adducts include (i) the angle between bonded atoms N4=C3–C2; changing from 111.1250° to 122.7894°, (ii) lengthening of the N4–C3 and C3–C26 bonds by 0.157 Å and ~0.100 Å respectively.

The optimised σ^H-adducts (obtained from the C3-C26 bond coordinate scan) were submitted for a dihedral angle DA(N4,C3,C26,O25) scan at 5° steps for a 360° rotation, **Figure 3.7**. This produced GMSs for Int. **1-Aa** and **1-Ba** of –25.72 kcal/mol and –23.47 kcal/mol respectively, relative to the respective reactants. The energy difference between the LMS and GMS of Int. **1-Aa** is 1.4 kcal/mol and 0.5 kcal/mol for Int. **1-Ba**. These energy differences are minor. Furthermore, it should be noted that the rotational energy barriers are rather small (between 3-4 kcal/mol) and of comparable values for both intermediates. These observations suggest that (i) molecular fragments can "freely" rotate along the DA(N4,C3,C26,O25), (ii) either geometrical structure, whether LMS or GMS, is feasible in the reaction vessel, and (iii) both intermediates can be classified as equally stable. This therefore strongly suggests the absence of any significant steric hindrance that might influence progress at this stage of the reaction. The DA(N4,C3,C26,O25) scan of each intermediate is attached to the CD.
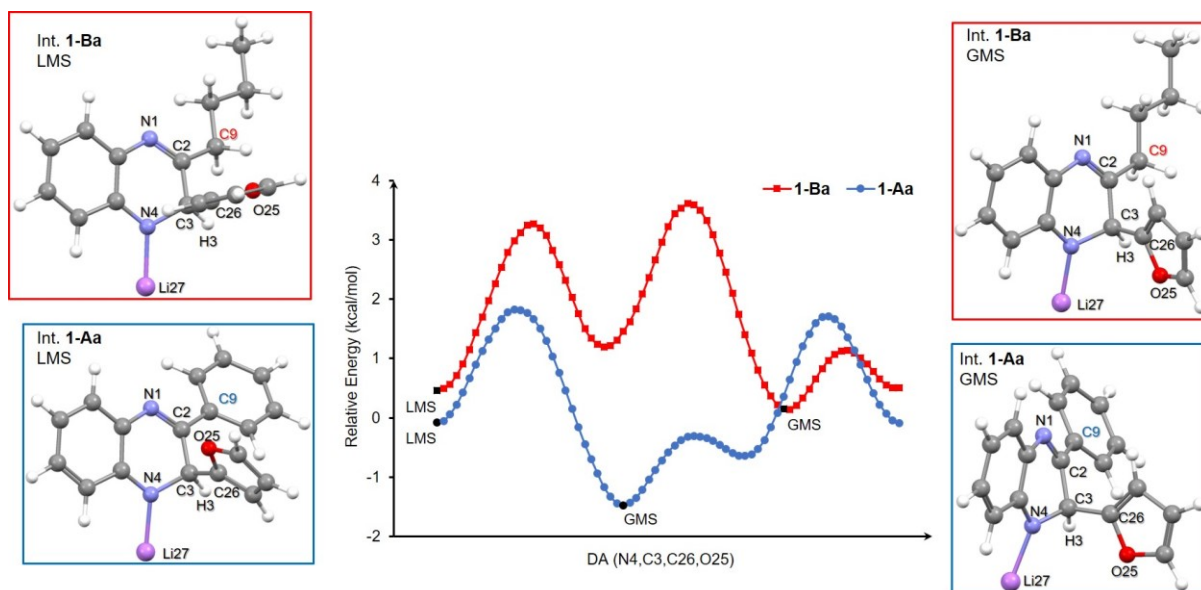
Figure 3.7: Dihedral angular scan profiles (showing a relative E change in kcal/mol) of the DA(N4,C3,C26,O25) angle for Int. **1-Aa** of 2-phenylquinoxaline and Int. **1-Ba** of 2-butylquinoxaline with lithiofuran. The relevant input (LMS) and global minimum (GMS) structures are also shown

One would expect at this point that the C3–H3 bond of the σ^H-adduct intermediate would be elongated due to the presence of a new C3–C26 bond. However, the α-hydrogen (H3) remains strongly bonded to C3 at a bond length of 1.095 Å.

The free energy difference between TS and Int. for reactions involving **1-Aa** and **1-Ba** is -24.28 kcal/mol and –20.82 kcal/mol respectively (**Figure 3.4**). The energies are significant, therefore both intermediates are sufficiently stable for experimental isolation. Thus both Int. **1-Aa** and **1-Ba** are less likely to dissociate and form Add. **1-Aa** and **1-Ba** respectively. This is in agreement with experimental reports.[5-7]

The enthalpy energies shown in **Table 3.1** show that reactions involving **1-Aa** and **1-Ba**, have comparable energy values (±0.5 kcal/mol difference). However, the intermediates are 2.24 kcal/mol apart; this causes the reaction involving **1-Aa** to be –1.25 kcal/mol more exothermic than that involving **1-Ba**. The energy difference is minimal and thus both reactions are similarly exothermic.

Furthermore, when looking at **Table 3.1**, it can be seen that the energies of the corrected zero-point vibrational energy (ZPVE) and thermal enthalpy mimic each other. Thus, the energy profile of the ZPVE reaction should follow a trend such as that of the enthalpy.

Table 3.1: Stationary points involved in nucleophilic addition reaction of 2-phenylquinoxaline (**A**) and 2-*n*-butylquinoxaline (**B**) with lithiofuran (**a**). Structures are optimised in implicit THF solvent at –78 °C. Changes in energies are measured relative to separate reactants (**R$_X$** + **a**). **R$_X$** = **A**, **B**

Systems	E	E_{ZPVE}	H	G
	Energy term in a.u.			
Reactants				
2-phenylquinoxaline (**A**)	–649.21024	–649.00667	–649.00095	–649.02883
Lithiofuran (**a**)	–237.04795	–236.97100	–236.96738	–236.98881
2-*n*-butylquinoxaline (**B**)	–575.40101	–575.16529	–575.15883	–575.18838
Nucleophilic Addition Reaction				
Add. **1-Aa**	–886.27440	–886.01131	–886.00188	–886.03993
Add. **1-Ba**	–812.46455	–812.16924	–812.15916	–812.19879
TS **1-Aa**	–886.25185	–885.98912	–885.98054	–886.01534
TS **1-Ba**	–812.44180	–812.14656	–812.13748	–812.17296
Int. **1-Aa**	–886.29806	–886.03272	–886.02426	–886.05862
Int. **1-Ba**	–812.48470	–812.18788	–812.17858	–812.21458
	Change in energy term (kcal/mol)			
	ΔE	ΔE_{ZPVE}	ΔH	ΔG
Add. **1-Aa**	–10.17	–21.11	–21.05	–13.99
Add. **1-Ba**	–9.78	–20.68	–20.68	–13.56
TS **1-Aa**	3.98	–7.18	–7.66	1.44
TS **1-Ba**	4.50	–6.44	–7.07	2.65
Int. **1-Aa**	–25.02	–34.54	–35.10	–25.72
Int. **1-Ba**	–22.42	–32.37	–32.86	–23.47

3.2.1.1 C2–C26 bond formation

An alternative reaction pathway was modelled in search of possible competing reactions that may explain the vast difference in reaction yields. Although **R$_X$** (**R$_X$** = **A**, **B**) already has a substituent at position C2, the molecule is still electrophilic at both position C2 and C3 and is thus susceptible to nucleophilic attack at both positions.[1]

A C2–C26 bond coordinate scan was conducted using the GMS Add. **1-Aa** shown in **Figure 3.3** – the data obtained are shown in **Figure 3.8**. A C2–C26 bond formation was simulated from an inter-nuclear distance d(C2, C26) of 3.564 Å in –0.01 Å steps. The adduct forms TS **1-Aa**$_{C2–C26}$ at ΔG = 15.95 kcal/mol relative to the sum of free energy reactants R = **A** + **a**. The free activation energy for C2–C26 bond formation is $\Delta G^{\ddagger}$ = 29.94 kcal/mol; this is 14.51 kcal/mol more energy than the C26 addition at the C3 position (**Figure 3.8**). This significantly higher activation energy makes it highly unlikely that C2–C26 would compete with C3–C26. Therefore, a bond formation of C3–C26 is highly favoured over that of C2–C26.
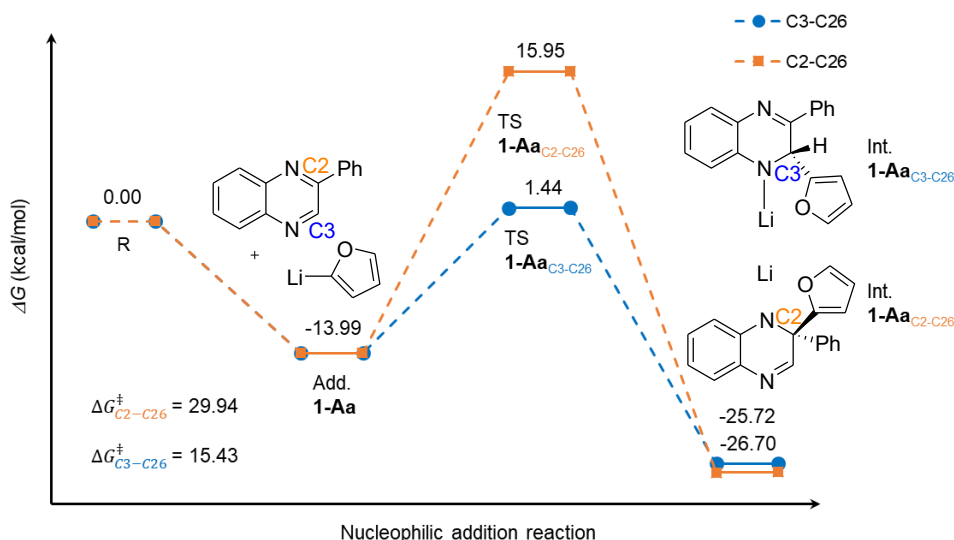
Figure 3.8: Nucleophilic addition reaction at C2 versus C3 of 2-phenyl quinoxaline using Add. Int. **1-Aa** as starting material. Both reactions were modelled in implicit THF solvent at –78 °C

The addition of C26 at the C2 position forms a σ^C-complex intermediate, while the addition at C3 forms a σ^H-complex intermediate (Int.). Int. **1-Aa**$_{C2–C26}$ at –26.70 kcal/mol free energy is –0.98 kcal/mol lower in energy than Int. **1-Aa**$_{C3–C26}$. The energy difference is minimal and thus both adducts are similarly stable.

Regarding **Table 3.2** and **Table 3.1**, if both reactions (C2 and C3 addition) are modelled using the same adduct, the reaction involving the addition of C26 at C3 is ±10 kcal/mol more exothermic than the addition at the C2 position.

Table 3.2: Stationary points involved in nucleophilic addition reaction of 2-phenyl-quinoxaline (**A**) with lithiofuran (**a**) at the C2 position. Changes in energies are measured relative to separate reactants

Systems	E	E_{ZPVE}	H	G
	Energy term in a.u.			
Reactants				
2-phenylquinoxaline (**A**)	–649.21024	–649.00667	–649.00095	–649.02883
Lithiofuran (**a**)	–237.04795	–236.97100	–236.96738	–236.98881
Nucleophilic Addition Reaction				
Add. **1-Aa**$_{C2–C26}$	–886.27440	–886.01131	–886.00188	–886.03993
TS **1-Aa**$_{C2–C26}$	–886.22901	–885.96700	–885.95867	–885.99222
Int. **1-Aa**$_{C2–C26}$	–886.27794	–886.01425	–885.99612	–886.06019
	Change in energy term (kcal/mol)			
	ΔE	ΔE_{ZPVE}	ΔH	ΔG
Add. **1-Aa**$_{C2–C26}$	–10.17	–21.11	–21.05	–13.99
TS **1-Aa**$_{C2–C26}$	18.31	6.70	6.07	15.95
Int. **1-Aa**$_{C2–C26}$	–12.40	–22.95	–21.44	–26.70

3.2.2 Hydrolysis reaction

Hydrolysis (**2**) is the second step investigated towards the full reaction mechanism of oxidative nucleophilic substitution of hydrogen (ONSH).[2] H_2O was therefore introduced to the Int. **1-R$_X$a** (**R$_X$ = A, B**) system to further model the substitution of the α-H3. **Figure 3.9** shows global minimum structures (GMSs) obtained from the optimisations of Int. **1-R$_X$a** in the presence of an H_2O molecule. The H_2O molecule placed in various positions at a close distance (~3 Å) to Int. **1-R$_X$a** led to several local minima – see **Table 0.2** (Appendix **A**).

The H_2O molecule interacts non-covalently with the atoms of Int. **1-R$_X$a**, some stronger than others, especially H35···O25, H36O34···Li27, O25···H3, and H35···N4 (**Figure 3.9**). All these interactions contribute strongly to the stability of the GMSs and thus provide evidence of the viability of the hydrolysis reaction.
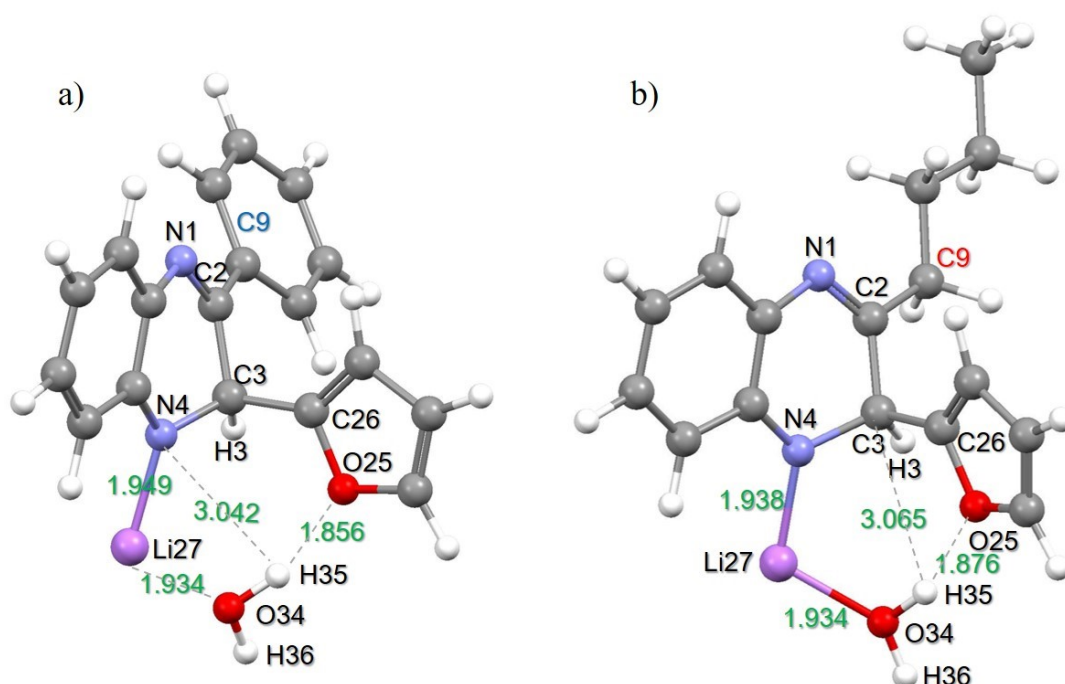
Figure 3.9: Adducts a) **2-Aa** and b) **2-Ba** formed from the geometrical optimisation of Int. **1-R$_X$a** with an H_2O molecule

A N4–H35 covalent bond coordinate scan was conducted using Add. **2-R$_X$a** (see **Figure 3.9**). Atoms N4 and H35 were brought closer together in steps of –0.01 Å to form an N4–H35 covalent bond. From the relative energy plot shown in **Figure 3.10**, the formation of the N4–H35 bond essentially results in a spontaneous hydrolysis reaction. Both **2-R$_X$a** reactions were modelled at –78 °C (195.15 K) and follow the same reaction mechanism.
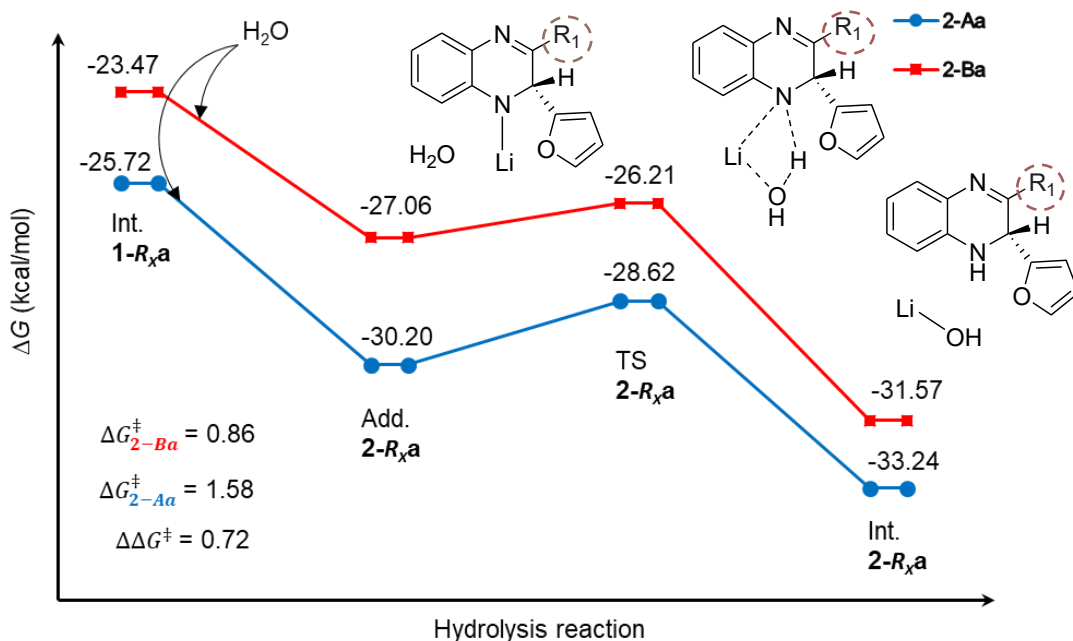
Figure 3.10: Gibbs free energy profile of the hydrolysis reaction from Add. **2-R$_x$a** (**R$_x$** = 2-butylquinoxaline (**B**), 2-phenylquinoxaline (**A**), R$_1$ = phenyl-, butyl-)

The presence of the water molecule stabilises Int. **1-Aa** and **1-Ba** by –4.48 kcal/mol and -3.59 kcal/mol to form adducts – Add. **2-Aa** and **2-Ba** respectively (as shown in **Figure 3.10**). Adducts **2-Aa** and **2-Ba** are formed at $\Delta G_{2\text{-}Aa}$ = –30.20 kcal/mol and $\Delta G_{2\text{-}Ba}$ = –27.06 kcal/mol relative to the separate reactants (R), **R$_x$** and **a**, corresponding to an energy gap of -3.14 kcal/mol in favour of Add. **2-Aa**

Adducts **2-Aa** and **2-Ba** reach TSs of –28.62 kcal/mol and –26.21 kcal/mol respectively. Hence the energy barriers for reactions involving **2-Aa** and **2-Ba** are very small, namely 1.58 and 0.86 kcal/mol respectively. The energy difference of 0.72 kcal/mol is insignificant, indicating that both hydrolysis reactions are comparably reactive.

The TSs obtained (**Figure 3.11**) were submitted for intrinsic reaction coordinate (IRC) calculations. IRC data show the steepest pathway down the reaction profile from the TS to the energy minima on either side of the TS, representing the intermediate (Int.) and Adduct (Add.). Unexpectedly, the IRC profile seen in **Figure 3.12** shows the beautiful formation of the LMS (2.56 kcal/mol above the GMS) prior to the formation of the TS.
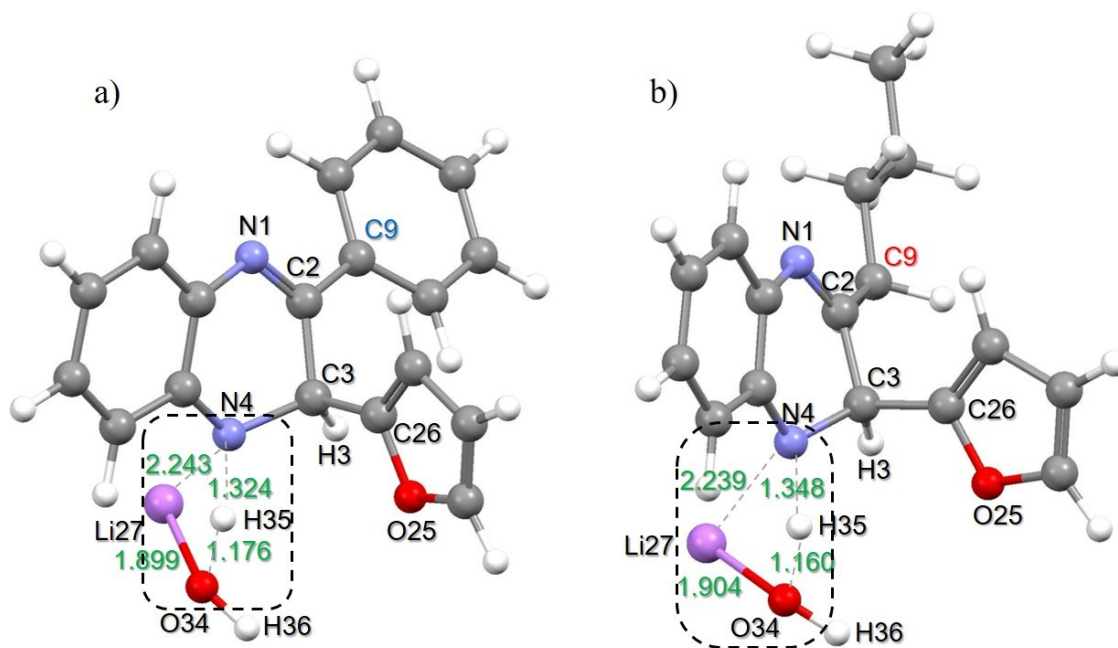
Figure 3.11: Transition states of the hydrolysis reaction of a) Int. **1-Aa** and b) Int. **1-Aa**. The grey dashed lines show the bond cleavage of H35–O34 and N4–Li27, and the bond formation of N4–H35 and O34–Li27
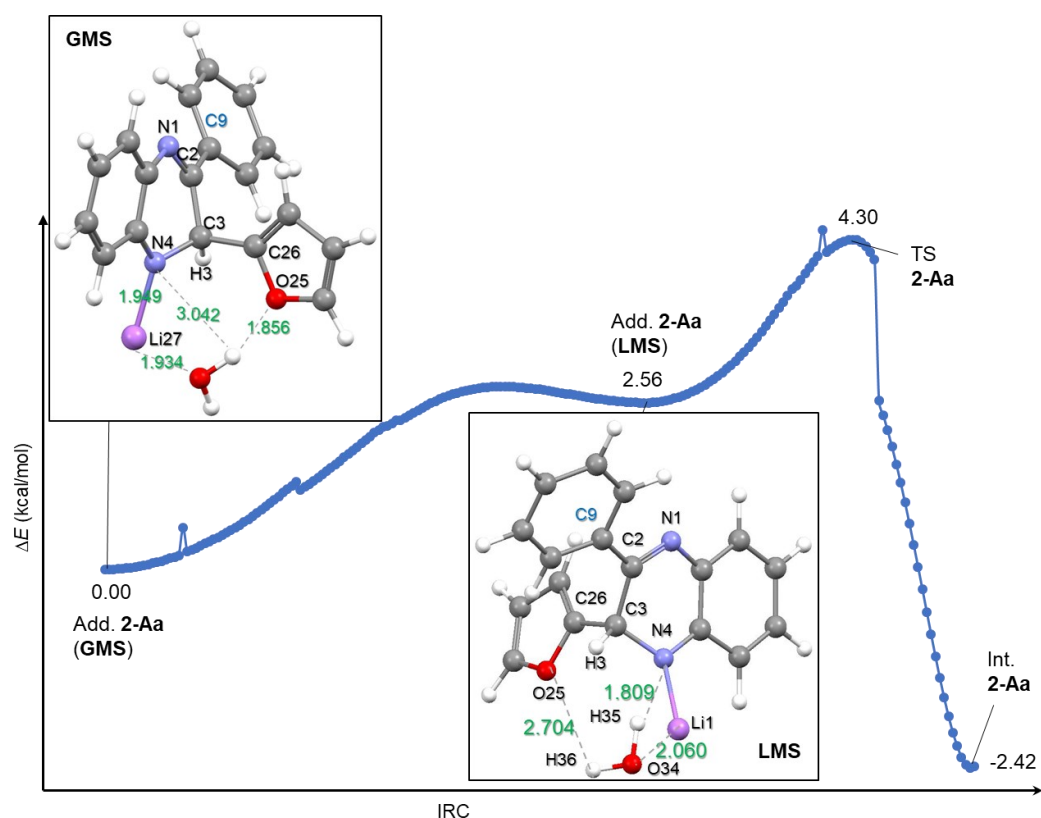
Figure 3.12: IRC profile of the hydrolysis reaction of Add. **1-Aa** that forms the LMS prior to the formation of a TS. Energies are measured relative to the GMS

51

According to the IRC profile, the GMS (Add. **1-Aa**) rearranges and destabilises to form a local minimum structure (LMS) prior to the formation of the TS. The LMS has a similar geometry to the GMS, with atom H35 moving from O25 closer to N4, but the former is better pre-organised for the subsequent step. The rearrangement allows a smooth reaction profile to form a TS of $\Delta E^{\ddagger} = 4.30$ kcal/mol higher than the GMS, and a stable Int. that is –2.42 kcal/mol lower in energy than the GMS. These energies are negligible, hence the spontaneous formation of the intermediates.

The TSs **2-Aa** and **2-Ba** were further submitted for TS geometry optimisation. The calculations produced a single negative imaginary frequency for each structure of the reaction that depicts the attack of N4 to H35 and the bond breaking of HO···H35.

In the absence of a "tight" geometry optimisation, the vibrational frequency is between N4, H35, O34 and Li27 atoms. The atomic vibrations represent the TSs **2-Aa** and **2-Ba** with frequencies of –950.51 cm^{-1} and –1038.29 cm^{-1} respectively. The difference in vibrational frequency between the TSs is –87.78 cm^{-1} and suggests that TS **2-Ba** represents a region on the potential energy surface (PES) which is more curved than that of TS **2-Aa**.
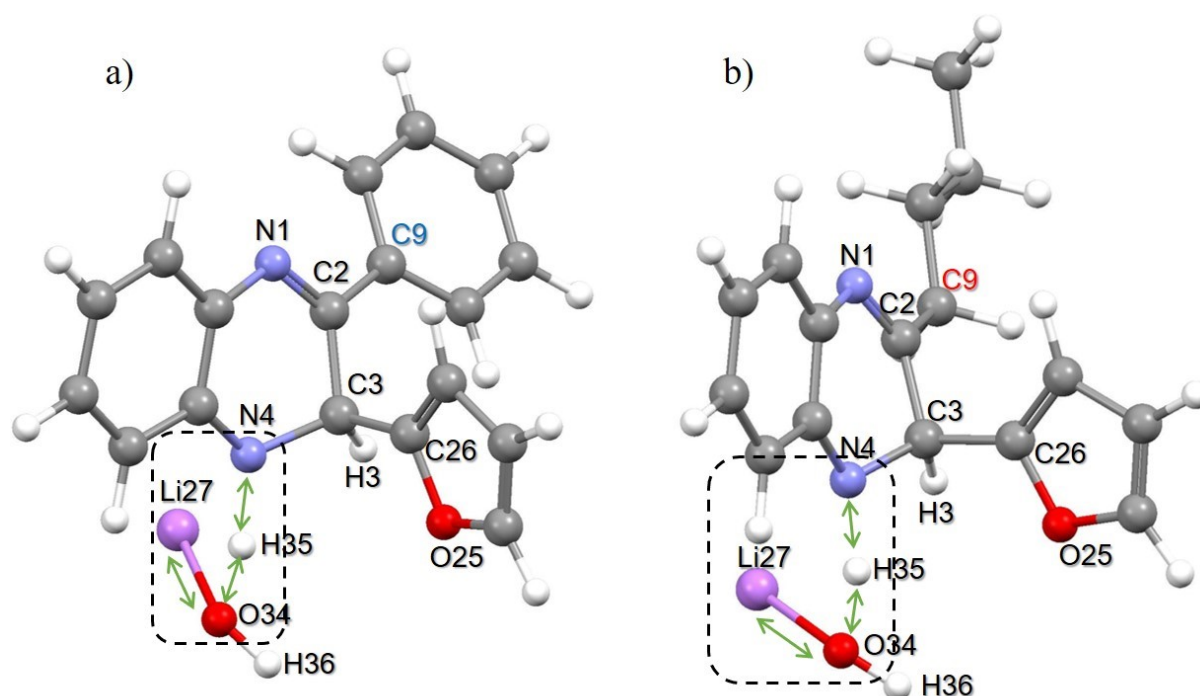
Figure 3.13: Transition states (a) **2-Aa** and (b) **2-Ba**, showing the proton transfer from the breaking of the H$_2$O molecule to Int. **1-R$_X$a**. The vectors show the vibrational frequency of the reaction and the dashed line enclosing all atoms involved in the formation of the TSs

During hydrolysis, the water molecule is broken (H36O34···H35) to allow proton (H35) to transfer to the N4. The transfer occurs prior to the attack of the remaining hydroxide ion ($^-$O34H36) with the leaving group Li27. The anionic $^-$O34H36 molecule acts as a hydroxo ligand (a monodentate ligand), and thus it is susceptible to coordinate with Li27$^+$ (an alkali metal ion) to form a weak coordination complex, Li27–O34H36, as a by-product.[8,9] The exchange of Li27 to $^-$O34H36 encourages the exchange of H35 from the H$_2$O molecule to N4. The by-product Li27–O34H36 is formed concomitantly with the bond formation of N4–H35. A coordinate scan of each reaction is attached on the CD.

The overall hydrolysis reaction involves the formation of an amine at N4 (Int. **2-R$_x$a**), see **Figure 3.14**. The intermediates **2-R$_x$a** have an increased electron donor strength at N4 as the electron-donating amine (sp^3-hybridised) C3N4–H35 was changed from an electron-accepting imine (sp^2-hybridised).
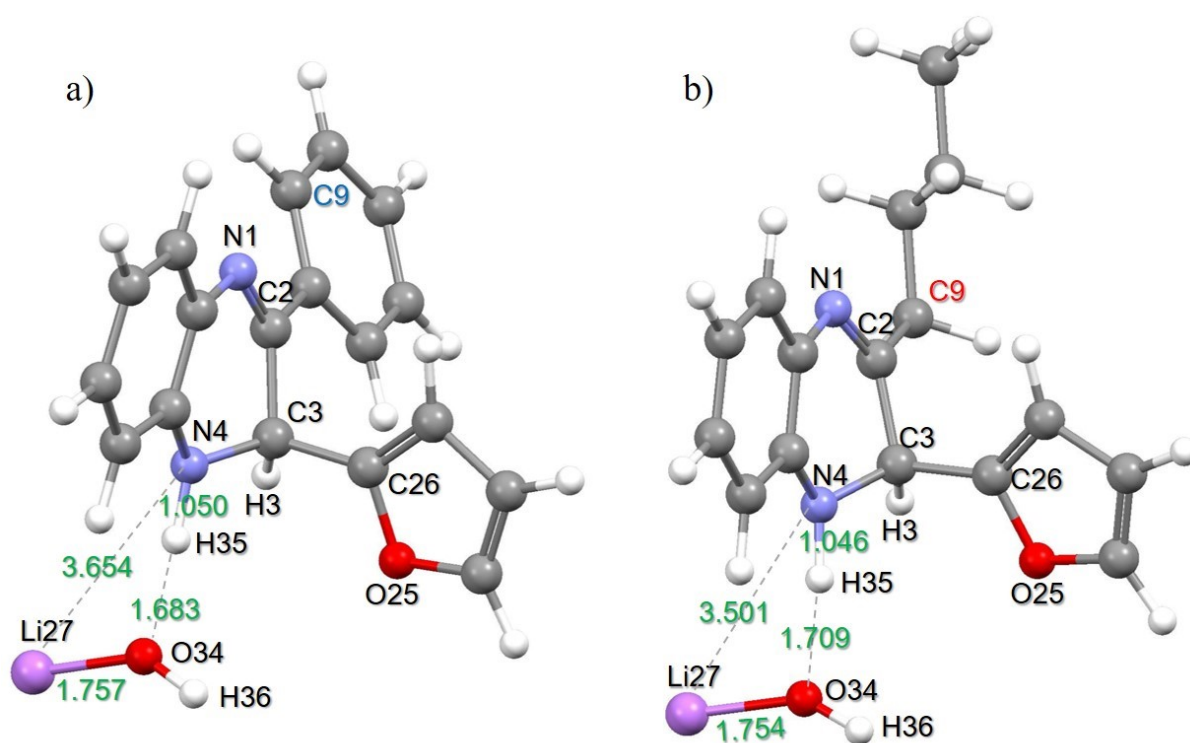
Figure 3.14: Hydro-quinoxaline intermediates a) **2-Aa** and b) **2-Ba** that form from amination and result in the formation of Li27–O34H36 as a by-product

Optimisation of both intermediates shown in **Figure 3.14** in the absence of the by-product (Li27–O34H36) raised the free energy to ±0.32 kcal/mol. The energy difference is insignificant

and therefore the presence of the by-product is minor in terms of the energy and stability of the intermediates.

The enthalpy energy profile shown in **Figure 3.15** shows that the intermediate **2-Aa** is -1.67 kcal/mol lower in energy than Int. **2-Ba**. Reactions involving **2-Aa** and **2-Ba** are $\Delta H_{\text{1-Aa}} = -2.58$ kcal/mol and $\Delta H_{\text{1-Ba}} = -1.14$ kcal/mol exothermic. However, reactions involving **2-Aa** are -1.44 kcal/mol more exothermic than reaction **2-Ba**. These energy differences are insignificant and thus both reactions are predicted to be equally exothermic.
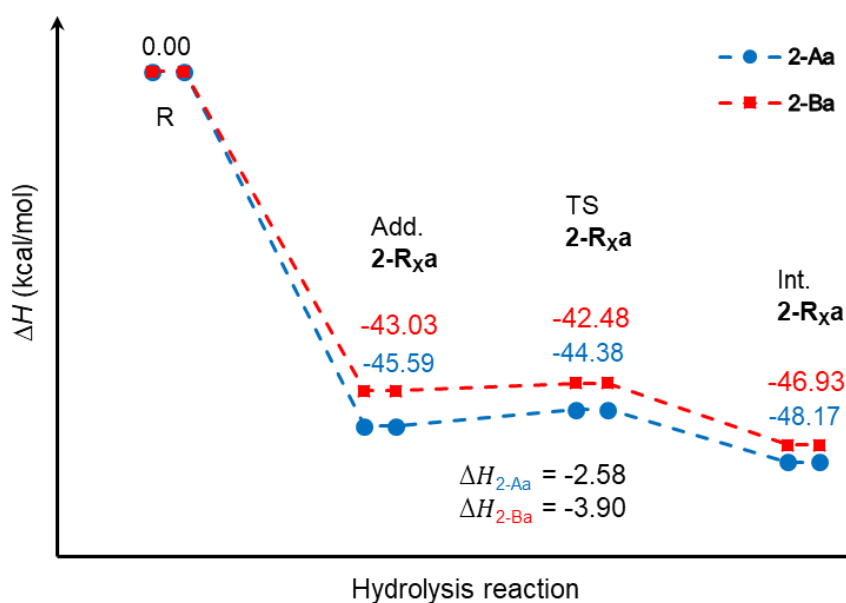
Figure 3.15: Enthalpy energy profile of the hydrolysis reaction from Add. **2-R$_x$a**. **R$_x$** = 2-butylquinoxaline (**B**), 2-phenylquinoxaline (**A**), R$_1$ = phenyl-, butyl-, and **2** = hydrolysis reaction step

Modelling of the nucleophilic addition (**1**) and hydrolysis (**2**) reaction steps of the ONSH reaction mechanism shows that all structures of the **Aa** reaction are lower in energy than those of **Ba** (see **Table 3.2** and **Table 3.3**). These energy differences are negligible and thus the presence of either a phenyl or *n*-butyl group at position C2 of quinoxaline has no significant effect on either reaction – which is contradictory to yields reported in the literature.[1]

54

Table 3.3: Stationary points involved in hydrolysis reaction of Int. **1-R$_X$a** with H$_2$O. Change in energies are measured relative to separate reactants (Int. **1-R$_X$a** + H$_2$O). **R$_X$ = A, B**

Systems	E	E_{ZPVE}	H	G
	Energy term in a.u.			
Reactants				
Int. **1-Aa**	−886.29806	−886.03272	−886.02426	−886.05862
H$_2$O	−76.46503	−76.44382	−76.44135	−76.45433
Int. **1-Ba**	−812.48470	−812.18788	−812.17858	−812.21458
Hydrolysis Reaction				
Add. **2-Aa**	−962.78243	−962.49233	−962.48233	−962.52008
Add. **2-Ba**	−888.96892	−888.64670	−888.63613	−888.67464
TS **2-Aa**	−962.77558	−962.49009	−962.48041	−962.51758
TS **2-Ba**	−888.96309	−888.64552	−888.63526	−888.67329
Int. **2-Aa**	−962.78655	−962.49670	−962.48645	−962.52493
Int. **2-Ba**	−888.97504	−888.65319	−888.64235	−888.68181
	Change in energy term (kcal/mol)			
	ΔE	ΔE_{ZPVE}	ΔH	ΔG
Add. **2-Aa**	−37.15	−44.45	−45.59	−30.20
Add. **2-Ba**	−34.46	−41.78	−43.03	−27.06
TS **2-Aa**	−32.85	−43.05	−44.38	−28.62
TS **2-Ba**	−30.81	−41.04	−42.48	−26.21
Int. **2-Aa**	−39.74	−47.19	−48.17	−33.24
Int. **2-Ba**	−38.30	−45.86	−46.93	−31.57

3.2.3 Oxidation reaction

The concomitant oxidation reaction reported by Chupakin[2] proposed that the introduction of an oxidising agent to an intermediate of hydrolysis affords an oxidative nucleophilic substitution of hydrogen (ONSH) product. As discussed earlier, Nxumalo and Ndlovu[1] used atmospheric oxygen as an oxidising agent to produce an ONSH product, thus we modelled the oxidation reaction and explicitly introduced O$_2$ as our external reagent to Int. **2-R$_X$a**. The reaction was modelled at 25 °C (298.15 K).

A spontaneous reaction was noted when O$_2$ was introduced to Int. **2-R$_X$a** during the geometrical optimisation of the system. This resulted in re-arrangement of Int. **2-R$_X$a** through a process of de-amination to form the desired products, Prod. **3-R$_X$a** (**Figure 3.16**). The de-amination converts the electron-donating amine (C3N4–H35, sp^3-hybridised) back to an electron-accepting imine (N4=C3, sp^2-hybridised).

The spontaneity resulted in several transformations forming the products, and the following were noted: C3–H3, N4–H35 and Li27O34–H36 bond cleavage, substitution of α-hydrogen (H3), formation of H_2O_2 by-product, and the restoration of the quinoxaline's aromaticity.
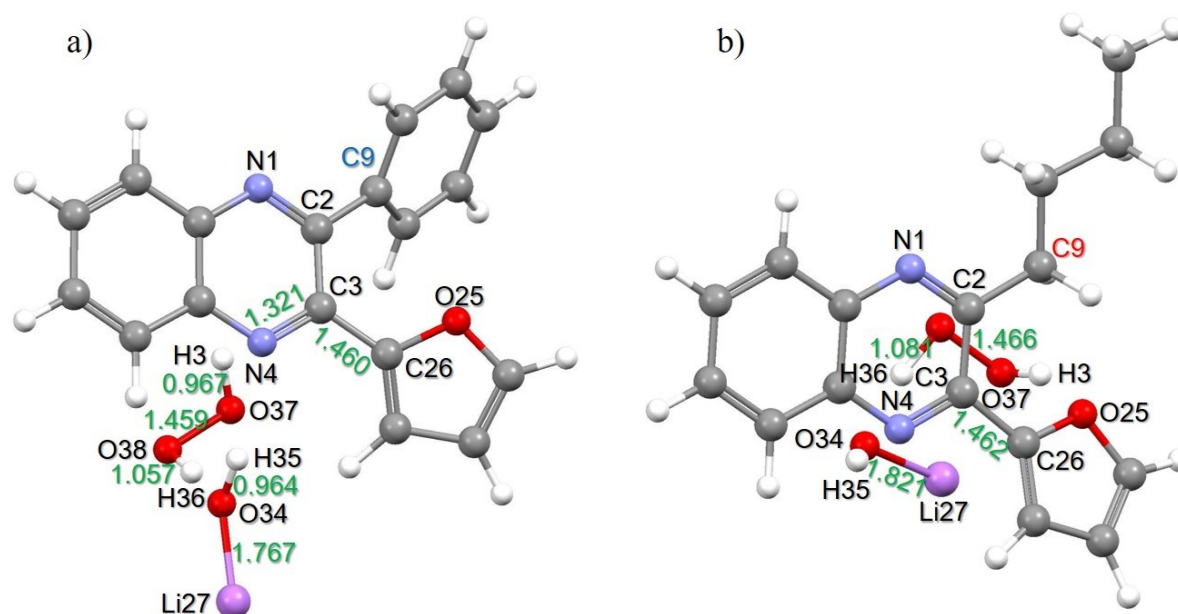
Figure 3.16: Structural minima of products a) Prod. **3-Aa** and b) Prod. **3-Ba** that result from the spontaneous oxidation reaction through geometry optimisation of Int. **2-R_xa** + O_2

The aim was to investigate the displacement of the strongly bonded α-H3. It is through geometry optimisation of Int. **3-Rxa** + O_2 that the covalent bond between α-H3 and C3 started to cleave during the formation of Prod. **3-Rxa**.

The cleavage of C3–H3, N4–H35 and Li27O34–H36 bonds occurred simultaneously. Due to this, the simultaneous transfer of hydrogens was viable; α-H3 is transferred to O37, H35 to O34 and H36 to O38. These changes are associated with the occurrence of a side-reaction that forms H_2O_2 (O37H3O38H36) and a LiOH complex (Li27O34H35) as by-products of ONSH. With LiOH taking part in the transfer of hydrogens, it acts as a precursor in the formation of the final product.

The newly formed peroxide (H_2O_2) is hypothesised to later break down into water and oxygen gas during experimental work-up. The equation is shown in **Scheme 3.2**.[8]

$$2H_2O_2 \rightarrow 2H_2O\ (l) + O_2\ (g)$$
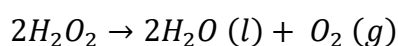
Scheme 3.2: Decomposition of hydrogen peroxide into water and oxygen

The minima products formed (Prod. **3-R$_X$a**) for both reactions involving **Aa** and **Ba** are highly stable structures with free energy values for Prod. **3-Aa** and Prod. **3-Ba** of –77.80 kcal/mol and –78.83 kcal/mol respectively (see **Table 3.4**).

Table 3.4: Minima involved in oxidation reaction of Int. **2-R$_X$a** with O$_2$ to form ONSH products, Prod. **2-R$_X$a**. Change in energies is measured relative to separate reactants (Int. **2-R$_X$a** + O$_2$). **R$_X$** = A, B

Systems	E	E_{ZPVE}	H	G
	Energy term in a.u.			
Reactants				
Int. **2-Aa**	–962.78655	–962.49670	–962.47550	–962.54755
O$_2$	–150.30980	–150.30610	–150.30279	–150.32502
Int. **2-Ba**	–888.97504	–888.65319	–888.63108	–888.70503
Oxidation Reaction				
Prod. **3-Aa**	–1113.21149	–1112.91650	–1112.89219	–1112.97412
Prod. **3-Ba**	–1039.40966	–1039.08209	–1039.05775	–1039.13623
	Change in energy term (kcal/mol)			
	ΔE	ΔE_{ZPVE}	ΔH	ΔG
Prod. **3-Aa**	–111.98	–106.45	–107.24	–77.80
Prod. **3-Ba**	–116.63	–110.82	–112.24	–78.83

Looking at **Figure 3.17** b), the enthalpy energy difference between Prod. **3-R$_X$a** and Add. **1-R$_X$a** is ΔH_{Aa} = –86.19 kcal/mol and ΔH_{Ba} = –91.56 kcal/mol. These energy differences show that the ONSH reaction of **a** with **A** is –5.37 kcal/mol less exothermic than with **B**. However, the energy difference is insignificant. Thus, both ONSH reactions are comparably exothermic.

Due to the two processes, namely (i) hydrolysis, having a minor activation barrier and (ii) oxidation reaction having no activation barrier, the nucleophilic addition reaction is the rate-determining step (RDS). A coordination scan of the three reaction steps that make up the ONSH mechanism is attached on the CD. The Gibbs free energy difference between Prod. **3-R$_X$a** and TS **1-R$_X$a** is ΔG_{Aa} = –79.24 kcal/mol and ΔG_{Ba} = –80.81 kcal/mol (**Figure 3.17**, a)). Due to the high energies, it is impossible for both Prod. **3-Aa** and **3-Ba** to dissociate and overcome the reverse energy to form Add. **1-Aa** and **1-Ba** respectively.
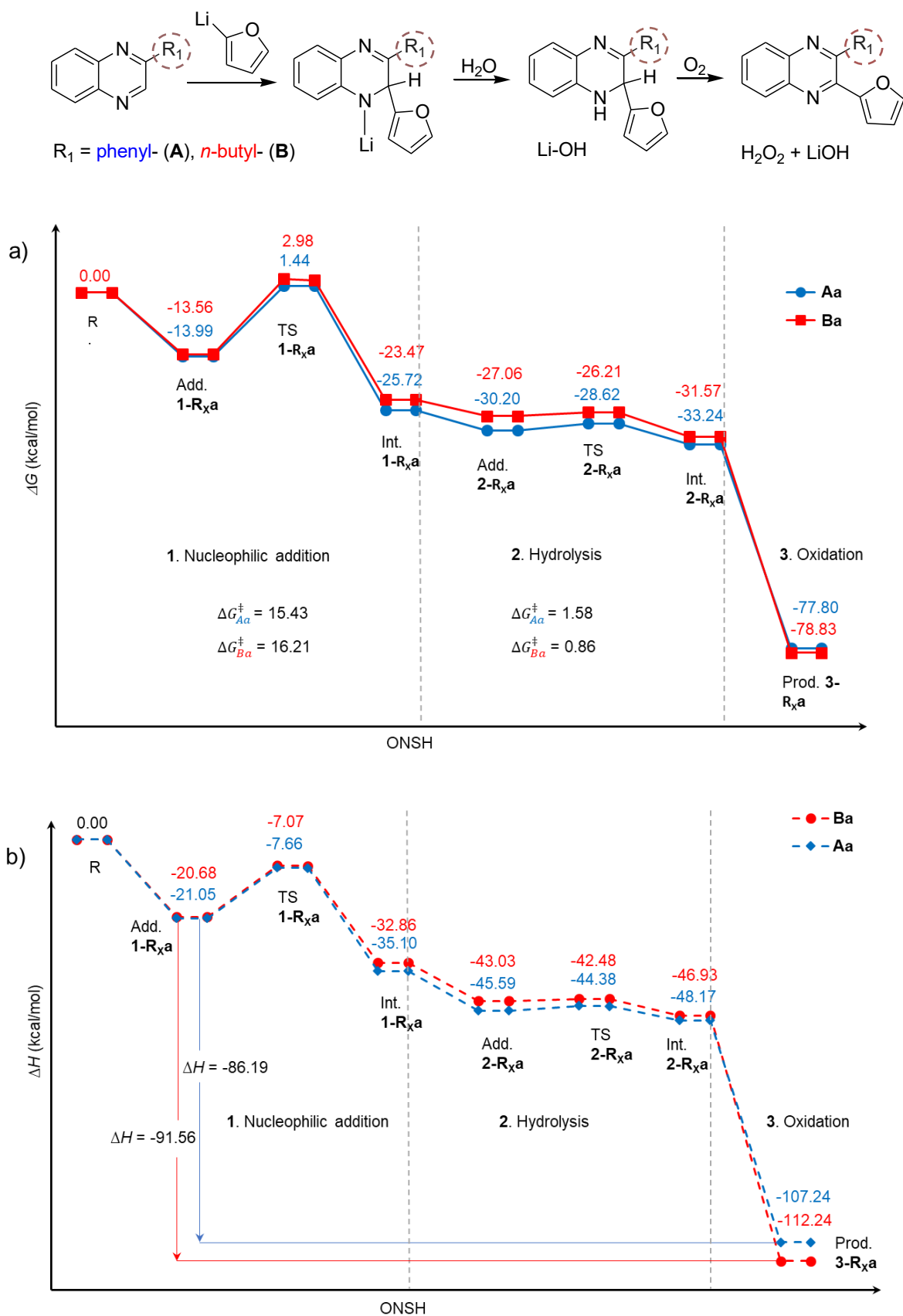
Figure 3.17: The free and enthalpy energy profile of oxidative nucleophilic substitution of hydrogen (ONSH) for lithiofuran (**a**) with 2-phenyl quinoxaline (A) and 2-butyl quinoxaline (**B**). Energies are measured relative to the reactants (R), and the activation energies are measured relative to the adducts (Add.)

3.2.4 Effects of temperature on nucleophilic addition and hydrolysis reaction

The entire ONSH reaction mechanism has not been well studied with regard to the effects of temperature on the hydrolysis or the preferred temperature for the whole reaction. A single-point frequency calculation for each stationary point of **1-R$_X$a** to **2-R$_X$a** was performed at 25 °C (298.15 K) to study the effects of temperature. The calculated energy for each complex is relative to the sum of the reactants and the activation energies are relative to the adducts of that particular reaction step.

It is known that most organolithium compounds and Grignard reagents are not reactive at high temperatures.[13] They are broken down in the presence of water due to the sensitivity of the highly polar metal-carbon bonds contained within them. Even so, it is important to study the reactions at these temperatures as the nucleophile is only used in the first step of ONSH. The study therefore focuses on the nucleophilic addition and hydrolysis reaction.

3.2.4.1 Effects of temperature on the nucleophilic addition reaction

When looking at **Figure 3.18**, it can be seen that the reactant complexes (Add. **1-R$_X$a**) at 298.15 K of each reaction, Add. **1-Aa**$_{298.15}$ and Add. **1-Ba**$_{298.15}$, are destabilised by 0.98 kcal/mol and 1.42 kcal/mol respectively relative to the reactants (R). These energy differences are negligible. The difference in energy between Add. **1-Aa**$_{195.15}$ and Add. **1-Aa**$_{298.15}$ is -14.97 kcal/mol, and the energy difference between Add. **1-Ba**$_{195.15}$ and Add. **1-Ba**$_{298.15}$ is -14.96 kcal/mol. Thus, by lowering the temperature of the reaction, a ~-15.00 kcal/mol more stable adduct is formed for both reactions.

Adducts **1-R$_X$a**$_{298.15}$ form TS **1-Aa**$_{298.15}$ and **1-Ba**$_{298.15}$ of 17.54 kcal/mol and 19.06 kcal/mol respectively (**Figure 3.18**). Transition states **1-Aa**$_{298.15}$ and **1-Ba**$_{298.15}$ are 16.10 kcal/mol and 16.41 kcal/mol higher in energy than TSs **1-Aa**$_{195.15}$ and **1-Ba**$_{195.15}$ respectively. However, the difference in activation energies between the same reactions involving **1-Aa** at different temperatures is 1.13 kcal/mol and 1.36 kcal/mol for reactions involving **1-Ba**. These are minor energies and thus both reactions are similarly reactive.

59
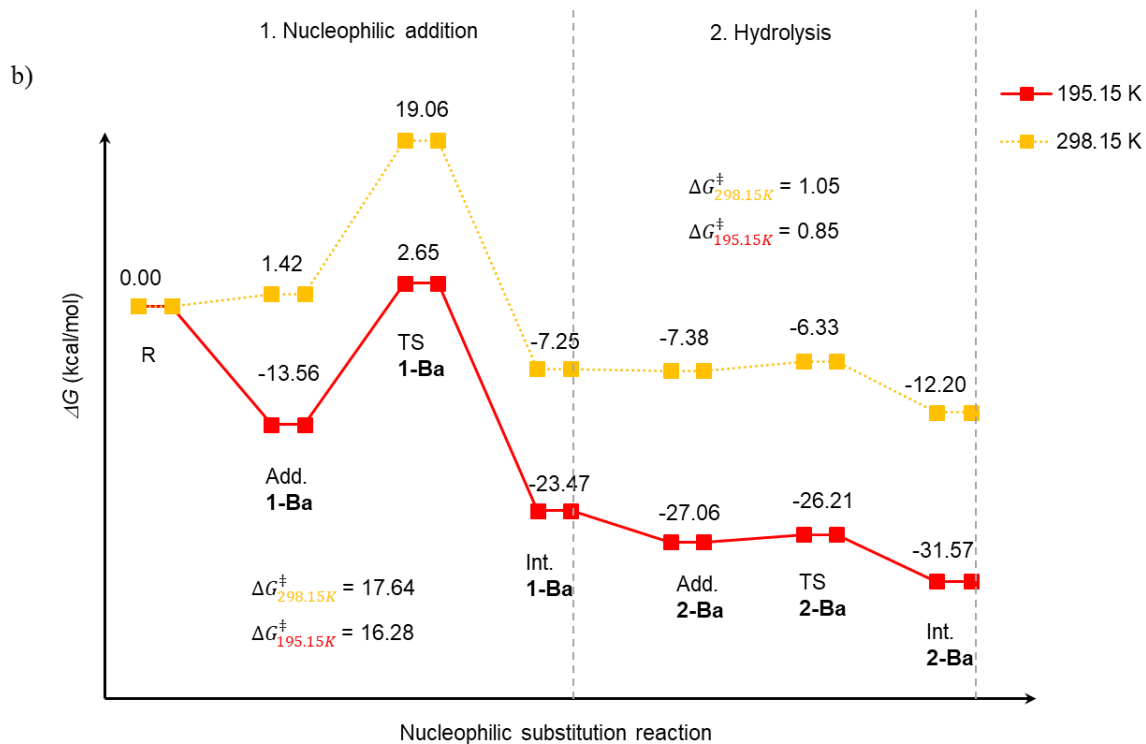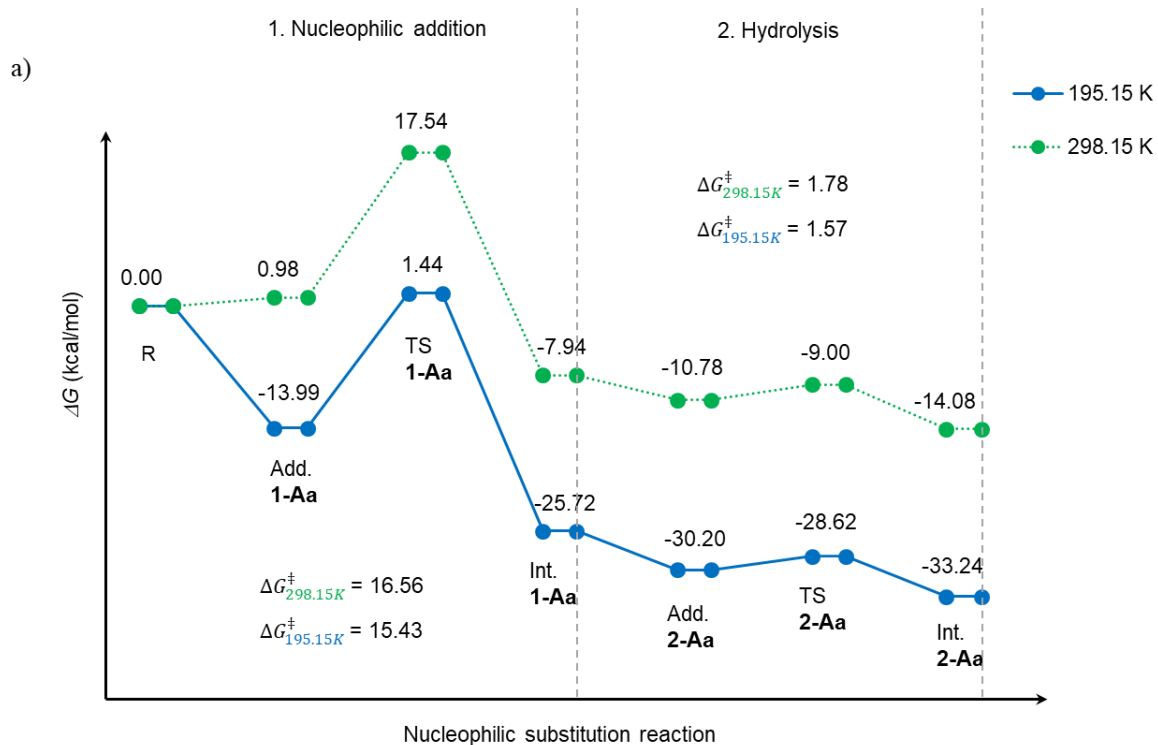
Figure 3.18: Change in free energy profiles showing the effects of temperature increase on the nucleophilic addition and hydrolysis reactions of lithiofuran (**a**) with a) **A** and b) **B**. The energies are measured relative to the reactants (R), and the activation energies are measured relative to the adducts (Add. **1-R$_X$a**)

All stationary points modelled at 298.15 K have higher energy than those modelled at 195.15 K. The stationary points of reaction **1-Aa** are of lower energy than those of reaction **1-Ba** at both temperatures (**Figure 3.18**).

Although the nucleophilic addition reaction at high temperatures consists of unstable stationary points compared to those at low temperatures, both reactions can smoothly form the intermediate **1-R$_X$a**. However, reaction step **1** at lower temperature is the preferred method due to the breaking down of organolithium compounds at high temperatures. Once the organolithium compound has reacted, the reaction must be allowed to be at equilibrium with the intermediate **1-Rxa**$_{195.15}$; the temperature can then be increased to 298.15 K, subsequently allowing a hydrolysis reaction to occur.

3.2.4.2 Effects of temperature on hydrolysis reaction

As per the experimental reaction procedure[1], water was not explicitly introduced into the reaction system but rather the system was left to warm up to room temperature from –78 °C, and later exposed to atmospheric oxygen. Furthermore, Chupakin *et al.*[2] reported that the increase in temperature from 0 to 100 °C converted σ^H-adduct to give the final product 2-phenylpyridine. The conversion is equated to hydrolysis to give the second intermediate of ONSH, Int **2-R$_X$a** (**Figure 3.14**).[2]

At low temperatures of 195.15 K, water molecules would freeze, thus not allowing the hydrolysis reaction to occur. At high temperatures of 298.15 K, Add. **2-Rxa**$_{298.15}$ can easily revert to Int. **1-Rxa**$_{298.15}$, but it is not as easy for Int. **1-Rxa**$_{298.15}$ to revert to Add. **1-Rxa**$_{298.15}$ due to the high energy between TS and Int. **1-Rxa**$_{298.15}$.

Regarding the effects of temperature, the change to high temperatures destabilised the stationary points of the hydrolysis (**2**) more than the stationary points of the nucleophilic addition (**1**). However, the hydrolysis reaction at high temperatures remains spontaneous. Changing the temperature resulted in a minor 0.2 kcal/mol increase in free activation energy for both reactions (**2-R$_X$a**). The stationary points of hydrolysis, in both reactions involving **2-Aa** and **2-Ba**, are ±19 kcal/mol higher in free energy at 298.15 K than at 195.15 K.

61

3.2.5 Presence of explicit THF solvent molecules

Geometrical optimisation of R_x (**A**, **B**) was simulated with a_e, where the a_e molecule is the nucleophile lithiofuran explicitly solvated with two THF molecules (**Figure 3.19**), a version of **a** (lithiofuran). The subscript **e** indicates two explicit THF solvent molecules. The explicitly solvated lithiofuran (a_e) was subjected to conformational search, and this resulted in eight conformers (see Appendix A, **Table 0.2**). The chosen structure was selected based on its stability and its non-steric geometry. The lowest energy structure was used throughout the computational modelling of the ONSH reaction mechanism to study the effects of solvation on the reaction mechanism(s).

A single THF solvent molecule was modelled with reactant **a** and then optimised to a minimum. Furthermore, the number of solvent molecules was increased one at a time until the THF molecules did not remain coordinated to the Li27 atom. Geometry optimisation of two THF molecules with the solute resulted in both molecules coordinating to the solute, as shown in **Figure 3.19**. Notably, an optimisation with three THF solvent molecules resulted in only two of the solvent molecules coordinating to **a**.
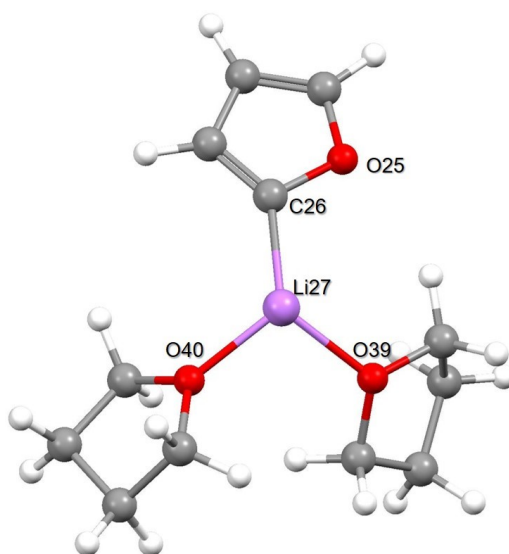
Figure 3.19: Global minimum structure of lithiofuran with two explicit THF solvent molecules coordinated to the Li27 atom

The reaction mechanism was modelled in implicit THF solvent in the presence of two explicit THF molecules. This was (i) to reduce computational cost and (ii) to make the modelling more experimentally relevant.

The **a$_e$** was optimised with **A** and **B** to form adducts, Add. **1-Aa$_e$** and Add. **1-Ba$_e$**, respectively. The inclusion of explicit THF solvent molecules resulted in lower-energy adducts for reactions involving **1-Aa$_e$** and **1-Ba$_e$**, and a change in the geometry of the THF solvent in the vicinity of the solute; this then resulted in the change in free energy.[9]

The adduct structures, Add. **1-R$_X$a$_e$** and Add. **1-R$_X$a**, show similar non-covalent atomic interactions for N4···Li27, C26···C3 and O25···H3. The two Add. **1-R$_X$a$_e$** structures in **Figure 3.20** were used to carry out a C3–C26 bond coordinate scan starting at d(C3, C26) ~3.656 Å, taking steps of –0.01 Å. The formation of the new C3–C26 bond results in a nucleophilic addition reaction (**1**).
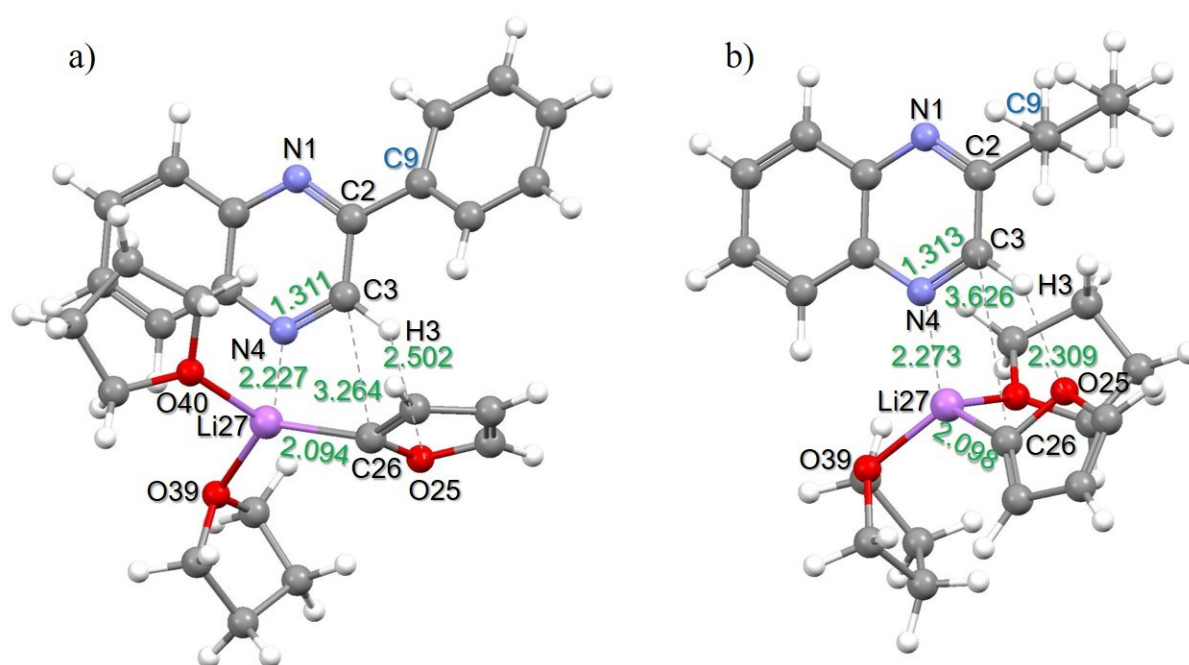
Figure 3.20: Adduct a) **1-Aa$_e$** and b) **1-Ba$_e$**. The subscript **e** represents the presence of two explicit THF solvent molecules covalently bonded to Li27 of the nucleophile (lithiofuran)

In reactions leading to **1-Aa$_e$** and **1-Ba$_e$**, the electronic activation energy of the rate-determining step (RDS) is decreased by 4.41 kcal/mol and 3.76 kcal/mol respectively. Similar to reactions involving **1-R$_X$a**, the reactions involving **1-Aa$_e$** and **1-Ba$_e$** have comparable electronic activation energies and thus both reactions have similar reactivity (**Figure 3.21**).

63
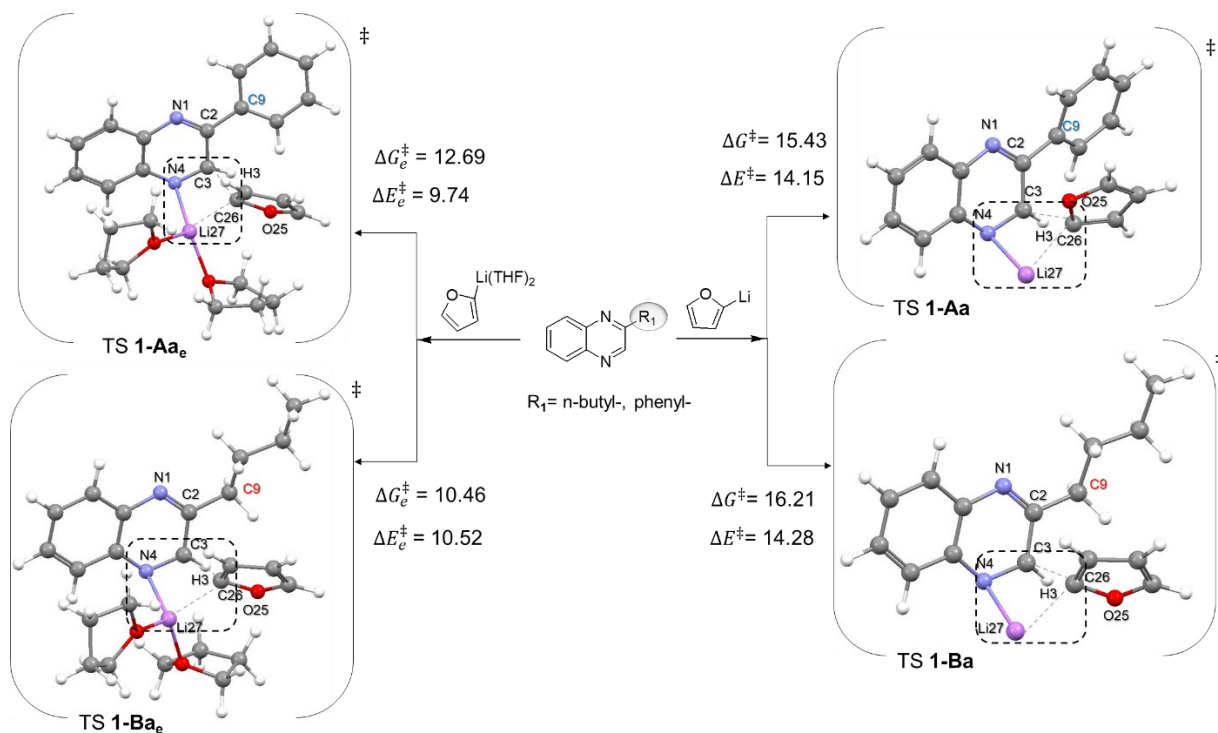
Figure 3.21: Activation energies for the rate-determining nucleophilic addition reaction of lithiofuran in implicit and explicit THF solvent with **A** (2-phenylquinoxaline) and (**B**) 2-*n*-butylquinoxaline. Stationary points involving two explicit THF molecules are indicated by subscript **e** – energies are given in kcal/mol

The formation of TS **1-R$_x$a$_e$** shows similar vibrational frequencies as TS **1-R$_x$a**. However, TSs **1-R$_x$a$_e$** have a single negative frequency of -251.74 cm^{-1} and -271.97 cm^{-1} for TS **1-Aa$_e$** and TS **1-Ba$_e$** respectively. The vibrational frequencies of TS **1-Aa$_e$** and **1-Ba$_e$** are -48.33 cm^{-1} and -19.68 cm^{-1} lower than those of TS **1-Aa** and **1-Ba** respectively. Thus, the PES is less curved in the presence of two explicit THF molecules than in their absence. The vibrational movements of these coordinates are included in the attached CD.

64
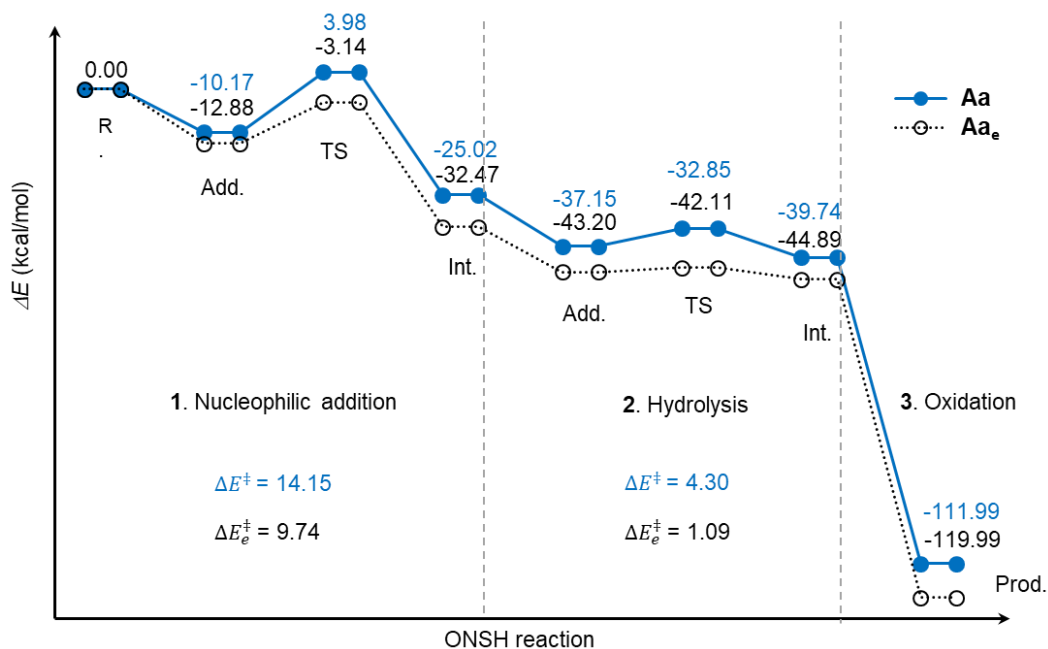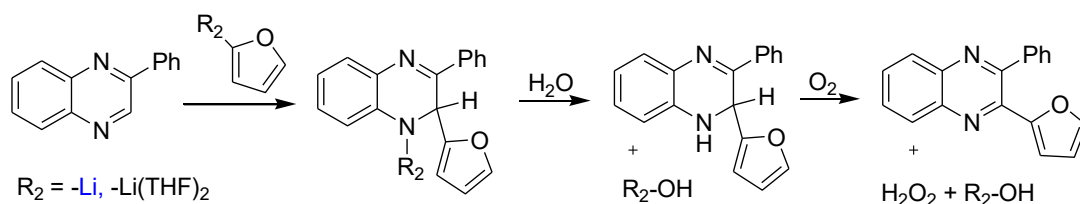
Figure 3.22: Electronic energy profile for the full reaction mechanism of oxidative nucleophilic substitution of hydrogen (ONSH) for 2-phenyl-quinoxaline (**A**) with **a** = lithiofuran versus **a_e** = lithiofuran-(THF)₂. Reaction energy profiles involving two explicit THF molecules are indicated by subscript **e**
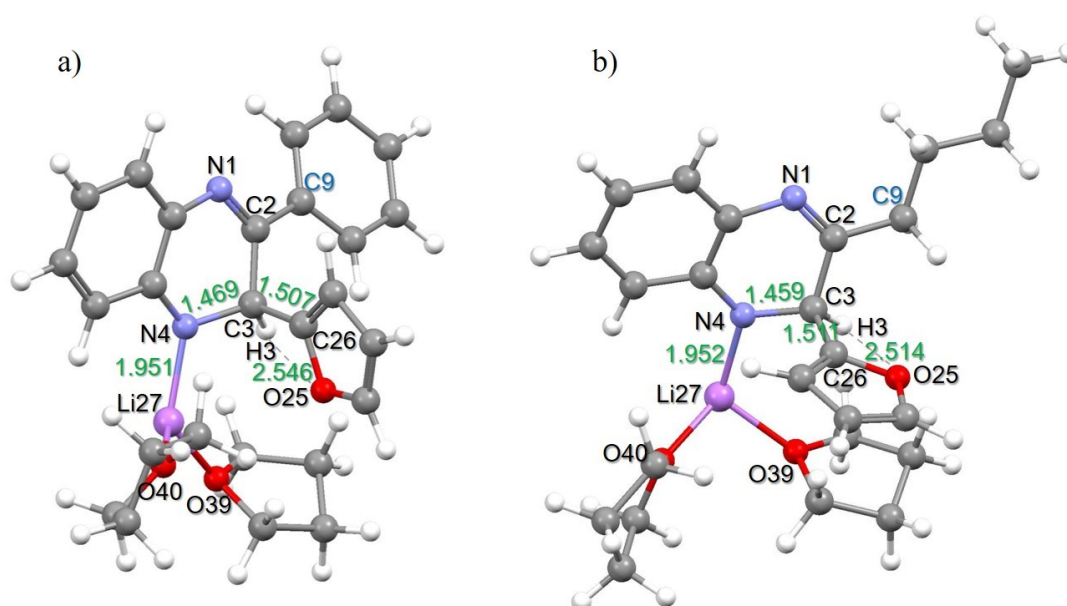
Figure 3.23: Intermediate **1-R_Xa_e** (σ^H-adduct) formed from the nucleophilic addition of lithiofuran-(THF)₂ (**a_e**) to a) 2-phenylquinoxaline (**A**) and b) 2-*n*-butylquinoxaline (**B**). **R_X** = **A**, **B**

65

The presence of the H_2O molecule subjects Int. **1-Rxa_e** to a hydrolysis mechanism similar to the hydrolysis reaction modelled in the absence of two explicit THF molecules. The H_2O molecule is broken down to form an amine at N4, concomitantly forming Li27–O34H36 as a by-product (see **Table 3.4**).

The change from N4–Li27 to N4–H35 occurs through the simultaneous bond cleavage of O34–H35 and N4–Li27, and the bond formation of N4–H35 and O34–Li27. These transformations represent a single negative frequency of -346.53 cm^{-1} and -1007.84 cm^{-1} for TS **1-Aa_e** and **1-Ba_e** respectively. These frequencies are -603.88 cm^{-1} and -30.45 cm^{-1} lower than the frequencies of TS **1-Aa** and **1-Ba** respectively. Thus, the PES of the hydrolysis reaction is flat rather than curvy in the presence of two explicit THF molecules; however, at TS **1-Ba_e** the PES is curvy rather than flat, contrary to TS **1-Ba_e**.

The electronic activation energy barrier in reactions involving **2-Aa_e** and **2-Ba_e** is 3.21 kcal/mol and -3.76 kcal/mol lower than in reactions involving **2-Aa** and **2-Ba**. However, these energy differences are negligible and thus both reactions involving **2-Aa_e** and **2-Ba_e** remain spontaneous to form Int. **2-Rxa_e**.

Table 3.5: Stationary points involved in the hydrolysis of Int. **1-Aa_e** and **1-Ba_e** to form an amine. Energies are measured in kcal/mol, relative to separate reactants (Int. **1-R_Xa_e** + H_2O). **R_X = A, B**

Add. **2-Aa_e** ($\Delta G = -18.38$, $\Delta E = -43.21$)	Add. **2-Ba_e**, ($\Delta G = -19.23$, $\Delta E = -39.95$)
TS **2-Aa_e** ($\Delta G = -17.85$, $\Delta E = -42.12$)	TS **2-Ba_e** ($\Delta G = -18.86$, $\Delta E = -37.68$)
Int. **2-Aa_e** ($\Delta G = -18.79$, $\Delta E = -44.91$)	Int. **2-Ba_e** $\Delta G = -22.48$, $\Delta E = -43.21$)
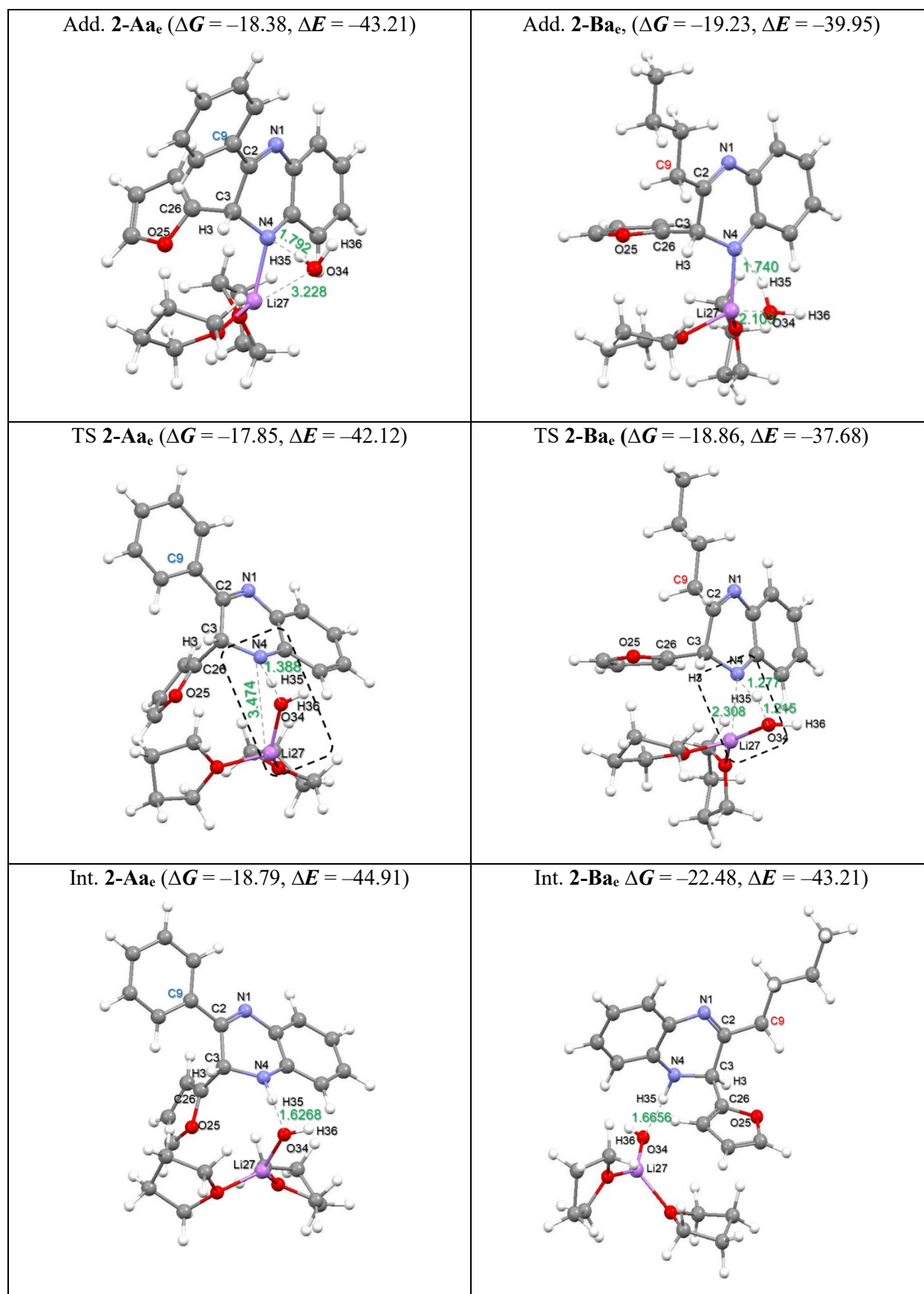
A spontaneous oxidation reaction results after the formation of the intermediates (Int. **2-Rxa_e**). In the presence of an oxidising reagent, O_2, the C3–H3 and N4–H35 bonds are cleaved to form H_2O_2; the highly stable ONSH products (Prod. **3-Rxa_e**) are concomitantly formed. Product **3-Aa_e** has an energy difference of –119.99 kcal/mol and –126.71 kcal/mol for Prod. **3-Ba_e** relative to the reactant (R). Product **3-Aa_e** is –6.72 kcal/mol lower in electronic energy than Prod. **3-Ba_e**. The energy difference is negligible, and since both reactions have a similar reactivity, both the products are unlikely to reverse to form adducts (Add.) (see **Figure 3.22** and **Figure 3.24**).
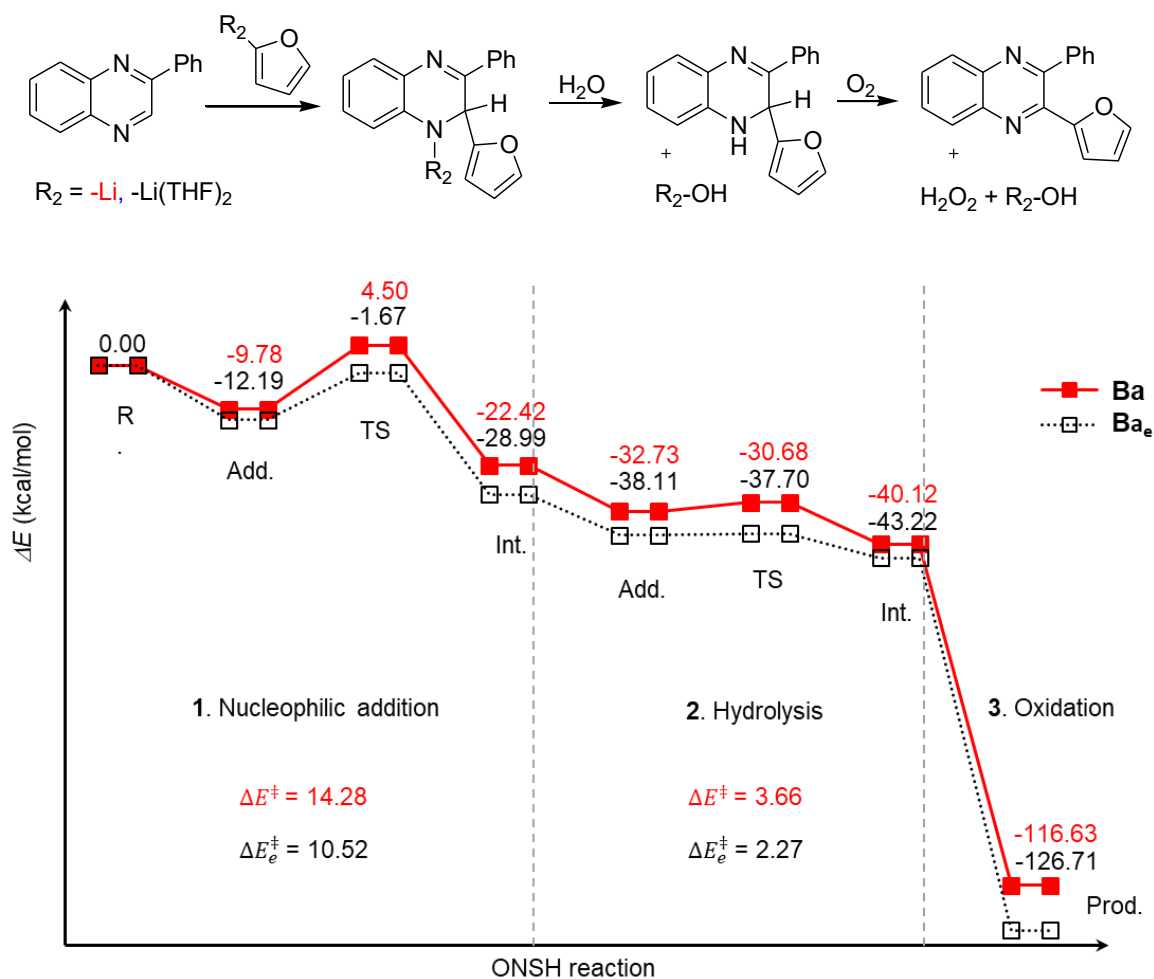
Figure 3.24: Electronic energy profile for the full reaction mechanism of oxidative nucleophilic substitution of hydrogen (ONSH) for 2-phenyl-quinoxaline (**A**) with **a** = lithiofuran versus **a_e** = lithiofuran-(THF)$_2$. Reaction profiles involving two explicit THF molecules are indicated by a subscript **e**
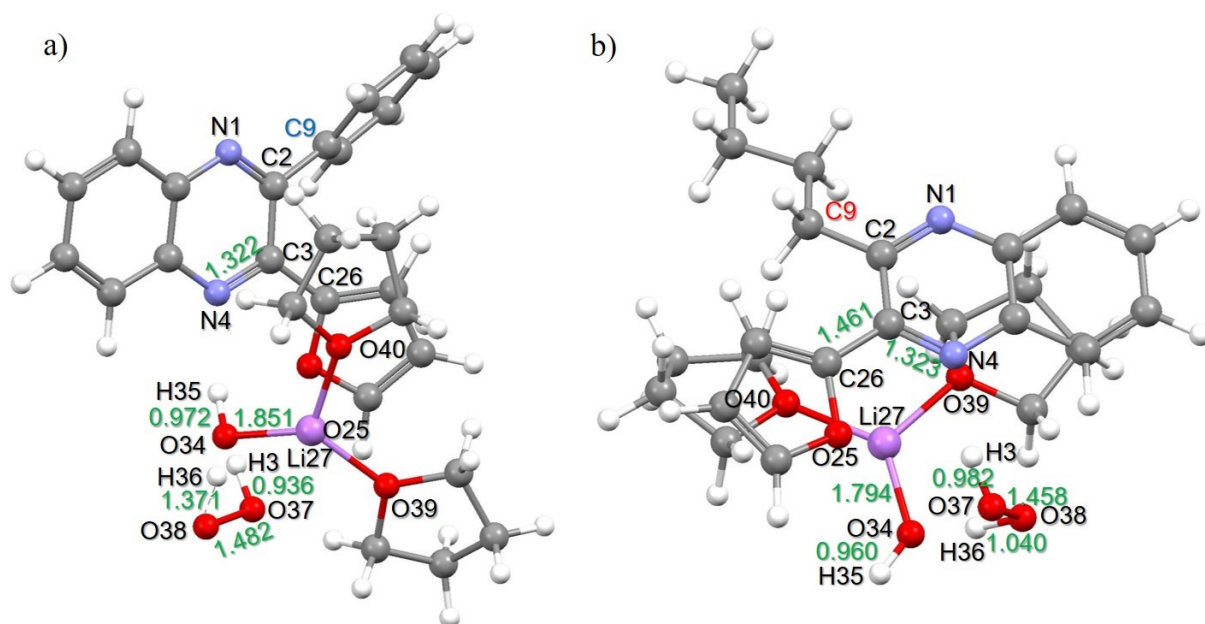
Figure 3.25: Products of ONSH: a) Prod. **3-Aa$_e$** b) Prod. **3-Ba$_e$**; 2,3-disubstituted quinoxaline and by-products (H$_2$O$_2$ and LiOH)

Table 3.6: Stationary points involved in ONSH reaction – all data results from optimised structures at –78 °C

Systems	E	E_{ZPVE}	H	G
	Energy term in a.u.			
Reactants				
Lithiofuran (**a**$_e$)	–702.14086	–701.84671	–701.83662	–701.87652
2-phenylquinoxaline (**A**)	–649.21024	–649.00667	–649.00095	–649.02883
2-***n***-butylquinoxaline (**B**)	–575.40101	–575.16529	–575.15883	–575.18838
H_2O	–76.46503	–76.44382	–76.44135	–76.45433
O_2	–150.30980	–150.30610	–150.30393	–150.31757
1. Nucleophilic Addition				
Add. **1-Aa**$_e$	–1351.37163	–1350.87185	–1350.85584	–1350.90947
Add. **1-Ba**$_e$	–1277.56132	–1277.02888	–1277.01241	–1277.06657
TS **1-Aa**$_e$	–1351.35611	–1350.85544	–1350.84076	–1350.88924
TS **1-Ba**$_e$	–1277.54456	–1277.01272	–1276.99678	–1277.04991
Int. **1-Aa**$_e$	–1351.40284	–1350.90060	–1350.88558	–1350.93578
Int. **1-Ba**$_e$	–1277.58810	–1277.05422	–1277.03851	–1277.09009
2. Hydrolysis				
Add. **2-Aa**$_e$	–1427.88500	–1427.35831	–1427.34160	–1427.39612
Add. **2-Ba**$_e$	–1354.07059	–1353.51255	–1353.49542	–1353.55015
TS **2-Aa**$_e$	–1427.88326	–1427.35981	–1427.34398	–1427.39526
TS **2-Ba**$_e$	–1354.06698	–1353.51262	–1353.49577	–1353.54956
Int. **2-Aa**$_e$	–1427.88770	–1427.36086	–1427.34452	–1427.39676
Int. **2-Ba**$_e$	–1354.07579	–1353.51715	–1353.49985	–1353.55532
3. Oxidation				
Prod. **3-Aa**$_e$	–1578.31718	–1577.78519	–1577.76708	–1577.82387
Prod. **3-Ba**$_e$	–1504.51864	–1503.95146	–1503.93348	–1503.98780
	Change in energy term (kcal/mol)			
	ΔE	ΔE_{ZPVE}	ΔH	ΔG
1. Nucleophilic Addition				
Add. **1-Aa**$_e$	–12.88	–11.59	–11.46	–2.58
Add. **1-Ba**$_e$	–12.19	–10.53	–10.60	–0.87
TS **1-Aa**$_e$	–3.14	–1.29	–2.00	10.11
TS **1-Ba**$_e$	–1.67	–0.39	–0.79	9.58
Int. **1-Aa**$_e$	–32.47	–29.63	–30.12	–19.09
Int. **1-Ba**$_e$	–28.99	–26.43	–26.98	–15.63
2. Hydrolysis				
Add. **2-Aa**$_e$	–43.21	–38.35	–40.15	–18.38
Add. **2-Ba**$_e$	–39.95	–35.54	–36.74	–19.23
TS **2-Aa**$_e$	–42.12	–39.28	–41.65	–17.85
TS **2-Ba**$_e$	–37.68	–35.58	–36.96	–18.86
Int. **2-Aa**$_e$	–44.91	–39.94	–41.98	–18.79
Int. **2-Ba**$_e$	–43.21	–38.42	–39.52	–22.48
3. Oxidation				
Prod. **3-Aa**$_e$	–119.99	–114.14	–116.43	–87.52
Prod. **3-Ba**$_e$	–126.70	–118.87	–120.90	–94.58

3.3 Conclusion

The mechanism of the reaction of lithiofuran (**a**) with 2-phenylquinoxaline (**A**) and 2-butylquinoxaline (**B**) followed the oxidative nucleophilic substitution of hydrogen (ONSH) route. The reaction results in three reaction steps: (i) nucleophilic addition, (ii) hydrolysis and (iii) oxidation. The nucleophilic addition reaction that forms σ^H-adduct was determined to be the rate-determining step (RDS).

The inclusion of an H_2O molecule stabilises the σ^H-adduct and spontaneously forms a Li-OH complex as a by-product that acts as a precursor in the concomitant oxidation reaction. Thus, its presence is crucial for the completion of the reaction. The oxidation occurs in the presence of an oxidant, O_2. The oxidant affords the elimination of the α-hydrogen to form the second by-product H_2O_2, as shown in **Scheme 3.3**. To the best of our knowledge, no detailed mechanism has been reported detailing the ONSH reaction mechanism and the by-products that form with it.
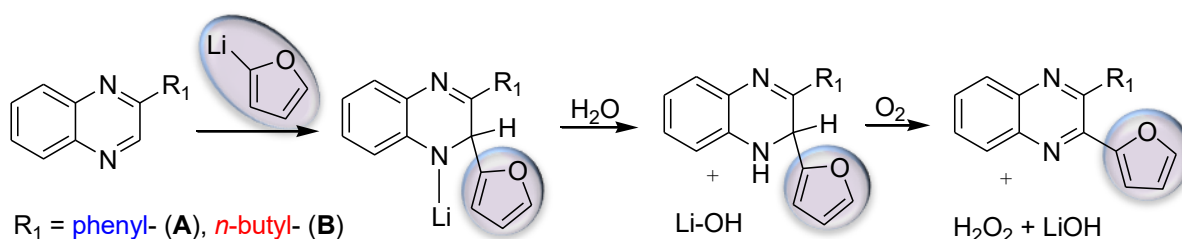
Scheme 3.3: Oxidative nucleophilic substitution of hydrogen (ONSH) of lithiofuran with 2-monosubstituted quinoxaline that forms 2,3-disubstituted quinoxaline and by-products (LiOH and H_2O_2). (R_1 = phenyl, -n-butyl)

Due to the deterioration of organolithium compounds at high temperatures, changing the temperature of the reactions to 25 °C (298.15 K) is only viable for the hydrolysis and oxidation reactions.

All stationary points that contribute to the ONSH reaction mechanism are stabilised with the inclusion of two explicit THF solvent molecules. It is worth noting that modelling using a hybrid solvation model (HSM) is necessary for experimentally relevant results. In both the presence and absence of explicit THF molecules, the ONSH reaction of **a** with **B** is more exothermic than the reaction with **A**. When considering (i) the rate-determining step, (ii) the Gibbs free activation energy, (iii) the exothermic effect, and (iv) the solvent effect, the σ^H-

71

adduct formation is more favourable for the reaction of lithiofuran with **B** than with **A**, but only by a negligible energy difference.

It is therefore concluded that the substituents present at position 2 (R_1 = phenyl-, *n*-butyl-) of 2-R_1-quinoxaline have no significant effect on the reactivity of the nucleophilic substitution reaction of 2-R_1-quinoxaline with **a**. Thus, both reactions have a similar reactivity and should afford similar reaction yields. From this work it follows that, since product yields can also be affected by a number of experimental errors during the synthesis of the products, the initial conditions/steps of the synthetic process must be carefully examined and optimised.

3.4 References

1. Ndlovu, N. T. & Nxumalo, W. Nucleophilic substitution on 2-monosubstituted quinoxalines giving 2,3-disubstituted quinoxalines: Investigating the effect of the 2-Substituent. *Molecules* **21**, (2016).

2. Kovalev, I. S. *et al.* Organolithium compounds in the nucleophilic substitution of hydrogen in arenes and hetarenes. *Russ. Chem. Rev.* **84**, 1191–1225 (2015).

3. Gilman, H. & Edward, J. T. Studies in the Preparation of Antimalarials From Pyridine. *Can. J. Chem.* **31**, 457–468 (1953).

4. Geissman, T. A., Schlatter, M. J., Webb, I. D. & Roberts, J. D. The synthesis of some intermediates for use in the preparation of analogs of salicylaldehyde ethylenediimine cobalt ("salcomine"). *J. Org. Chem.* **11**, 741–750 (1946).

5. Fraenkel, G. & Cooper, J. C. Structure of butyllithium-pyridine adducts. *Tetrahedron Lett.* **9**, 1825–1830 (1968).

6. Bubnov, Y. N., Klimkina, E. V, Starikova, Z. A. & Ignatenko, A. V. Reductive mono- and diallylation of the bis (pyridine) dihydropyridyllithium dimer by triallylborane. *Russ. Chem. Bull.* **50**, 1078–1084 (2001).

7. Giam, C. S. & Stout, J. L. Isolation and characterisation of crystalline σ-complexes from organolithium compounds and pyridine derivatives. *J. Chem. Soc. D Chem. Commun.* 142 (1969).

8. Housecroft, C. E. & Sharpe, A. G. *Inorganic chemistry*. (Pearson, 2012).

9. Poonia, N. S. & Bajaj, A. V. Coordination Chemistry of Alkali and Alkaline Earth Cations. *Chem. Rev.* **79**, 389–445 (1979).

10. Ortiz, V., Angélica Rubio, M. & Lissi, E. A. Hydrogen peroxide deposition and decomposition in rain and dew waters. *Atmos. Environ.* **34**, 1139–1146 (2000).

11. Liao, C. H. & Gurol, M. D. Chemical Oxidation by Photolytic Decomposition of Hydrogen Peroxide. *Environ. Sci. Technol.* **29**, 3007–3014 (1995).

12. Watts, R. J., Foget, M. K., Kong, S. H. & Teel, A. L. Hydrogen peroxide decomposition in model subsurface systems. *J. Hazard. Mater.* **69**, 229–243 (1999).

13. Contigiani, R. A., Bertorello, H. E. & de Bertorello, M. M. Reactions and thermal decomposition of organolithium compounds derived from 4,4′-dibromooctafluorobiphenyl. *J. Organomet. Chem.* **32**, 7–15 (1971).

14. Plata, R. E. & Singleton, D. A. A case study of the mechanism of alcohol-mediated morita baylis-hillman reactions. the importance of experimental observations. *J. Am. Chem. Soc.* **137**, 3811–3826 (2015).

Chapter 4

APPLYING ONSH ON 2-PHENYLQUINOXALINE WITH LITHIOTHIOPHENE USING DFT

4.1 Introduction and aim

In an S_N2 reaction a nucleophile displaces an electrophile, resulting in a nucleophilic substitution reaction. The reactivity and type of reaction will depend on the strength of both the electrophile and nucleophile separately, which in turn are determined by the nature of the substituents of each reactant.

Nxumalo and Ndlovu[1] conducted a study on the alkyl and arylation of quinoxaline derivatives using various organolithium compounds. The two reactions, shown in **Scheme 4.1**, consist of two different nucleophiles (lithiofuran (**a**) and lithiothiophene (**b**)) and the same electrophile (2-phenylquinoxaline, **A**). These reactions were reported to give products of 46% yield for reaction 1 and 22% yield for reaction 2. This presumably indicates that the reactivity is influenced by the differences in the nucleophiles.

Scheme 4.1: Experimental reactions to be modelled[1]

R_1 = phenyl-, *n*-butyl-
R_2 = thiophen-, furan-
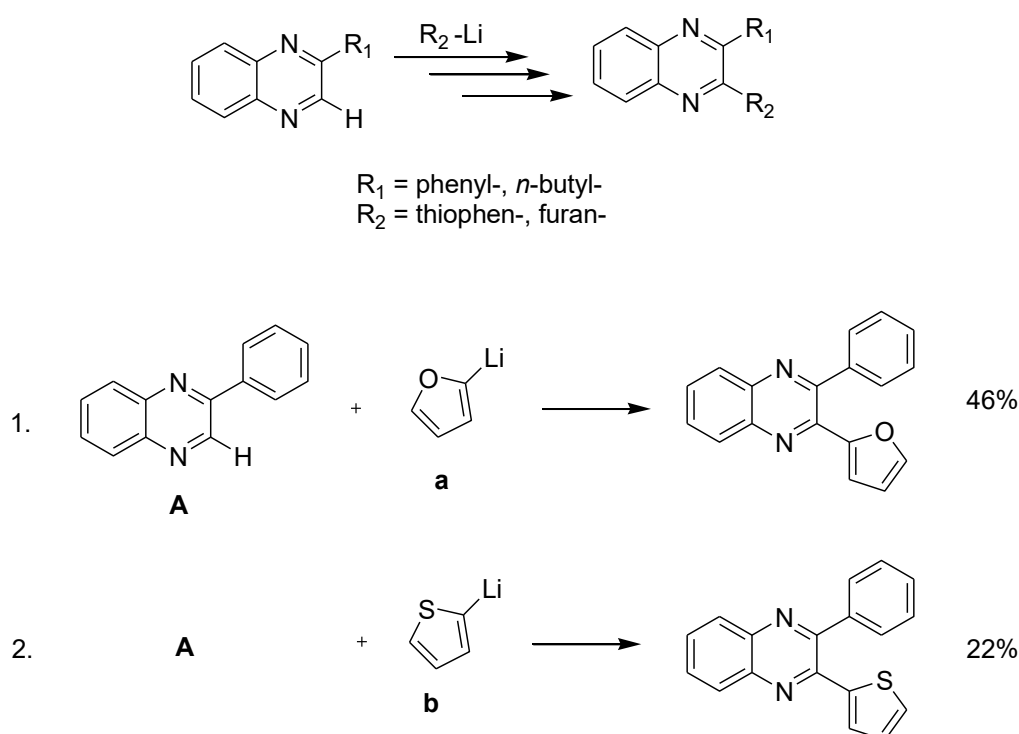
It is widely known that furan is more reactive than thiophene towards electrophilic substrates,[2] although the former is more aromatic than the latter.[3] The study reported focuses on the influence of the sulphur atom which appears to be responsible for the observed drop in the yield. The study also provides insight into the role played by the lithiated 5-membered ring when reacting with 2-phenylquinoxaline.

75

4.2 Results and discussion

4.2.1 Sulphur versus oxygen containing 5-membered cyclic rings

The structure of each nucleophile is shown in **Figure 4.1**. The C–S bonds are longer than the C–O bonds, a phenomenon that has been shown to affect the aromaticity of the ring and thus its stability. A study conducted by *Zora et al.*[4] shows the association of longer bonds with reduced aromaticity and shorter bonds with enhanced aromaticity. That being said, aromaticity is conveyed by the merger of various properties,[5–8] and it was further reported by Schleyer *et al.*[9] that there is no direct relationship between aromaticity and thermodynamic stability of heterocyclic isomers. In the case in hand, thiophene is more aromatic than furan,[3] and structure **b)** is more stable in terms of electronic energy than structure **a)**.
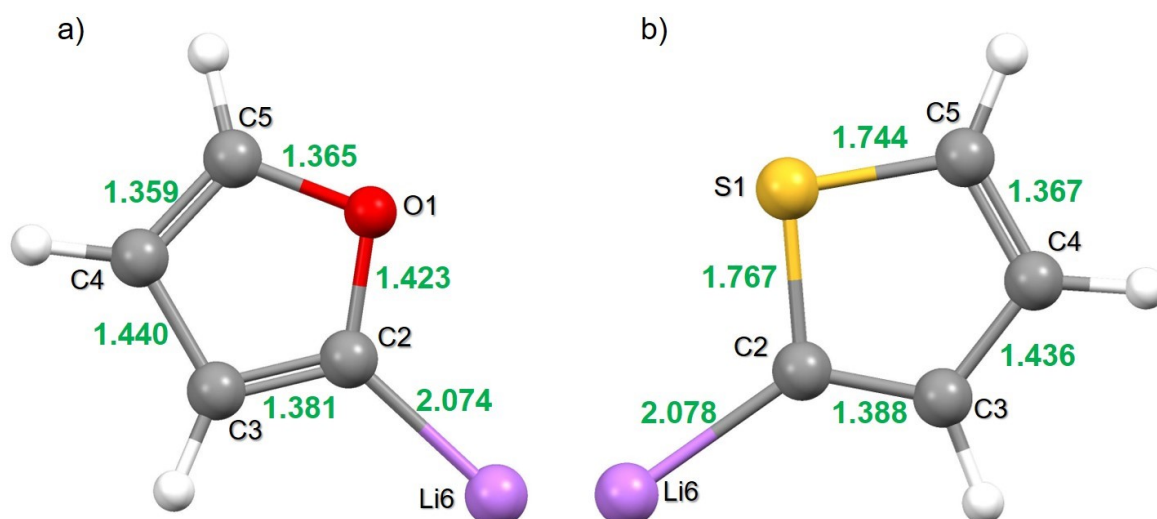
Figure 4.1: 5-membered heterocyclic ring nucleophiles: a) lithiofuran (**a**) and b) lithiothiophene (**b**) – the atomic distances, measured in Å, are shown in green

All reported structures are optimised in implicit THF solvent at 195.15 K (–78 °C). The **1-Aa** and **1-Ab** notations stand for nucleophilic addition (step-**1**) of 2-phenylquinoxaline (**A**) with lithiofuran (**a**)/lithiothiophene (**b**). A symbol of R_2 represents both **a** and **b** nucleophiles.

A geometrical optimisation of **A** with R_2 (R_2 = **a/b**) formed stable adducts (Add.) **1-Aa** and **1-Ab** with $\Delta G_{1\text{-Aa}}$ = –13.99 kcal/mol and $\Delta G_{1\text{-Ab}}$ = –2.26 kcal/mol, relative to the reactants R (R = A + R_2). This energy difference (–11.73 kcal/mol) between the adducts is significant and thus **A** interacting with **a** will have stronger inter-atomic (in general, inter-molecular) interactions that stabilise the adduct **1-Aa** more than **A** with **b**.

76
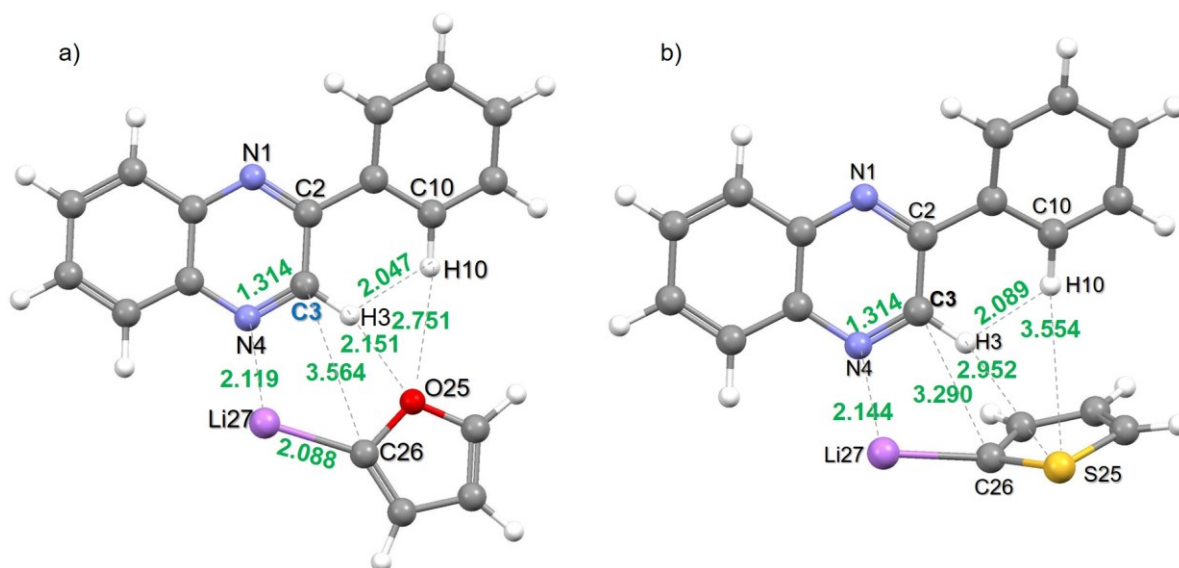
Figure 4.2: The adducts formed prior to the nucleophilic addition reaction of 2-phenylquinoxaline (**A**) with a) lithiofuran (**a**) and b) lithiothiophene (**b**)

The two adducts show different geometrical and atomic interactions between the reactants R. The different interactions between the reactants and the significance of the energy difference of the adducts evidently show that sulphur and oxygen atoms play a considerable role in the affinity of the rings to electrophiles. Furan in general is more reactive than thiophene.[2] Therefore there should presumably be a reactivity pattern of the lithiated 5-membered rings when reacting with electrophiles.

The highly electronegative O25 has, based on the inter-nuclear distances, strong non-covalent interaction with H3 and H10. This therefore reduces the d(H3,H10) in Add. **1-Aa** so that the two H atoms are, relative to the equilibrium structure of **A**, closer to O25, irrespective of the H3···H10 repelling effect.[10] The d(H3,H10) in Add. **1-Ab** is 0.042 Å further apart than in Add. **1-Aa**. The atoms involved in S25···H3 and S25···H10 interactions in Add. **1-Ab** are both ~0.802 Å further apart than the O25···H3 and O25···H10 atom-pairs of Add. **1-Aa**. In a report by Johnston and Cheong,[11] it was shown that the nonclassical hydrogen bonds (CH···O) are key stereo-controlling elements in a number of reactions. Thus, the reported data correlate well with that reported in the literature.

Both adducts, however, have a common N4···Li27 interaction. This is due to the lone pair of electrons on N4 which makes the quinoxaline derivative a Lewis base, allowing it to act as a monodentate ligand that binds with metal ions, here Li27, to form a coordinated complex, as

77

shown in **Figure 4.3**.[12–14] This strong interaction, together with other interactions between the reactants, contributes to the stability of the stationary points.
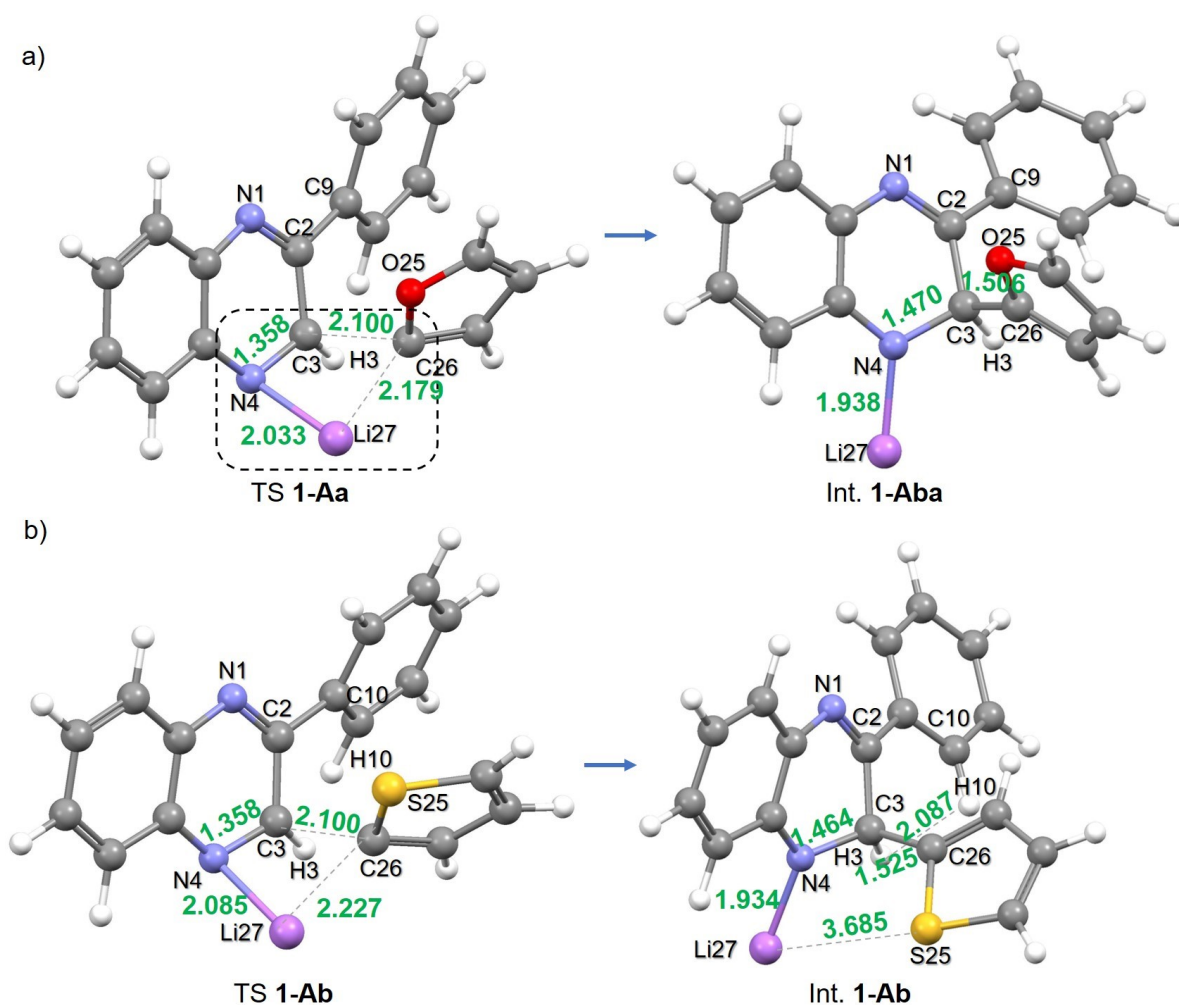
Figure 4.3: The transition state (TS) and subsequent intermediate (Int.) of the nucleophilic addition reaction of 2-phenylquinoxaline (**A**) with a) lithiofuran (**a**) and b) lithiothiophene (**b**)

The adducts were submitted for a C3–C26 reaction coordinate scan relative to the two reactants, which are involved in a nucleophilic addition reaction (step **1**). **Figure 4.4** shows the energy reaction profile of step **1**. The adducts **1-Aa** and **1-Ab** form transition states (TSs) **1-Aa** and **1-Ab** of $\Delta G_{1\text{-Aa}}$ = 1.44 kcal/mol and $\Delta G_{1\text{-Ab}}$ 13.20 kcal/mol in energy, relative to the reactants R. Both TS structures have similar geometry; however, a significant energy difference of 11.76 kcal/mol is noted between the TSs. An intrinsic reaction coordinate (IRC) scan of each reaction is attached in the CD.

78
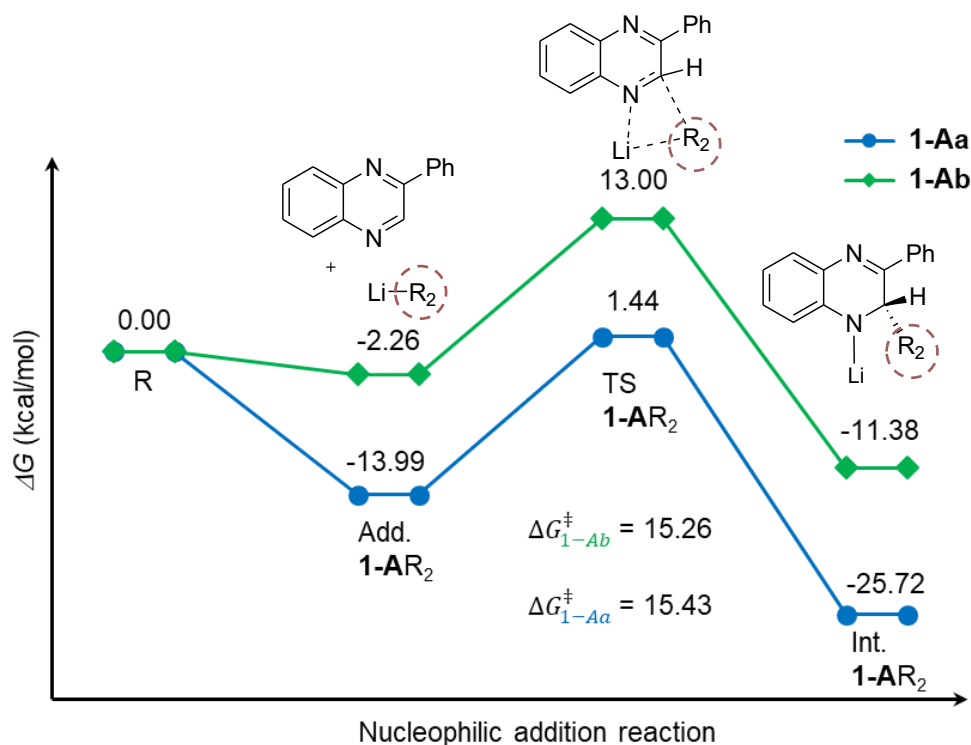
Figure 4.4: Gibbs free energy reaction profile of the nucleophilic addition (**1**) of 2-phenylquinoxaline (**A**) with lithiofuran (**a**) and lithiothiophene (**b**)

Although the stationary points of a reaction involving **1-Aa** are significantly more stable than those of **1-Ab**, both reactions have a comparable activation energy, $\Delta G^{\ddagger}$, of 15.43 kcal/mol and 15.26 kcal/mol respectively. Thus, the two reactions have comparable reactivity.

There is, however, a more significant energy difference between the intermediates **1-Aa** and **1-Ab** than there is for the adducts and TSs. The nucleophilic addition of **A** with **a** forms a σ^{H}-adduct intermediate that is 14.34 kcal/mol more stable than that formed with **b**. **Figure 4.5** shows the global minimum structure (GMS) of Int. **1-Aa** simulated from a 360° dihedral angle scan of DA(N4,C3,C26,O25) in 5° steps. The GMS of Int. **1-Ab** is shown in **Figure 4.3**. Intermediate **1-Aa** shows the non-classical intramolecular hydrogen bonds C3H3···O25 and C10H10···O25; such interactions were analysed in detail during the early 1960s to 1990s, and have been noted to be stabilising factors in reactions.[15–18] A DA scan of each intermediate **1-Aa** is attached to the CD.
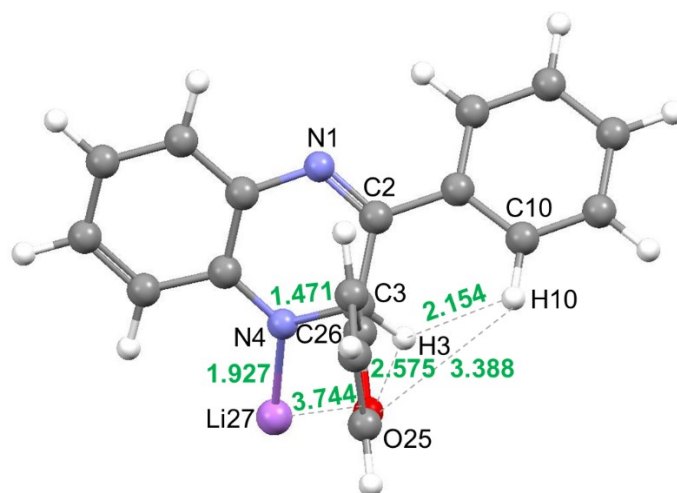
Figure 4.5: Global minimum structure (GMS) of the intermediate **1-Aa**. The grey dashed lines represent non-covalent interactions that stabilise the structure

The intermediate in **Figure 4.5** seems to have competing affinities for O25 between H3 and Li27. The d(Li27,O25) and d(H3,O25) are 3.744 Å and 2.575 Å, respectively. Due to C3 changing from sp^2 to sp-hybridisation (Add. to Int.) it makes H3 more acidic, thus leading to a stronger H3···O25 interaction than Li27···O25.[19–21] The O25 atom must have a net negative atomic charge and such atoms in molecules have an affinity for metals, as noted in Chapter 3 (Section 3.2.5), in which Li27 forms a coordination compound with two THF solvent molecules.[12]

When one looks at **Table 4.1**, it can be seen that the enthalpy energies (ΔH) for a reaction involving **1-Aa** are lower than the enthalpy energies involving **1-Ab**. It can also be deduced that the former reaction is 2.05 kcal/mol more exothermic than the latter. Furthermore, looking at the zero-point vibrational energies (ZPVE), it can be seen that they are comparable to the enthalpy energies and consequently both should have a similar reaction profile.

Table 4.1: Stationary points involved in nucleophilic addition reaction of 2-phenylquinoxaline (A) with lithiofuran (a) and lithiothiophene (b). Structures are optimised in implicit THF solvent at –78 °C. Changes in energies are measured relative to separate reactants (A + R₂). R_2 = a, b

Systems	E	E_{ZPVE}	H	G
	Energy term in a.u.			
Reactants				
2-phenylquinoxaline (**A**)	–649.21024	–649.00667	–649.00095	–649.02883
Lithiofuran (**a**)	–237.04795	–236.97100	–236.96738	–236.98881
Lithiothiophene (**b**)	–560.03717	–559.98197	–559.97862	–559.99933
Nucleophilic Addition Reaction				
Add. **1-Aa**	–886.27440	–886.01131	–886.00188	–886.03993
Add. **1-Ab**	–1209.26371	–1209.00325	–1208.99386	–1209.03176
TS **1-Aa**	–886.25185	–885.98912	–885.98054	–886.01534
TS **1- Ab**	–1209.24176	–1208.98150	–1208.97292	–1209.00744
Int. **1-Aa**	–886.29806	–886.03272	–886.02426	–886.05862
Int. **1- Ab**	–1209.28250	–1209.02027	–1209.01169	–1209.04629
	Change in energy term (kcal/mol)			
	ΔE	ΔE_{ZPVE}	ΔH	ΔG
Add. **1-Aa**	–10.17	–21.11	–21.05	–13.99
Add. **1-Ab**	–10.22	–9.17	–8.96	–2.26
TS **1-Aa**	3.98	–7.18	–7.66	1.44
TS **1- Ab**	3.55	4.48	4.17	13.00
Int. **1-Aa**	–25.02	–34.54	–35.10	–25.72
Int. **1- Ab**	–22.02	–19.85	–20.16	–11.38

4.2.2 Hydrolysis and oxidation reactions

The hydrolysis reaction energy profile shown in **Figure 4.6** involves the inclusion of H_2O in each σ^H-adduct intermediate of step-**1**. Both intermediates **1-A**R_2 are stabilised by the inclusion of the H_2O molecule to form adducts **2-Aa** and **2-Ab**; intermediate **1-Aa** and **1-Ab** are stabilised by –4.48 kcal/mol and –1.66 kcal/mol, respectively. Under hydrolytic conditions, the reaction involving **1-Aa** consists of stationary points of lower energy than the latter.

81
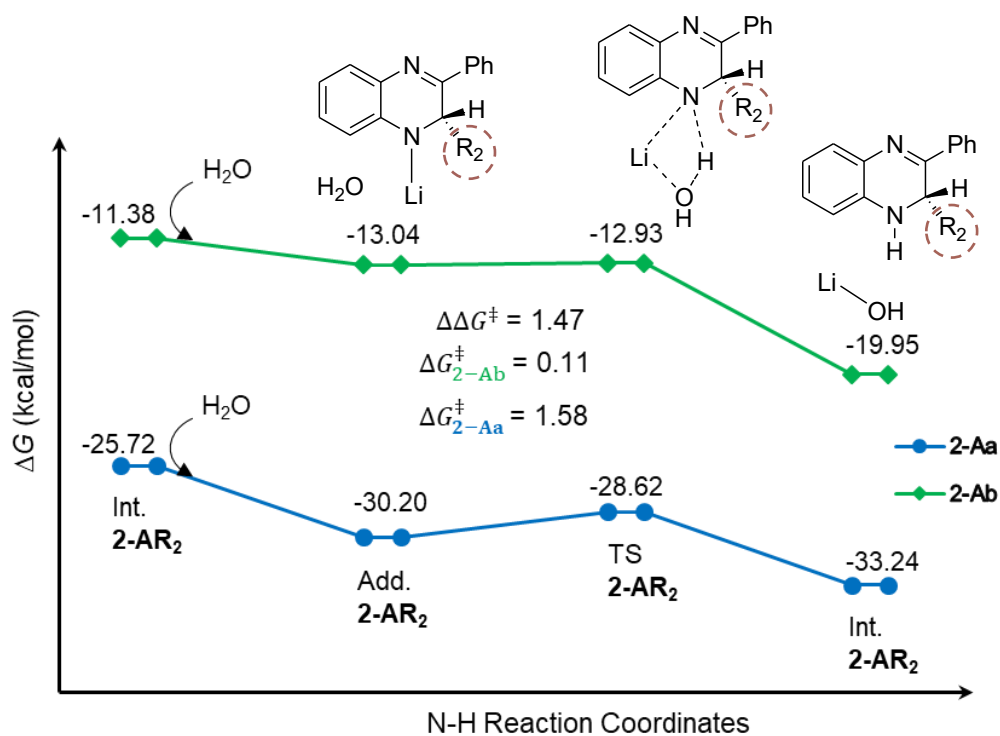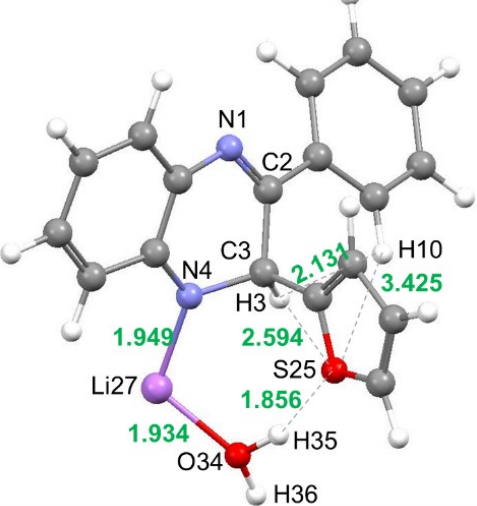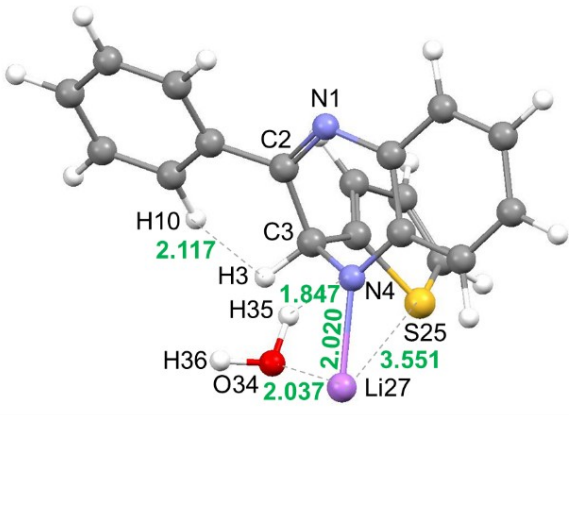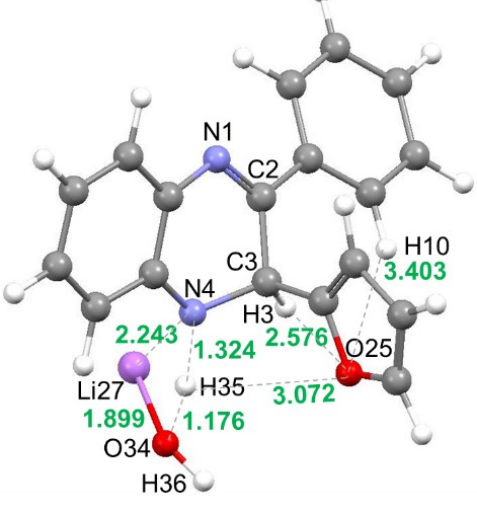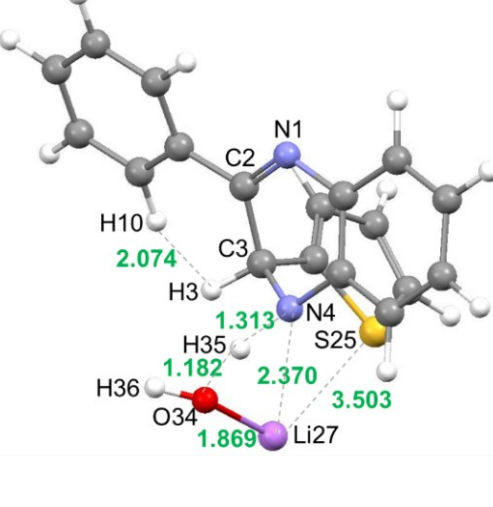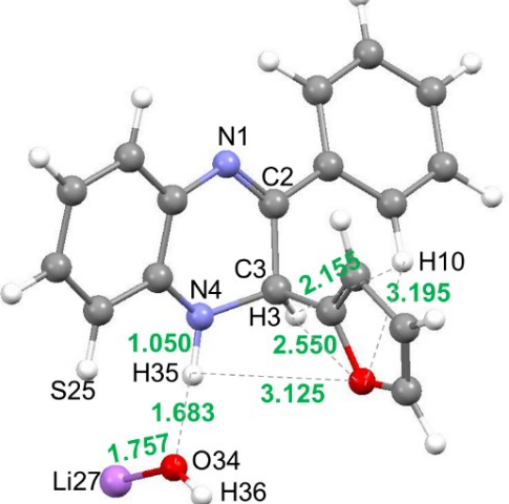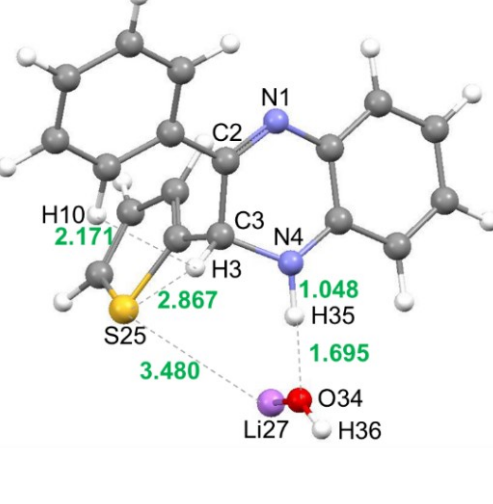
Figure 4.6: Free energy reaction profile of the hydrolysis of Int. **1-A**R$_2$, R$_2$ = -furan (**a**), -thiophene (**b**)

The adducts **2-Aa** and **2-Ab** form TSs of –12.93 and –28.62 kcal/mol respectively in free energy. The difference in energy between the respective adducts and TSs results in activation energies of $\Delta G^{\ddagger}_{2-Aa}$ = 1.58 kcal/mol and $\Delta G^{\ddagger}_{2-Ab}$ = 0.11 kcal/mol which are comparable (see **Figure 4.6**). This suggests that both reactions are comparably reactive and essentially spontaneous.

Reactions involving **2-A**R$_2$ result in the cleaving of the water molecule and the coordination complex (N4–Li27) allowing a hydride ion to be exchanged for a lithium ion (Li27$^+$), thus forming Li27–O34H36 and N4–H35 bonds at the intermediate (Int. **2-A**R$_2$) (**Table 4.2**). A detailed description of the reaction mechanism is reported in Chapter 3, Section 3.2.2.

Table 4.2: Stationary points involved in the hydrolysis reaction. All structures were optimised in implicit THF solvent using B3LYP/6-311++G(d,p) at 298.15 K (energies in kcal/mol)

Add. **2-Aa** ($\Delta G = -10.78$, $\Delta E_{ZPVE} = -32.26$)	Add. **2-Ab** ($\Delta G = -5.08$, $\Delta E_{ZPVE} = -27.19$)
TS. **2-Aa** ($\Delta G = -9.00$, $\Delta E_{ZPVE} = -30.96$)	TS. **2-Ab** ($\Delta G = -4.80$, $\Delta E_{ZPVE} = -27.23$)
Int. **2-Aa** ($\Delta G = -14.08$, $\Delta E_{ZPVE} = -35.10$)	Int. **3-Ab** ($\Delta G = -12.11$, $\Delta E_{ZPVE} = -33.72$)

83

The stationary points of the hydrolysis reactions modelled at 195.15 K were submitted for a single-point frequency calculation at a higher temperature of 298.15 K (25 °C), and the two reactions were compared (**Figure 4.7**). Reactions **2-A**R_2 have similar trends. At higher temperatures, the minima and saddle points became destabilised in both reactions. Destabilisation of the stationary points also resulted in a minor energy increase in free activation energy by ~0.2 kcal/mol. The change to high temperature, however, destabilised the reaction, which involved **2-Aa** significantly more than the reaction involving **2-Ab**. Each of the three stationary points of the hydrolysis reactions of the latter are destabilised as they are ~8 kcal/mol higher in energy, while the former are ~20 kcal/mol higher in energy.
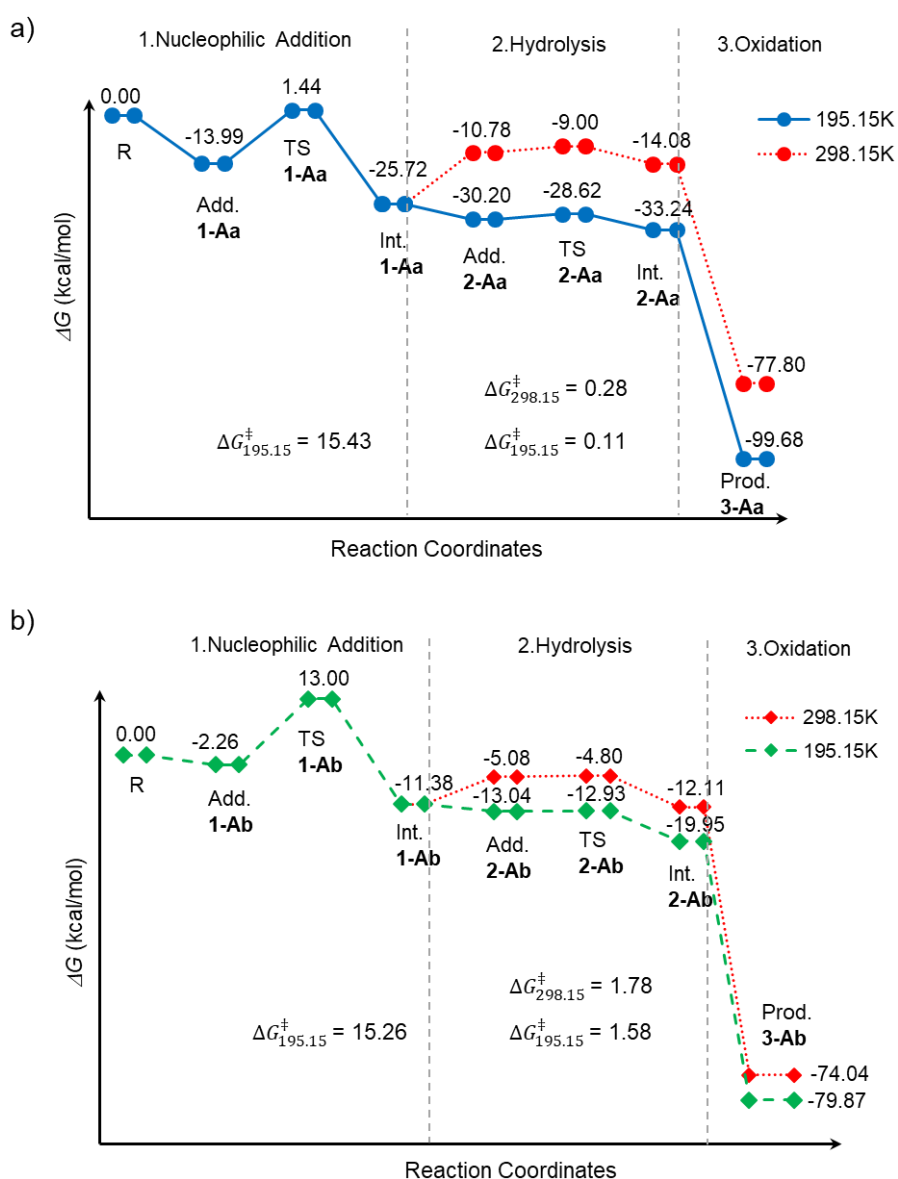
Figure 4.7: Gibbs free energy profile of the ONSH reaction of 2-phenylquinoxaline (**A**) with a) lithiofuran (**a**) and b) lithiothiophene (**b**), with the hydrolysis and oxidation reactions represented in both temperatures of 298.15 K and 195.15 K

The formation of Add. **2-Aa**$_{298.15}$ from Int. **1-Aa**$_{195.15}$ requires a significant amount of free energy of +14.94 kcal/mol, contrary to a reaction involving **b**, where the energy increase is +6.31 kcal/mol. Therefore, it is much easier to form Add. **2-Ab**$_{298.15}$ from temperatures of 195.15 K than Add. **2-Aa**$_{298.15}$. It should be noted, however, that both reactions at high temperatures are also spontaneous and have comparable reactivity.

The same pattern can be seen in **Table 4.3** with enthalpy energies (ΔH), in which the change to 298.5 K has a more significant effect on the stability of stationary points involved in a reaction of **2-Aa** than in a reaction involving **2-Ab**. Furthermore, Int. **1-Ab**'s energy is lowered more than that of **1-Aa**, thus the energy difference between the intermediate and adduct shows a more exothermic reaction for **1-Ab** by 3.73 kcal/mol. However, the energy difference is minimal and hence both the reactions are comparably exothermic.

85

Table 4.3: Stationary points involved in the hydrolysis reaction of σ^H-adduct intermediate at both 195.15 K and 298.15 K

Systems	E	E_{ZPVE}	H	G
	Energy term in a.u.			
Reactants at 195.15 K				
2-phenylquinoxaline (**A**)	–649.21024	–649.00667	–649.00095	–649.02883
Lithiothiophene (**b**)	–560.03717	–559.98197	–559.97862	–559.99933
Lithiofuran (**a**)	–237.04795	–236.97100	–236.96738	–236.98881
H_2O	–76.46503	–76.44382	–76.44135	–76.45433
Reactants at 298.15 K				
H_2O	–76.46503	–76.44382	–76.44004	–76.46147
Lithiofuran (**a**)	–237.04795	–236.99026	–236.98401	–237.01877
Lithiothiophene (**b**)	–560.03717	–559.98197	–559.97555	–560.01091
2-phenylquinoxaline (**A**)	–649.21026	–649.00667	–648.99445	–649.04487
Hydrolysis Reaction				
Add. **2-Aa**$_{298.15}$	–962.78243	–962.49233	–962.48233	–962.52008
Add. **2-Aa**$_{195.15}$	–962.78243	–962.49232	–962.47133	–962.54229
Add. **2-Ab**$_{298.15}$	–1285.76250	–1285.47579	–1285.45473	–1285.52534
Add. **2-Ab**$_{198.15}$	–1285.76250	–1285.47579	–1285.46591	–1285.50327
TS **2-Aa**$_{298.15}$	–962.77558	–962.49009	–962.48041	–962.51758
TS **2-Aa**$_{195.15}$	–962.77558	–962.49009	–962.46970	–962.53945
TS **2-Ab**$_{298.15}$	–1285.75808	–1285.47586	–1285.45513	–1285.52491
TS **2-Ab**$_{198.15}$	–1285.75808	–1285.47586	–1285.46612	–1285.50309
Int. **2-Aa**$_{298.15}$	–962.78655	–962.49670	–962.48645	–962.52493
Int. **2-Aa**$_{195.15}$	–962.78655	–962.49670	–962.47550	–962.54755
Int. **2-Ab**$_{298.15}$	–1285.773153	–1285.48620	–1285.46479	–1285.53655
Int. **2-Ab**$_{198.15}$	–1285.773153	–1285.48642	–1285.47623	–1285.51428
Change in energy term (kcal/mol)				
	ΔE	ΔE_{ZPVE}	ΔH	ΔG
Add. **2-Aa**$_{298.15}$	–37.15	–44.45	–45.59	–30.20
Add. **2-Aa**$_{195.15}$	–37.14	–32.36	–33.15	–10.78
Add. **2-Ab**$_{298.15}$	–31.40	–27.19	–28.04	–5.08
Add. **2-Ab**$_{198.15}$	–31.41	–27.19	–28.23	–13.04
TS **2-Aa**$_{298.15}$	–32.85	–43.05	–44.38	–28.62
TS **2-Aa**$_{195.15}$	–32.84	–30.96	–32.13	–9.00
TS **2-Ab**$_{298.15}$	–28.62	–27.23	–28.30	–4.80
TS **2-Ab**$_{198.15}$	–28.63	–27.23	–28.36	–12.93
Int. **2-Aa**$_{298.15}$	–39.74	–47.19	–48.17	–33.24
Int. **2-Aa**$_{195.15}$	–39.72	–35.10	–35.77	–14.08
Int. **2-Ab**$_{298.15}$	–38.08	–33.72	–34.35	–12.11
Int. **2-Ab**$_{198.15}$	–38.09	–33.86	–34.71	–19.95

With the hydrolysis reaction preferably occurring at temperatures above 0 °C, the subsequent oxidation reaction is also forced to proceed at higher temperatures. Explicitly introducing oxygen to Int. **2-Aa** and **2-Ab** significantly stabilises the intermediates to form product (Prod.) **3-Aa** and **3-Ab** of –77.80 kcal/mol and –74.04 kcal/mol in free energy respectively.

4.3 Conclusion

A theoretical study of the reactions of 2-phenylquinoxaline (**A**) with lithiothiophene (**b**) and lithiofuran (**a**) was undertaken to understand the reactivity of heterocyclic nucleophiles of different aromaticity, based on the reported experimental study by Nxumalo and Ndlovu.[1] Their study suggested that the reaction of **A** and **a** results in a greater yield than with **b**. As established in Chapter 3, the reactions of **a** and **A** involve three reactive steps: nucleophilic addition, hydrolysis and oxidation reaction.

Using a less reactive nucleophile, lithiothiophene (**b**), the reaction of **A** with **b** resulted in the same reaction mechanism consisting of the three reaction steps as in the reaction of **A** + **a**. The latter, however, results in a pronounced increase in the stability of stationary points over the former reaction. The high stability is influenced by the nonclassical hydrogen bonds (NCHB) C3H3···O25 and C10H10···O25. Such interactions are not available in a reaction involving **b**, thus this reaction results in stationary points of higher energy compared to those of reaction **A** + **a**. These stabilising interactions, apart from increasing the temperature of the reaction to 295.15 K, made no difference to the reactivity of the two reactions. The activation energy difference between the two reactions is $\Delta\Delta G^{\ddagger} = 0.17$ kcal/mol at the same reaction conditions. This energy difference is minor and suggests both reactions have comparable reactivity. Thus, they should result in comparable reaction yields.

Overall, because **b** is more aromatic than **a**, we can conclude that high aromaticity is not equivalent to stability in a reaction. However, the presence of an oxygen atom-containing molecule stabilises the stationary points involved in the nucleophilic substitution reaction in the presence of hydrocarbons (C–H) to form strong CH···O interactions, and results in even greater (shorter distance) H···O interactions if the hydrogen is acidic.

4.4 References

1. Ndlovu, N. T. & Nxumalo, W. Nucleophilic substitution on 2-monosubstituted quinoxalines giving 2,3-disubstituted quinoxalines: Investigating the effect of the 2-Substituent. *Molecules* **21**, 1304 (2016).

2. Ghomri, A. & Mekelleche, S. M. Reactivity and regioselectivity of five-membered heterocycles in electrophilic aromatic substitution: A theoretical investigation. *J. Mol. Struct. THEOCHEM* **941**, 36–40 (2010).

3. Horner, K. E. & Karadakov, P. B. Chemical bonding and aromaticity in furan, pyrrole, and thiophene: A magnetic shielding study. *J. Org. Chem.* **78**, 8037–8043 (2013).

4. Zora, M. & Özkan, I. Nucleus-independent chemical shift evaluation for benzo- and dibenzo-fused pyrrole, furan and thiophene derivatives. *J. Mol. Struct. THEOCHEM* **638**, 157–162 (2003).

5. Cyrañski, M. K., Krygowski, T. M., Katritzky, A. R. & Schleyer, P. V. R. To what extent can aromaticity be defined uniquely? *J. Org. Chem.* **67**, 1333–1338 (2002).

6. Von Ragué Schleyer, P. Aromaticity: Introduction. *Chem. Rev.* **101**, 1115–1117 (2001).

7. von Schleyer, P. R. & Jiao, H. What is aromaticity? *Pure Appl. Chem.* **68**, 209–218 (1996).

8. Krygowski, T. M., Cyrañski, M. K., Czarnocki, Z., Häfelinger, G. & Katritzky, A. R. Aromaticity: A theoretical concept of immense practical importance. *Tetrahedron* **56**, 1783–1796 (2000).

9. Subramanian, G., von Ragué Schleyer, P. & Jiao, H. Are the Most Stable Fused Heterobicycles the Most Aromatic? *Angew. Chemie Int. Ed. English* **35**, 2638–2641 (1996).

10. Simmons, H. E. & Williams, J. K. An Empirical Model for Nonbonded H~H Repulsion Energies in Hydrocarbons. *J. Am. Chem. Soc.* **86**, 3222–3226 (1964).

11. Johnston, R. C. & Cheong, P. H. Y. C-H···O non-classical hydrogen bonding in the stereomechanics of organic transformations: Theory and recognition. *Org. Biomol. Chem.* **11**, 5057–5064 (2013).

12. Bellemin-Laponnaz, S. & Dagorne, S. Group 1 and 2 and early transition metal

complexes bearing N-heterocyclic carbene ligands: Coordination chemistry, reactivity, and applications. *Chem. Rev.* **114**, 8747–8774 (2014).

13. Seggio, A., Chevallier, F., Vaultier, M. & Mongin, F. Lithium-mediated zincation of pyrazine, pyridazine, pyrimidine, and quinoxaline. *J. Org. Chem.* **72**, 6602–6605 (2007).

14. Kovalev, I. S. *et al.* Organolithium compounds in the nucleophilic substitution of hydrogen in arenes and hetarenes. *Russ. Chem. Rev.* **84**, 1191 (2015).

15. Sutor, D. J. 204. Evidence for the existence of C–H··· O hydrogen bonds in crystals. *J. Chem. Soc.* 1105–1110 (1963).

16. Taylor, R. & Kennard, O. Crystallographic Evidence for the Existence of C-H···O, C-H···N, and C-H···Cl Hydrogen Bonds. *J. Am. Chem. Soc.* **104**, 5063–5070 (1982).

17. Burley, S. K. & Petsko, G. A. Amino-aromatic interactions in proteins. *FEBS Lett.* **203**, 139–143 (1986).

18. Rzepa, H. S., Smith, M. H. & Webb, M. L. A crystallographic AM1 and PM3 SCF-MO investigation of strong OH··· π-alkene and alkyne hydrogen bonding interactions. *J. Chem. Soc. Perkin Trans. 2* 703–707 (1994).

19. Scheiner, S. & Kar, T. Red- versus blue-shifting hydrogen bonds: Are there fundamental distinctions? *J. Phys. Chem. A* **106**, 1784–1789 (2002).

20. Zhou, Y., Parisini, T. & Polycarpou, M. M. Detection of drift sensor faults in a class of nonlinear uncertain systems. *Proc. IEEE Conf. Decis. Control* **54rd IEEE**, 3169–3174 (2015).

21. Alcamí, M., Mó, O. & Yáñez, M. Modelling intrinsic basicities and acidities. *J. Phys. Org. Chem.* **15**, 174–186 (2002).

Chapter 5

THE INFLUENCE OF -NO$_2$ ON THE STABILITY OF σ^H-ADDUCTS

5.1 Introduction and aim

One of the highlighted topics of current organic chemistry is the direct C–H functionalisation of aromatics without the incorporation of a halogen or other functionalities, which therefore corresponds to the principles of green chemistry.[1] The development of C–H functionalisation techniques can help in the understanding of organic synthesis.

The C–H functionalisation in aromatic rings is referred to as nucleophilic aromatic substitution of hydrogen (S_NArH). It involves a nucleophilic addition reaction (step **1**) on an aromatic ring to form an intermediate (σ^H-adduct), followed by the re-aromatisation of the ring.[2–5] The susceptibility of the aromatic ring to nucleophilic attack is increased by the presence of an electron-withdrawing group (EWG) on the ring. It should, however, be noted that while the EWG on the aromatic ring facilitates reaction step **1**, it also constitutes the reversibility of the reaction.[4]

The σ^H-adducts which are formed in reaction step **1** are susceptible to dissociation; with a wide range of stability for these adducts being noted.[6–9] This stability varies from being easy-to-isolate to very unstable intermediates which are challenging to detect by spectroscopic techniques, contrary to the former. The "easy-to-isolate" adducts are unable to proceed further to aromatisation. The stability of σ^H-adducts is not only determined by the solvation effect, but also by structural (both electronic and steric) features of the reaction partners.

In this study, we focus on the nitro ($-NO_2$) and aza (R–N–R) EWGs and their influence on the stability of σ^H-adducts formed from the reaction of quinoxaline derivatives with lithiofuran (**a**). Similar to general S_NArH reactions, these reactions can be used to avoid using leaving groups such as halogens, NO_2, SO_2R and OR (R = Aryl, Alkyl) as substituents in aromatic rings. This consequently opens up new possibilities to extend the methodology and synthesise more complex C–H functionalised molecules. Therefore, using quinoxalines as electrophiles, a wide spectrum of properties of the newly established C–H functionalised molecules would be of significant importance.[10–16]

These new reactions have the potential to extend the conventional Heck, Sonogashira, Suzuki and other cross-coupling reactions,[17–20] which are renowned for using halogens and metal-based catalysts.

91

5.2 Results and discussion

5.2.1 Mesomeric effect

Effective nucleophilic addition of organolithium nucleophiles to form C–C bonds with aza aromatics, enabling one to carry out nucleophilic substitution of hydrogen (S_NH) reactions under mild conditions, has been suggested.[17] These reactions are studied to understand the influence of the nitro group substituent on the quinoxaline ring [2-phenylquinoxaline (**A**)]. The EWG, -NO_2, was placed at position 6 of the aromatic ring of **A** (noted to be electrophilic in previous chapters) to form 6-nitro-2-phenylquinoxaline (**C**). The resultant structure was geometrically optimised and is shown in **Figure 5.1**.
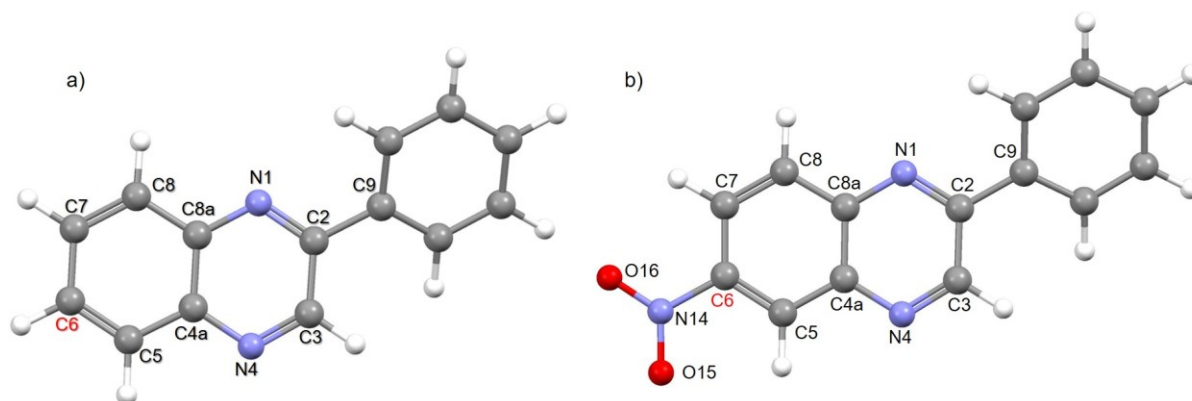
Figure 5.1: Two electrophiles a) 2-phenylquinoxaline (**A**) and b) 6-nitro-2-phenylquinoxaline (**C**) used in the nucleophilic addition reaction with lithiofuran

All reported structures are optimised in implicit THF solvent at –78 °C. The **1-Ca** and **1-Aa** notations stand for: nucleophilic addition (**1**) of 2-phenylquinoxaline (**A**)/6-nitro-2-phenylquinoxaline (**C**) with lithiofuran (**a**). The symbol **Rx** represents **A/C**. Energies that represent the stationary points are measured relative to the reactants R (R = **Rx** + **a**) and the activation energies are measured relative to the adducts (Add.).

The nitro group is a strong EWG, which is capable of significantly reducing the electron density of the aromatic ring system, thereby making the ring more susceptible to nucleophilic attack(s). Therefore, using lithiofuran (**a**) as a nucleophile, nucleophilic addition at C3 of **C** and **A** was modelled and compared in order to rationalise the influence of the nitro group on the aza-activated site, C3. A detailed nucleophilic addition (**1**) reaction of **a** with **A** is described in Chapter 3 (Section 3.2.1).

92

The geometrical optimisation of **C** with **a** at various distances apart resulted in several adducts – see Appendix C, **Table 0.1** and **Table 0.2**. The two most stable adducts of suitable geometry to facilitate the reaction involving **1-Ca** and **1-Aa** are shown in **Figure 5.2**.
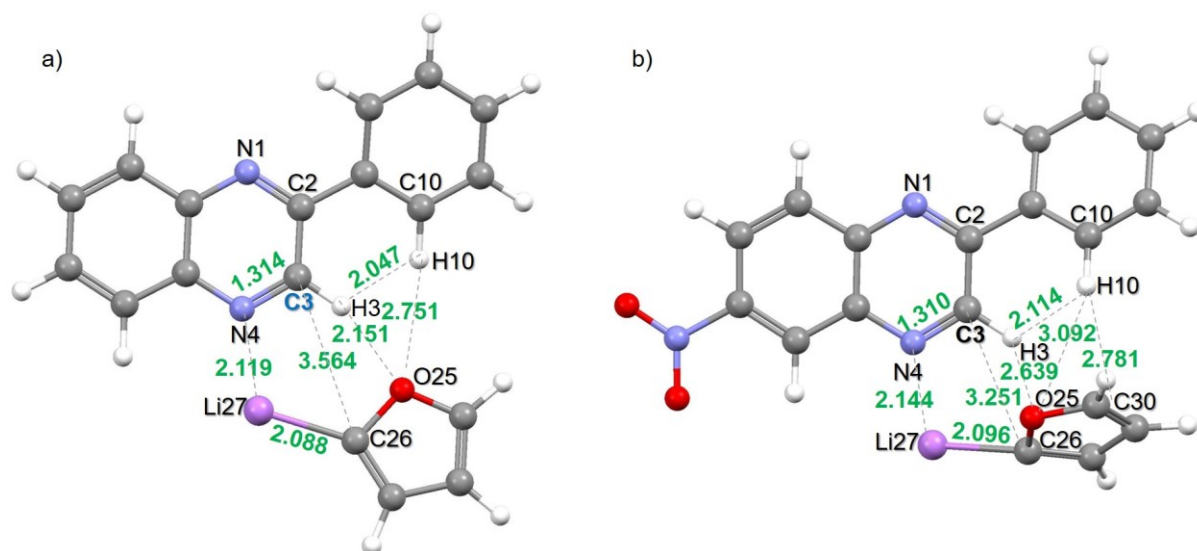
Figure 5.2: Adduct a) **1-Aa** and b) **1-Ca** involved in the nucleophilic addition reaction of 2-phenylquinoxaline (**A**)/6-nitro-2-phenylquinoxaline (**C**) with the nucleophile lithiofuran (**a**)

Both adducts have similar non-covalent interactions between the reactants (**Rx** and **a**), showing strong interactions for N4···Li27, O25···H3 and O25···H10 atom pairs. The strong interactions, together with the rest of the non-covalent interactions, contribute to the stability of each adduct. A C3–C26 reaction coordinate scan was conducted for both adducts, **1-Aa** and **1-Ca,** taking steps of –0.01 Å. A coordinate scan of each reaction is attached on the CD.

The C3–C26 reaction coordinate scan results in nucleophilic addition at C3, with H3 still bonded to C3 due to the thermodynamically unfavourable release of the hydride anion. Shown in **Figure 5.3** is a reaction involving **1-Ca** with activation free energy ($\Delta G^{\ddagger}$) of 10.55 kcal/mol, which is 4.82 kcal/mol less than the $\Delta G^{\ddagger}$ of a reaction involving **1-Aa**. Furthermore, both reactions are essentially spontaneous, and due to the minor energy difference they are comparably reactive.

When we look at **Figure 5.3**, we see that although the reaction energy profile in the presence of the nitro group is comparable to its absence, in principle the nitro group stabilises the stationary points and thus activates the quinoxaline derivative into a better electrophile, which correlates well with what is reported in the literature.[21]
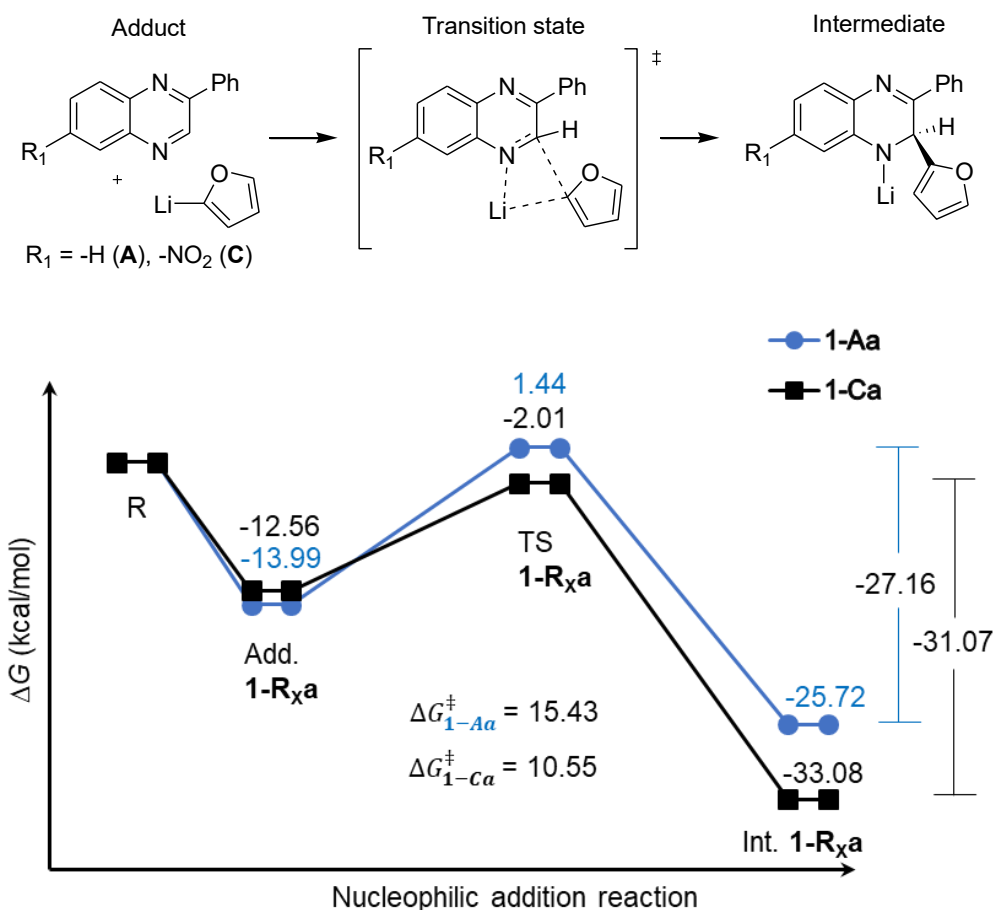
Figure 5.3: Gibbs free energy profile of the nucleophilic addition reaction of lithiofuran (**a**) with 6-nitro-2-phenylquinoxaline (**C**) and 2-phenylquinoxaline (**A**) at the C3-position. $\mathbf{R_X = A, C}$

Each TS, **1-Aa** and **1-Ca**, has a single negative vibration frequency of -300.06 cm^{-1} and -265.31 cm^{-1} respectively. The vibration frequencies represent vibrational movements between Li27, C3 and C26. According to the vibrational frequency values, both reactions involving **1-Aa** and **1-Ca** have a comparable potential energy surface (PES) that is curved at the region of the TSs.

The TSs form intermediates (Int.), namely σ^H-adducts. Intermediate **1-Ca** is formed at -33.08 kcal/mol, relative to the separate reactants R (**R$_X$** and **a**) – it is -7.36 kcal/mol lower in energy than Int. **1-Aa**. Therefore, a reaction involving **1-Ca** forms a more stable σ^H-complex compared to that involving **1-Aa**. Furthermore, the energy difference between Int. **1-R$_X$a** and TS **1-R$_X$a** is -31.07 kcal/mol and -27.16 kcal/mol for reactions involving **1-Ca** and **1-Aa** respectively. These energy differences are significant; thus, it is highly unlikely that both intermediates would dissociate to form Add. **1-R$_X$a** again.

94

5.2.2 Regio-selectivity

When analysing the reactivity of the quinoxaline ring with the incorporated two electron acceptors (the nitro and aza groups) towards nucleophilic reagents, both the relative reactivity of different quinoxaline derivatives and the site selectivity must be considered. To study which site on **C** has been activated more towards nucleophilic attack, three sites, namely C3 (aza-activated) and the nitro-activated C5 and C7 were modelled and compared. The reactive sites C5 and C7 in **C** are competing sites and thus lead to structural isomers.[23]

Nucleophilic addition reaction of lithiofuran (**a**) and 6-nitro-2-phenylquinoxaline (**C**) at two competing *ortho*-sites, C5 and C7, was modelled and compared with the addition at C3 (discussed in Section 5.2.1). Reaction coordinate scans of C5–C26 and C7–C26 bonds were carried out at intervals of –0.01 Å steps. **Figure 5.4** shows the local and global minimum structures (LMS and GMS) for the adducts (Add.) **1-Ca**$_{C5\text{-}C26}$ and **1-Ca**$_{C7\text{-}C26}$ that were used to carry out the scans. The two reactions result in similar structures.
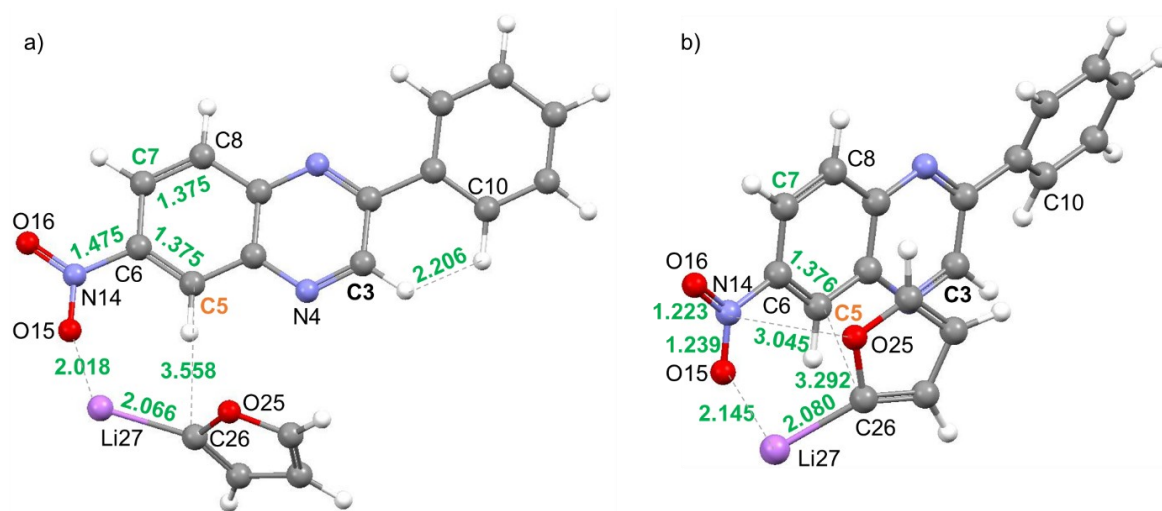
Figure 5.4: Reactants lithiofuran (**a**) and 6-nitro-2-phenylquinoxaline (C) geometrically optimised to form adduct **1-Ca** a) local minimum structure (LMS) and b) global minimum structure (GMS)

When we look at **Figure 5.4**, we see that the nitro-group on **C** has an affinity for **a**. Thus, **C** forms non-covalent interactions with **a** to form adduct (Add.) **1-Ca**. Several adducts have been produced, and most of them have a common strong non-covalent interaction involving O15···Li27 atoms, which has the shortest inter-atomic distance (~2.050 Å). Due to the delocalisation of -NO$_2$, two dissimilar oxygen atoms of negative charge are formed.[22] The bond distance d(N14,O16) is 0.016 Å shorter than d(N14,O15), thus O15 is likely to be negatively

charged, hence the strong O15···Li27 interaction. The reactions involving **1-Ca** at C5 and C7 result in an identical GMS adduct.

The formation of TS **1-Ca**$_{C5–C26}$ involves the cleavage of C26–Li27 bond and partial bond formation of C5–C26 and O15–Li27, whereas the formation of TS **1-Ca**$_{C7–C26}$ also involves the cleavage of the C26–Li27 bond and the partial bond formation of C7–C26. These transformations are associated with a single negative frequency of –251.46 cm^{-1} and –331.18 cm^{-1} for TS **1-Ca**$_{C5–C26}$ and **1-Ca**$_{C7–C26}$ respectively. The vibrational frequencies show that the C26 atom acts as a central atom and vibrates between C5 and the leaving group Li27 (**Figure 5.5**). The vibrational movements of these coordinates are included in the attached CD.

In TS **1-Ca**$_{C5–C26}$ the d(Li27,O15) is 1.992 Å and in TS **1-Ca**$_{C7–C26}$ the d(Li27,O16) is 4.602 Å. Due to the significant atomic distance of the latter and a lack of strong interactions between Li27 and any other close atom(s), a Li27$^+$ radical ion is formed in both the TS and Int. **1-Ca**$_{C7–C26}$. However, no radical ion in solution exists in isolation; the Li-metal ion will form coordination compounds with solvent molecules.[23]
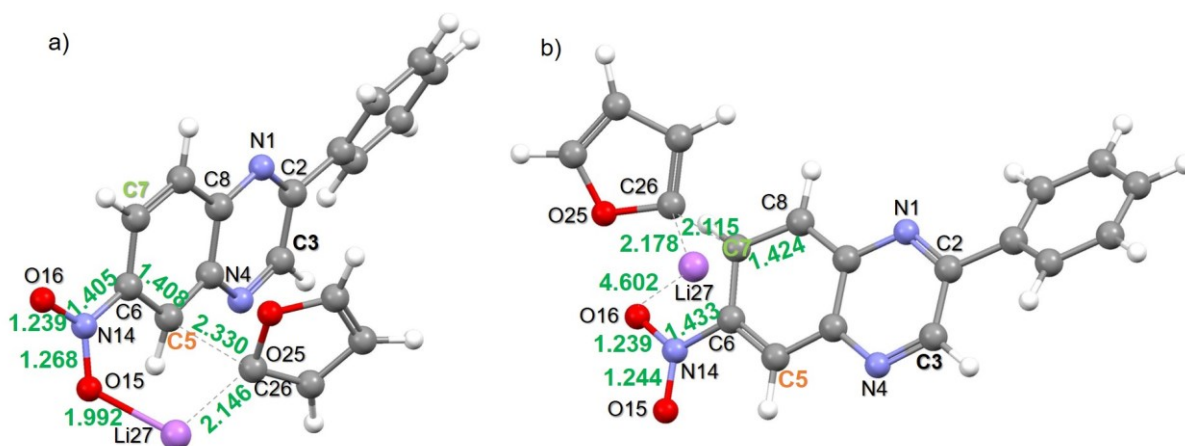
Figure 5.5: Transition states involved in the nucleophilic addition of 6-nitro-2-phenylquinoxaline (**C**) with lithiofuran (**a**) at two ortho-sites a) C5 and b) C7

All three structural adducts in **Figure 5.6** have comparable energy relative to the reactants R. The adducts form transition states (TSs) **1-Ca**$_{C5-C26}$ and **1-Ca**$_{C7-C26}$ of –5.31 kcal/mol and 10.38 kcal/mol respectively. This results in activation free energy (ΔG‡) of 5.11 kcal/mol and 20.81 kcal/mol for reactions involving **1-Ca**$_{C5-C26}$ and **1-Ca**$_{C7-C26}$ respectively. Both reactions are reactive; however, the energy difference between the two barriers of 15.70 kcal/mol is significant, thus the reaction involving **1-Ca**$_{C5-C26}$ is more reactive. Therefore, due to the

reactions forming regio-isomers, the nucleophilic addition at C7 is highly unlikely to occur and thus addition at C5 is favoured.
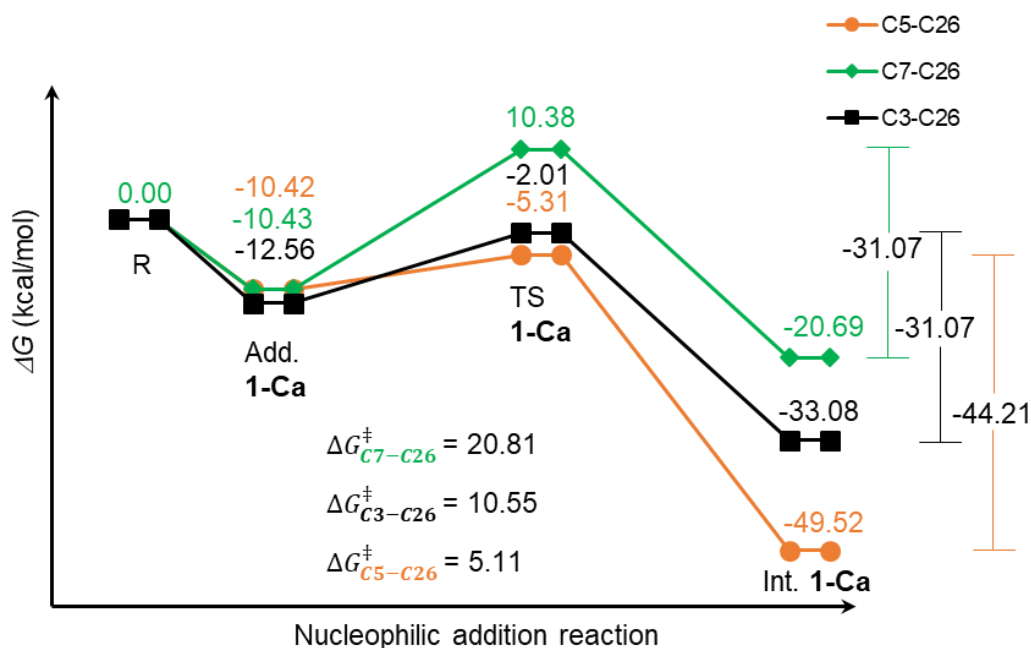
Figure 5.6: Gibbs free energy profile of the nucleophilic addition reaction of 6-nitro-2-phenylquinoxaline (**C**) with lithiofuran (**a**) at three electrophilic sites: C3, C5 and C7

The nucleophilic addition reaction at the azine-activated site C3 requires double the activation energy of the addition reaction at C5. However, this energy difference is insignificant and both reactions have minimum activation energies ($\Delta G^{\ddagger}_{C3-C26}$ = 10.55 kcal/mol and $\Delta G^{\ddagger}_{C5-C26}$ = 5.11 kcal/mol) (see **Figure 5.6**). Thus, the reaction paths are likely to also compete in forming the σ^{H}-adduct (Int. **1-Ca**) of regio-isomers.

The low-energy TSs stabilise to form intermediates at ΔG_{C3-C26} = –33.08, ΔG_{C5-C26} = -49.52 and ΔG_{C7-C26} = –20.69 kcal/mol relative to the separate reactants (R = **C** + **a**). Intermediate **1-Ca**$_{C3-C26}$ and **1-Ca**$_{C5-C26}$ shown in **Figure 5.7** are highly stable and are unlikely to revert to adducts. However, Int. **1-Ca**$_{C5-C26}$ is –16.44 kcal/mol lower in energy than Int. **1-Ca**$_{C3-C26}$. As a result, Int. **1-Ca**$_{C5-C26}$ is most likely to form among the two intermediates (Int. **1-Ca**$_{C3-C26}$ and **1-Ca**$_{C5-C26}$), but with a high chance of isomerisation. All three intermediates result in different Li27 interactions with **C** which plays a significant role in the stability of each structure. A similar mechanism of the formation of Int. **1-Ca**$_{C3-C26}$ is discussed in Chapter 3, Section 3.2.1.

97
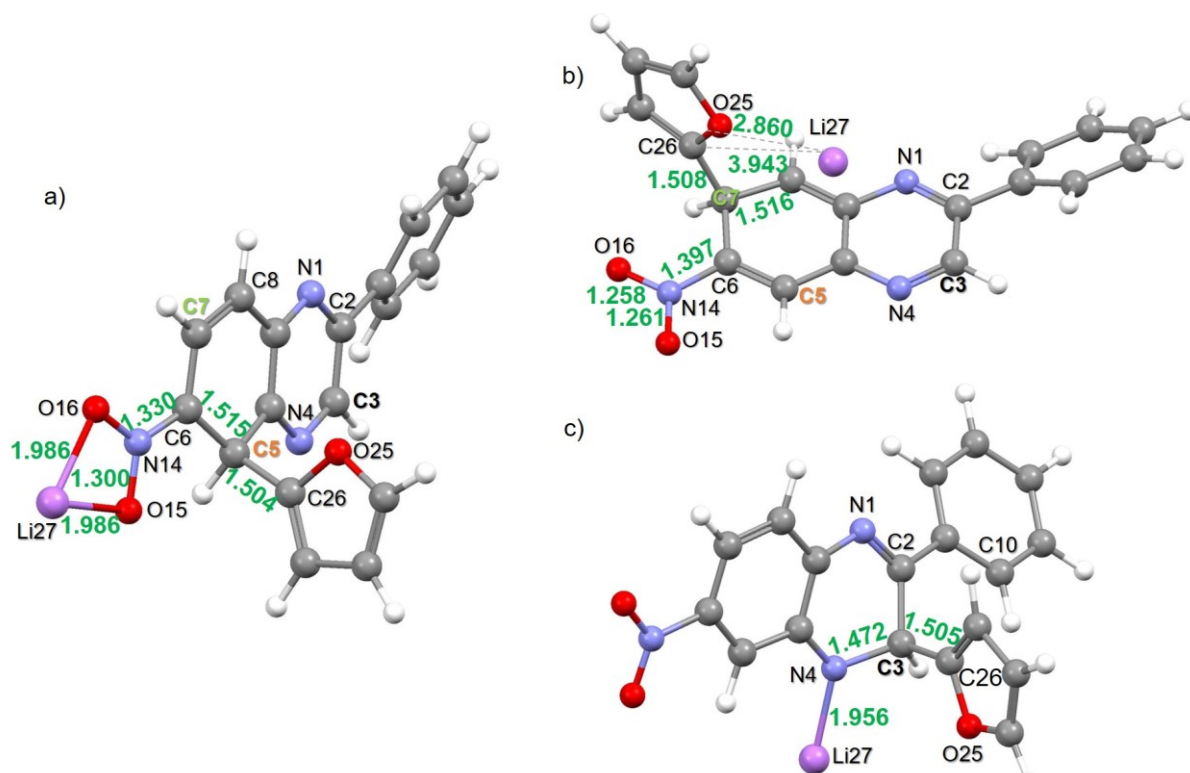
Figure 5.7: Intermediate a) **1-Ca**C5-C26, b) **1-Ca**C7-C26 and c) **1-Ca**C7-C26 involved in the nucleophilic addition of 6-nitro-2-phenylquinoxaline (**C**) with lithiofuran (**a**) at three electrophilic sites C5, C7 and C3 respectively

Intermediate **1-Ca**C5–C26 is more stable than **1-Ca**C3-C26 due to (i) the charge delocalisation not only in the ring but also in the -NO$_2$ group, (ii) reduced steric hindrance from not being adjacent to the phenyl ring and (iii) the bridging of the 4-membered complex shown in **Scheme 5.1**.
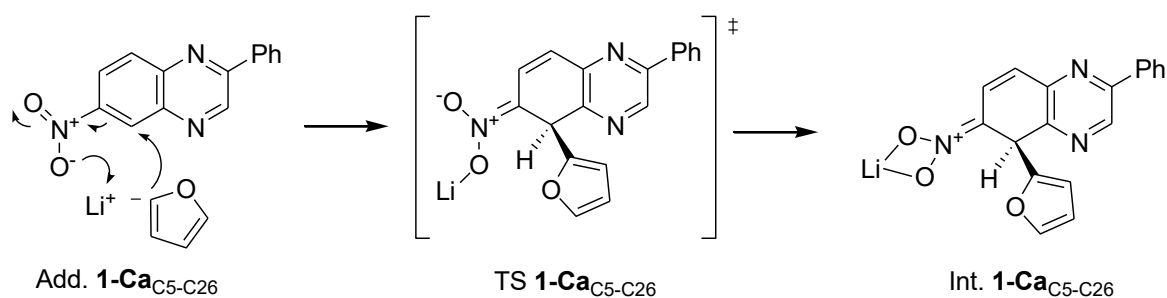
Scheme 5.1: Nucleophilic addition reaction of lithiofuran and 6-nitro-2-phenylquinoxaline at *ortho*-site C5

The formation of Int. **1-Ca**C7–C26 is also stabilised by charge delocalisation within the ring and the -NO$_2$ group. However, instead of a 4-membered complex, a radical Li$^+$ and two anionic oxygens are formed (**Scheme 5.2**). Looking at Int. **1-Ca**C5–C26 in **Scheme 5.1**, the oxygen anions

in **1-Ca**$_{C7-C26}$ occupy the bridging positions with lithium. Some neutral ligands such as THF have occasionally been reported in bridging roles to lithium,[24] but no form of coordination nor strong interaction occurs during the nucleophilic attack at C7.
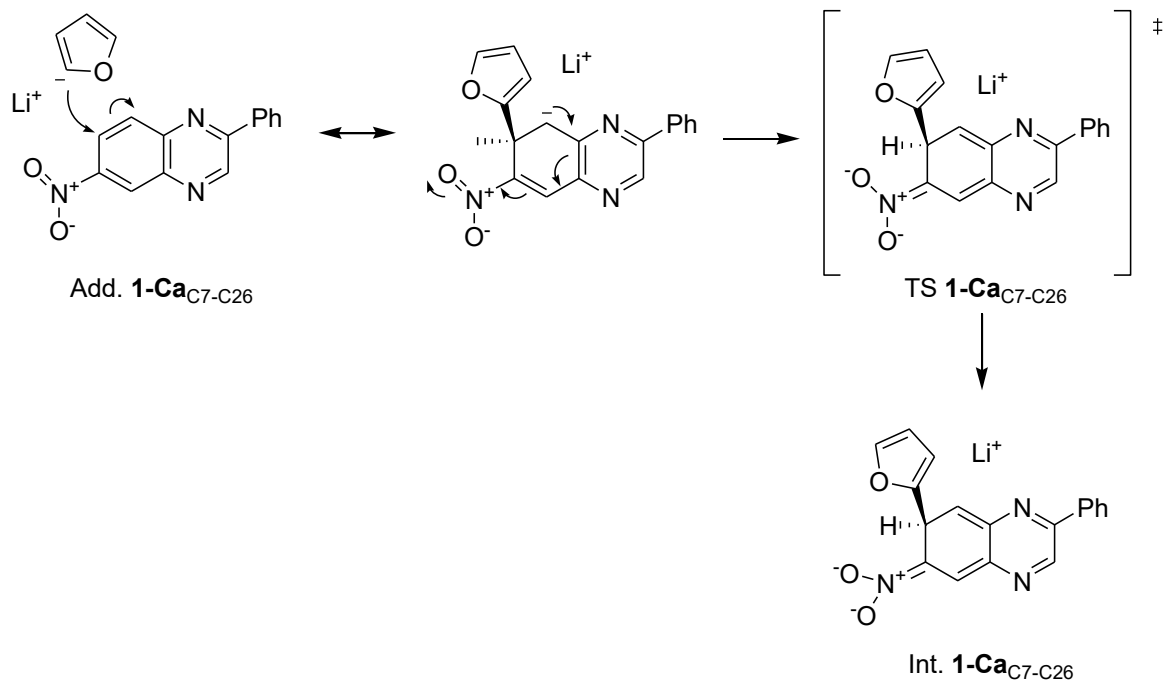
Scheme 5.2: Nucleophilic addition reaction of lithiofuran and 6-nitro-2-phenylquinoxaline at *ortho*-site C7

The formation of the 4-membered complex involves the elongation of bonds N14–O15 and N14–O16 by 0.032 Å and 0.046 Å (**Table 5.1**) respectively. Both intermediates involving C7 and C5 addition have comparable bond lengths of the newly formed C–C bonds (±1.506 Å).

Looking at enthalpy energies in **Figure 5.8**, it can be seen that all three reaction paths release energy (heat) via an exothermic reaction. However, the reaction involving C5–C26 bond formation is three and two times more exothermic than the reactions involving C7–C26 and C3–C26 bond formation respectively.

99
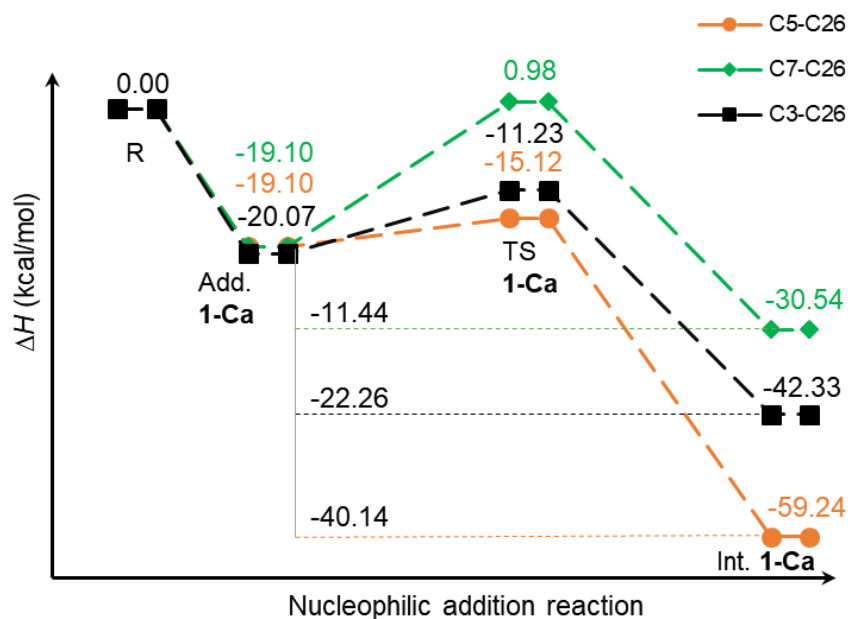
Figure 5.8: The reaction enthalpy energy profile of the nucleophilic addition reaction of 6-nitro-2-phenylquinoxaline (**C**) with lithiofuran (**a**) at three electrophilic sites: C3, C5 and C7

Furthermore, when we look at **Table 5.1**, we can see that the energies of the corrected zero-point vibrational energy (ZPVE) and thermal enthalpy are comparable (a difference between 0.3–0.64 kcal/mol). Thus, both the enthalpy and ZPVE reaction energy profiles have a similar trend to each other.

Table 5.1: Stationary points involved in the nucleophilic addition reaction of 6-nitro-2-phenylquinoxaline (**C**) and with lithiofuran (**a**) at different electrophilic sites (C3, C5 and C7). Structures are optimised in implicit THF solvent at –78 °C. Change in energies are measured relative to separate reactants

Systems	E	E_{ZPVE}	H	G
	Energy term in a.u.			
Reactants				
Lithiofuran (**a**)	–237.04795	–236.97100	–236.96738	–236.98881
6-nitro-2-phenylquinoxaline (**C**)	–853.77554	–853.57287	–853.56576	–853.59737
Nucleophilic Addition Reaction				
Add. **1-Ca**$_{C3-C19}$	–1090.84100	–1090.57581	–1090.56514	–1090.60620
Add. **1-Ca**$_{C5-C19}$	–1090.83910	–1090.57399	–1090.56358	–1090.60279
Add. **1-Ca**$_{C7-C19}$	–1090.83910	–1090.57399	–1090.56358	–1090.60280
TS **1-Ca**$_{C3-C19}$	–1090.82591	–1090.56099	–1090.55104	–1090.58939
TS **1-Ca**$_{C5-C19}$	–1090.83179	–1090.56698	–1090.55724	–1090.59464
TS **1-Ca**$_{C7-C19}$	–1090.80563	–1090.54150	–1090.53159	–1090.56964
Int. **1-Ca**$_{C3-C19}$	–1090.87791	–1090.61051	–1090.60060	–1090.63889
Int. **1-Ca**$_{C5-C19}$	–1090.90511	–1090.63726	–1090.62755	–1090.66510
Int. **1-Ca**$_{C7-C19}$	–1090.85800	–1090.59151	–1090.58181	–1090.61914
	Change in energy term (kcal/mol)			
	ΔE	ΔE_{ZPVE}	ΔH	ΔG
Add. **1-Ca**$_{C3-C19}$	–10.99	–20.04	–20.07	–12.56
Add. **1-Ca**$_{C5-C19}$	–9.80	–18.90	–19.10	–10.42
Add. **1-Ca**$_{C7-C19}$	–9.80	–18.90	–19.10	–10.43
TS **1-Ca**$_{C3-C19}$	–1.52	–10.74	-11.23	–2.01
TS **1-Ca**$_{C5-C19}$	–5.21	–14.50	–15.12	–5.31
TS **1-Ca**$_{C7-C19}$	11.20	1.49	0.98	10.38
Int. **1-Ca**$_{C3-C19}$	–34.15	–41.82	–42.33	–33.08
Int. **1-Ca**$_{C5-C19}$	–51.22	–58.60	–59.24	–49.52
Int. **1-Ca**$_{C7-C19}$	–21.66	–29.90	–30.54	–20.69

5.3   Conclusion

The reaction of quinoxaline derivatives with lithiofuran (**a**) involves a direct nucleophilic attack on an activated electron-deficient system, this eventually forms σ^H-adduct complexes of various stabilities. The presence of the nitro group ($-NO_2$) on a quinoxaline derivative forms a significantly more stable σ^H-adduct, thus allowing for easy isolation and detection of the complex by spectroscopic techniques. The $-NO_2$ group has a higher polarising effect than two of the already incorporated aza groups in the quinoxaline molecule. However, incorporating –

NO$_2$ to an already electrophilic quinoxaline ring results in regio-selectivity issues, forming σ^H-adduct regio-isomers and thus leading to competing reaction paths.

The favoured reaction path at C5 (*ortho* to –NO$_2$), directed by the –NO$_2$ group, forms a σ^H-adduct with the formation of a 4-membered ring. To the best of our knowledge, no such case has been reported on quinoxaline derivatives. The least-favoured reaction path, nucleophilic addition reaction at C7 (also *ortho* to –NO$_2$) forms a σ^H-adduct consisting of a radical Li$^+$ atom rather than a 4-membered complex. The preferred reactive site is at C5 and is favoured due to (i) reduced steric hindrance, (ii) the formation of the 4-membered complex, and (iii) charge delocalisation within the ring and the –NO$_2$ group.

Overall, the nitroarenes form better σ^H–adducts than azines. However, the incorporation of –NO$_2$ to an already electron-deficient quinoxaline ring is not ideal, unless the other reactive sites are deactivated/protected. Regio-selectivity of the reactions is likely to affect the isolation of the desired σ^H-adducts and the reaction yield of the final product.

5.4   References

1.   Sheldon, R. A., Arends, I. & Hanefeld, U. *Green chemistry and catalysis*. *John Wiley & Sons* (John Wiley & Sons, 2007).

2.   Gulevskaya, A. V & Pozharskii, A. F. Nucleophilic aromatic substitution of hydrogen as a tool for heterocyclic ring annulation. *Adv. Heterocycl. Chem.* **93**, 57–115 (2007).

3.   Idoux, J. P., Chupakhin, O. N., Charushin, V. N. & Plas, H. C. van der. Nucleophilic Aromatic Substitution of Hydrogen. *J. Am. Chem. Soc.* **118**, 2310 (1996).

4.   Chupakhin, O. N., Charushin, V. N. & Van der Plas, H. C. *Nucleophilic aromatic substitution of hydrogen*. (Academic Press, 1994).

5.   Charushin, V. N. & Chupakhin, O. N. Metal-free C–H functionalization of aromatic compounds through the action of nucleophilic reagents. in *Metal Free CH Functionalization of Aromatics* 1–50 (Springer, 2014).

6.   Clegg, W., Dunbar, L., Horsburgh, L. & Mulvey, R. E. Stoichiometric Dependence of the Long-Established Reaction of Butyllithium ith Pyridine: A Hidden Secondary Reaction That Produces a Pyridine Adduct. *Angew. Chemie.* **35**, 753 (1996).

7.   Kovalev, I. S. *et al.* Organolithium compounds in the nucleophilic substitution of hydrogen in arenes and hetarenes. *Russ. Chem. Rev.* **84**, 1191–1225 (2015).

8.   Fraenkel, G. & Cooper, J. C. Structure of butyllithium-pyridine adducts. *Tetrahedron Lett.* **9**, 1825–1830 (1968).

9.   Bubnov, Y. N., Klimkina, E. V, Starikova, Z. A. & Ignatenko, A. V. Reductive mono- and diallylation of the bis (pyridine) dihydropyridyllithium dimer by triallylborane. *Russ. Chem. Bull.* **50**, 1078–1084 (2001).

10.   Pereira, J. A. *et al.* Quinoxaline, its derivatives and applications: A State of the Art review. *Eur. J. Med. Chem.* **97**, 664–672 (2015).

11.   Sharma, B. K., Shaikh, A. M., Chacko, S. & Kamble, R. M. Synthesis, Spectral, Electrochemical and Theoretical Investigation of indolo[2,3-b]quinoxaline dyes derived from Anthraquinone for n–type materials. *J. Chem. Sci.* **129**, 483–494 (2017).

12.   Le Douaron, G. *et al.* Neuroprotective effects of a brain permeant 6-aminoquinoxaline derivative in cell culture conditions that model the loss of dopaminergic neurons in Parkinson disease. *Eur. J. Med. Chem.* **89**, 467–479 (2015).

13.   Le Douaron, G. *et al.* New 6-Aminoquinoxaline Derivatives with Neuroprotective Effect on Dopaminergic Neurons in Cellular and Animal Parkinson Disease Models. *J. Med. Chem.* **59**, 6169–6186 (2016).

14.   Potey, L. C., Kosalge, S. B. & Hadke, M. A. Synthesis and antimicrobial activity of quinoxaline sulfonamide. *Int. J. Adv. Sci. Technol* **2**, 126–134 (2013).

15.   Ramalingam, P., Ganapaty, S. & Rao, C. B. In vitro antitubercular and antimicrobial activities of 1-substituted quinoxaline-2, 3 (1H, 4H)-diones. *Bioorg. Med. Chem. Lett.* **20**, 406–408 (2010).

16.   Singh, D. P., Deivedi, S. K., Hashim, S. R. & Singhal, R. G. Synthesis and antimicrobial activity of some new quinoxaline derivatives. *Pharmaceuticals* **3**, 2416–2425 (2010).

17.   Ndlovu, N. T. & Nxumalo, W. Nucleophilic substitution on 2-monosubstituted quinoxalines giving 2,3-disubstituted quinoxalines: Investigating the effect of the 2-Substituent. *Molecules* **21**, 1304 (2016).

18.   Wu, Y., Wang, J., Mao, F. & Kwong, F. Y. Palladium-catalyzed cross-dehydrogenative functionalization of C(sp^2)-H bonds. *Chem. - An Asian J.* **9**, 26–47 (2014).

19. Girard, S. A., Knauber, T. & Li, C. The Cross-Dehydrogenative Coupling of C–H Bonds: A Versatile Strategy for C–C Bond Formations. *Angew. Chemie Int. Ed.* **53**, 74–100 (2014).

20. Heravi, M. M., Hashemi, E. & Azimian, F. Recent developments of the Stille reaction as a revolutionized method in total synthesis. *Tetrahedron* **1**, 7–21 (2014).

21. Smith, M. March's advanced organic chemistry : reactions, mechanisms, and structure. (2013).

22. Zhang, C. Review of the establishment of nitro group charge method and its applications. *J. Hazard. Mater.* **161**, 21–28 (2009).

23. Jarek, R. L., Miles, T. D., Trester, M. L., Denson, S. C. & Shin, S. K. Solvation of Li+ by acetone, THF, and diethyl ether in the Gas phase and the ion-molecule association mechanism. *J. Phys. Chem. A* **104**, 2230–2237 (2000).

24. Clegg, W., Horsburgh, L., Mackenzie, F. M. & Mulvey, R. E. Dis-assembling lithium amide ladder structures: structural elucidation of the lithium anilide solvate [{PhN(H)Li}6·8THF], a model intermediate En route to forming tetra-solvated ring dimers. *J. Chem. Soc. Chem. Commun.* 2011–2012 (1995).

Chapter 6

CONCLUSIONS

6.1 Conclusion

The nucleophilic substitution of hydrogen (S_NH methodology) complements conventional cross-coupling reactions,[1–4] and data acquired over the last two decades is starting to make the S_NH reaction look like a new chapter in aromatic chemistry. As a result of the common character of the S_NH reaction, synthesising and modelling of new reactions provides a possibility of extending these metal-catalysed cross-coupling reactions.

Density functional theory (DFT) was used to study the reaction mechanism of 2-monosubstituted quinoxalines with organolithium compounds. The study shows that the reaction of the case in hand follows the mechanism of oxidative nucleophilic substitution of hydrogen (ONSH). This is a sub-topic of the S_NH reaction mechanism. Among many advantages of the ONSH mechanism is its inessential use of catalysts (transition metals) and its non-requirement for preliminary functionalisation.

The energy barriers of the reactions studied (experimentally performed by Nxumalo[4]) were predicted using DFT. The entire ONSH reaction is controlled by the rate-determining nucleophilic addition (step-**1**, which involves the formation of the intermediate "σ^{H-}adduct") followed by the hydrolysis reaction (step-**2**) and finally the oxidation reaction (step-**3**).

It has been established that the reactants 2-monosubstituted quinoxaline and organolithium compounds must overcome a free energy barrier, $\Delta G^{\ddagger}$, of ~15 kcal/mol to form transition states (TSs), followed by the formation of very stable intermediates. For a reverse reaction from the intermediates to the reactants, the reaction must overcome +24 kcal/mol; this is a significant energy barrier which shows that the reverse reaction will not take place. The subsequent hydrolysis reaction has a minor energy barrier; hence hydrolysis is the preferred reaction path over the reverse reaction.

The formation of the σ^{H-}adduct intermediate results in sp-hybridised carbon (C3) of tetrahedral geometry. However, the acidic α-hydrogen (H3) remains bonded to C3, thus preventing the formation of LiH as a by-product of step-**1**. This is contrary to the literature, in which it was hypothesised that LiH is a by-product of the ONSH reaction.[7,8] In fact, computational modelling showed that no by-product is formed in step-**1** of this reaction.

Interestingly, introducing water to the σ^H-adduct intermediate results in a spontaneous hydrolysis reaction (step-**2**) from which a second intermediate and LiOH as the first by-product are formed. The formation of LiOH is associated with the formation of an amine-group at N4 of the quinoxaline derivative. Importantly, it has been discovered that the very same LiOH plays a role as a precursor in the subsequent oxidation reaction, which requires an external reagent O_2.

With the main issue being the elimination of the leaving group α-hydrogen, the presence of O_2 as the oxidising agent allowed the following:

(i)   Elimination of α-hydrogen

(ii)   Conversion from an amine (sp^3-hybridisation) molecule back to an imine (sp^2-hybridisation)

(iii)   Conversion of σ^H-adducts into stable products of 2,3-disubstituted-quinoxaline

(iv)   Formation of hydrogen peroxide (H_2O_2) as the second by-product of ONSH

(v)   Ring rearrangement to planar geometry and re-aromatisation,

Since the hydrogen peroxide can easily break down into water, and with the use of O_2 from the atmospheric air, the reaction is ecologically attractive because it provides a better match with the principles of green chemistry.[9]

The oxidation of the hydrolysis intermediates is essentially spontaneous and barrierless; it forms the crude products of ONSH. All three products (2,3-disubstituted-quinoxaline, Li–OH and H_2O_2) of each reaction contribute highly to the stability, Δ**G**, of the crude products with energies below –74 kcal/mol (Prod. **3-Aa** = –77.80 kcal/mol, Prod. **3-Ba** = –78.83 kcal/mol and Prod. **3-Ab** = –74.04 kcal/mol).

It is worth mentioning that prior to this study there was little evidence to suggest the mechanism reported in this work. As a matter of fact, to the best of our knowledge, no mechanism has been reported on the formation of the by-products mentioned. The findings reported are very insightful, and it is believed that most of these observations would not have been noted if other analytical approaches had been used.

Several factors affect the stability of the stationary points of the ONSH reaction:

(i)   The presence of phenyl and n-butyl substituents on 2-phenylquinoxaline (**A**) and 2-*n*-butylquinoxaline (**B**) have no significant influence on steric effect and stability.

(ii)   The use of lithiofuran (**a**) as a nucleophile instead of lithiothiophene (**b**) has a more stabilising effect (>10 kcal/mol) on the products of the ONSH reaction. This is influenced by the high electronegativity of the O-atom compared to the S-atom and its inter- and intra-molecular non-classical hydrogen bonds (NCHB) CH···O.

(iii) Changing the reaction temperature from 195.15 K to 298.15 K significantly destabilises all stationary points of the ONSH reaction. However, the reactions are viable at both temperatures, but due to the decomposition of organolithium compounds at high temperatures,[10] water freezing at low temperatures (below 273.15 K) and the introduction of atmospheric air,[4] step-**1** occurs preferentially at 195.15 K. Once it reaches equilibrium, the reaction can be warmed up to 298.15 K to allow step-**2,** which essentially allows step-**3**. According to experimental data water was never explicitly introduced in the reaction vessel, Chupakin et al.[11] did mention that an increase in the temperature of the system from 0 °C to 100 °C at the intermediates' σ^H-adducts formation step is equivalent to hydrolysis followed by oxidation.

(iv)   The inclusion of two explicit THF solvent molecules to the implicitly modelled reactions resulted in their coordination to the Li-atom. What is important is that it has been established that the solvent molecules stabilised the stationary points of the ONSH reactions. Modelling the reaction in explicit solvent resulted in a ~4 kcal/mol reduction in free energy barrier, $\Delta G^{\ddagger}$.

The points highlighted in (i), (ii) and (iii) above had little to no effect on the activation energy. As a result, all three reactions of **A** and **B** each with **a**, and **A** with **b,** have comparable reactivity. They should therefore afford similar reaction yields. From this work it follows that, since product yields can also be affected by several experimental errors during the synthesis of the products, the initial conditions/steps of the synthetic process must be carefully re-examined and optimised.

With only two reactive sites to 2-monosubstituted-quinoxaline, a possible competing nucleophilic reaction at C2 of **A** or **B** forms a σ^C-adduct. However, this nucleophilic addition

reaction has a dramatic free energy barrier of $\Delta G^{\ddagger} = 29.94$ kcal/mol, which makes it impossible for it to compete with the nucleophilic addition at C3.

The S_NArH mechanism has been known mostly as C–H functionalisation of haloaromatic compounds and para-deficient nitro (-NO$_2$) aromatic systems.[12,13] However, the scope of S_NArH reactions shows that it is not restricted by the participation of the substituent. Even so, aza (R-N-R) aromatic systems have been ignored due to the less polarising effect of the aza group compared to nitro-activated systems. To this effect, -NO$_2$ was placed at C6 of **A** to form 6-nitro-2-phenylquinoxaline (**C**), which made the quinoxaline derivative more susceptible to nucleophile "**a**" attack, therefore forming σ^H-adducts. The nucleophilic attack at C3 between **C** and **a** is –4.88 kcal/mol lower in activation energy than the reactions of **A** and **a**. However, the former reaction results in regio-isomers of the nucleophilic attack at C7 and C5. This means that the reaction results in three competing reactions.

The electrophilicity and, most importantly, the regio-selectivity of the **C** is mostly activated by the nitro groups. This allows for a more dominant reaction path and reactive reaction at C5. All three reactions (nucleophilic addition at C3, C5 and C7) are exothermic, with the reaction at C7 being the least exothermic. This makes the C7 σ^H-adduct intermediate more susceptible to dissociation to form reactants. This intermediate will therefore be hard to dissociate, which will make it hard to detect using spectroscopic techniques, contrary to the intermediates of reactions C5 and C3 attack.

In conclusion, we can say that the results of computational data require guidance from experimental data for validation. Experimental work may have the inability to reveal important mechanistic information that computational organic chemistry can reveal. However, this information must be standardised by experimental evidence to confirm its physical relevance. More importantly, a low-energy barrier does not mean that the process corresponds to what is happening in solution. Furthermore, a reaction path which is energetically viable does not mean that it is the only mechanistic pathway.

6.2   Future Work

The nucleophiles and temperature seem to influence the stability of the modelled reaction mechanism. Therefore, further studies should be conducted with other nucleophiles, such as n-BuLi, PhLi, and Mg-based nucleophiles (e.g. Me-MgCl, and *i*-PrMgCl) to determine whether they share the same reaction mechanism. Furthermore, the reaction temperature can be changed to anything between 298.15 K and 195.15 K to further understand the influence of temperature on the reaction steps. The addition of electron-withdrawing groups (EWG)/electron-donating groups (EDG) on 2-monosubstituted quinoxalines would provide insightful information that would reflect their influence on competing reactive sites and what affects the mechanism's activation energy most, in other words the reaction rates.

The competing reactions should be verified using experimental data, and products would have to be identified using analytical instruments. Further computational modelling is recommended to gain insight into the relative stability of complexes. This includes Interacting Quantum Atoms (IQA) and the Quantum Theory of Atoms in Molecules (QTAIM) as these can provide important insight into the strength and nature of atomic interactions. This kind of computational data could then be used to determine whether there is any correlation with geometric analysis, e.g. interatomic distances.

It is also advisable to use Grimme's empirical dispersion (GD3) together with an aug-cc-pVDZ basis set. This basis set is better to a small extent than 6-311++(G(d,p), which was the one used in this study. For an optimal computational study/results, one may optimise the most important B3LYP-generated structures at a higher level of theory, preferably CCSD. The differences in the level of theories and basis set would provide comparative data that should be useful in evaluating whether the B3LYP/aug-cc-pVDZ/GD3 level of theory is good enough to explain relatively small differences in reactivity, driving forces, etc. Due to the high demand in computational cost these calculations were not done in this study.

6.3 References

1. Girard, S. A., Knauber, T. & Li, C. The Cross-Dehydrogenative Coupling of C–H Bonds: A Versatile Strategy for C–C Bond Formations. *Angew. Chemie Int. Ed.* **53**, 74–100 (2014).

2. Wu, Y., Wang, J., Mao, F. & Kwong, F. Y. Palladium-catalyzed cross-dehydrogenative functionalization of C(sp 2)-H bonds. *Chem. - An Asian J.* **9**, 26–47 (2014).

3. Heravi, M. M., Hashemi, E. & Azimian, F. Recent developments of the Stille reaction as a revolutionized method in total synthesis. *Tetrahedron* **1**, 7–21 (2014).

4. Ndlovu, N. T. & Nxumalo, W. Nucleophilic substitution on 2-monosubstituted quinoxalines giving 2,3-disubstituted quinoxalines: Investigating the effect of the 2-Substituent. *Molecules* **21**, 1304 (2016).

5. Verbitskiy, E. V. *et al.* Synthesis, and structure-activity relationship for C(4) and/or C(5) thienyl substituted pyrimidines, as a new family of antimycobacterial compounds. *Eur. J. Med. Chem.* **97**, 225–234 (2015).

6. Verbitskiy, E. V. *et al.* Synthesis, spectral and electrochemical properties of pyrimidine-containing dyes as photosensitizers for dye-sensitized solar cells. *Dye. Pigment.* **100**, 201–214 (2014).

7. Geissman, T. A., Schlatter, M. J., Webb, I. D. & Roberts, J. D. The synthesis of some intermediates for use in the preparation of analogs of salicylaldehyde ethylenediimine cobalt ("salcomine"). *J. Org. Chem.* **11**, 741–750 (1946).

8. Gilman, H. & Edward, J. T. Studies in the Preparation of Antimalarials From Pyridine. *Can. J. Chem.* **31**, 457–468 (1953).

9. Utepova, I. A., Trestsova, M. A., Chupakhin, O. N., Charushin, V. N. & Rempel, A. A. Aerobic oxidative C-H/C-H coupling of azaaromatics with indoles and pyrroles in the presence of TiO2 as a photocatalyst. *Green Chem.* **17**, 4401–4410 (2015).

10. Contigiani, R. A., Bertorello, H. E. & de Bertorello, M. M. Reactions and thermal decomposition of organolithium compounds derived from 4,4′-dibromooctafluorobiphenyl. *J. Organomet. Chem. TA - TT -* **32**, 7–15 (1971).

11. Kovalev, I. S. *et al.* Organolithium compounds in the nucleophilic substitution of hydrogen in arenes and hetarenes. *Russ. Chem. Rev.* **84**, 1191–1225 (2015).

12. Blaziak, K., Danikiewicz, W. & Mąkosza, M. How Does Nucleophilic Aromatic Substitution Really Proceed in Nitroarenes? Computational Prediction and Experimental Verification. *J. Am. Chem. Soc.* **138**, 7276–7281 (2016).

13. Mąkosza, M. Reactions of nucleophiles with nitroarenes: Multifacial and versatile electrophiles. *Chem. - A Eur. J.* **20**, 5536–5545 (2014).

Appendix A

SUPPLEMENTARY INFORMATION FOR CHAPTER 3

Table 0.1: 2-butylquinoxaline conformers. All structures were optimised in implicit THF solvent at –78 °C (195.15 K)

Conformers	E (a.u.)	ΔE rel. (kcal/mol)
c1	–575.18789	0.30
c2	–575.18837	0.00
c3	–575.18802	0.22
c4	–575.18722	0.72
c5	–575.18624	1.33
c6	–575.18758	0.49
c7	–575.18740	0.61
c8	–575.18577	1.63
c9	–575.18585	1.58

Table 0.2: Conformers of lithiofuran (**a**) with two explicitly solvated THF molecules

Conformers	E (a.u.)	ΔE rel. (kcal/mol)
c1	–702.14042	0.22
c2	–702.14078	0.00
c3	–702.14027	0.32
c4	–702.14061	0.10
c5	–702.14018	0.38
c6	–702.13986	0.57

Table 0.3: Stationary points involved in the nucleophilic addition reaction of Int. **1-Aa$_e$** and Int. **1-Ba$_e$**, with the presence of two explicit THF solvent molecules. All structures were optimised in implicit THF solvent at –78 °C (energies in kcal/mol)

Add. **1-Ba$_e$** (ΔG = –0.87, ΔE = –12.19)	Add. **1-Aa$_e$**, (ΔG = –2.58, ΔE = –12.88)
TS **1-Ba$_e$** (ΔG = 9.58, ΔE = –1.67)	TS **1-Aa$_e$** (ΔG = 10.11, ΔE = –3.14)
Int. **1-Ba$_e$** (ΔG = –15.63, ΔE = –28.99)	Int. **1-Aa$_e$** ΔG = –19.99, ΔE = –32.47)

3
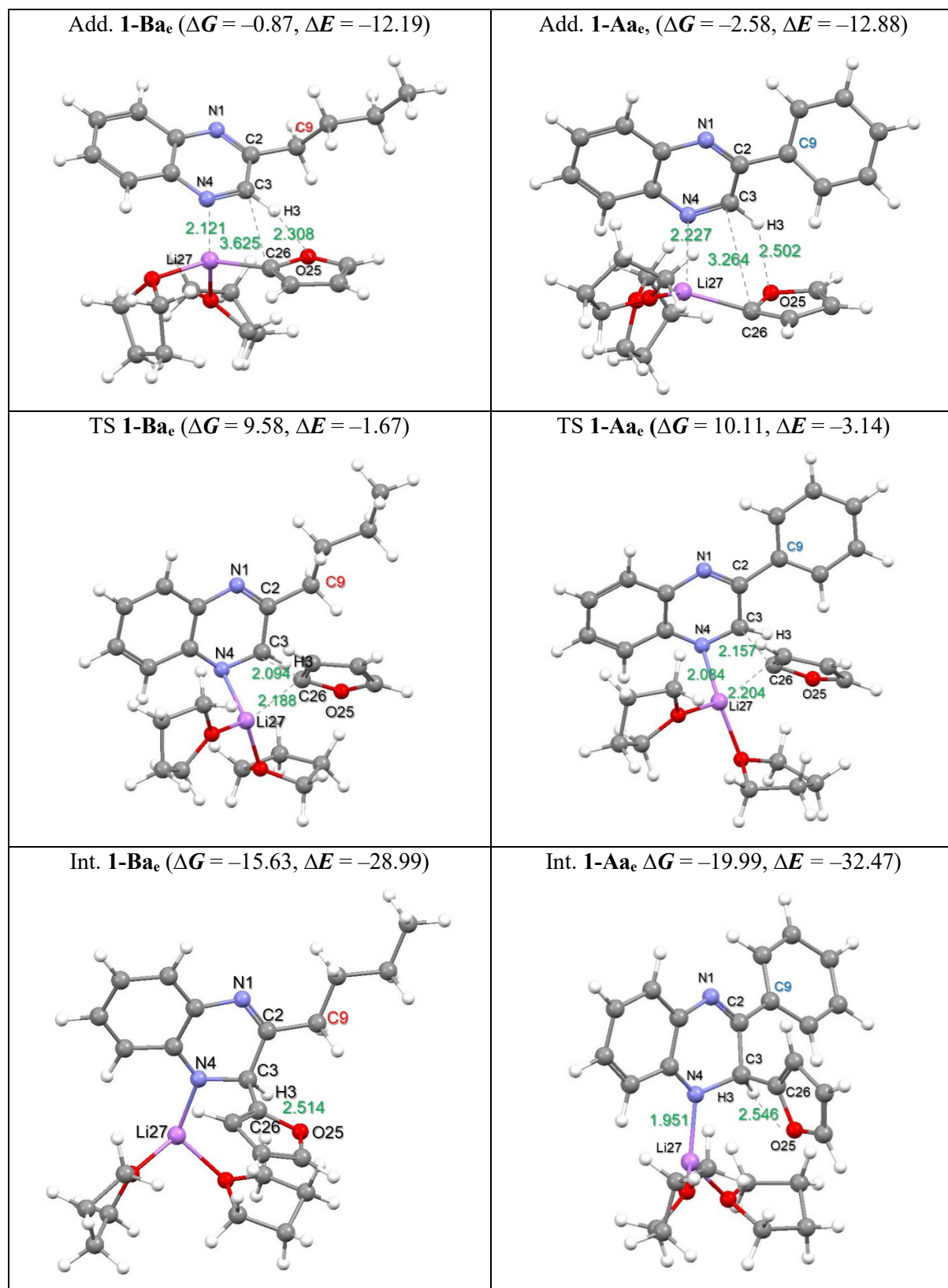
Table 0.4: Relative energies of conformational structures of the two THF explicitly solvated lithiofuran solvent molecules

Separate molecules	Conformers	E (a.u.)	ΔE (kcal/mol)
Single THF Molecule		–232.52394	
Lithiofuran		–237.04795	
Lithiofuran + 2 THF Molecules	c1	–702.14042	0.22
	c2	–702.14078	0.00
	c3	–702.14027	0.32
	c4	–702.14061	0.10
	c5	–702.14018	0.38

Table 0.5: Adduct stationary points involved in hydrolysis reaction. All data result from optimised structures in implicit THF solvent using B3LYP/6-311++G(d, p) at 25 °C

Systems	E	E_{ZPVE}	H	G
	Energy term in a.u.			
Reactants				
Lithiofuran **(a)**	–237.04795	–236.97100	–236.96738	–236.98881
2-phenylquinoxaline **(A)**	–886.29586	–886.03059	–886.02211	–886.05648
H_2O	–76.46503	–76.44382	–76.44004	–76.46147
Nucleophilic Addition				
Add. **1-Aa$_{c1}$**	–962.77778	–962.48903	–962.46768	–962.54095
Add. **1-Aa$_{c2}$**	–962.78243	–962.49232	–962.47133	–962.54229
Add. **1-Aa$_{c3}$**	–962.77883	–962.48888	–962.46829	–962.53761
Add. **1-Aa$_{c4}$**	–962.77897	–962.48919	–962.46840	–962.53869
Add. **1-Aa$_{c5}$**	–962.77821	–962.48841	–962.46743	–962.53876
Add. **1-Aa$_{c6}$**	–962.77535	–962.48613	–962.46464	–962.53704
	Change in energy term (kcal/mol)			
	ΔE	ΔE_{ZPVE}	ΔH	ΔG
Add. **1-Aa$_{c1}$**	–10.60	–9.18	–3.47	–14.43
Add. **1-Aa$_{c2}$**	–13.52	–11.24	–5.76	–15.27
Add. **1-Aa$_{c3}$**	–11.25	–9.08	–3.85	–12.33
Add. **1-Aa$_{c4}$**	–11.35	–9.27	–3.92	–13.01
Add. **1-Aa$_{c5}$**	–10.87	–8.78	–3.31	–13.06
Add. **1-Aa$_{c6}$**	–9.07	–7.36	–1.56	–11.98

Table 0.6: Stationary points involved in ONSH reaction. All data result from optimised structures in implicit THF solvent using B3LYP/6-311++G(d, p) at –78 °C

Systems	E	E_{ZPVE}	H	G
	Energy term in a.u.			
Reactants				
Lithiofuran **(a)**	–237.04795	–236.97100	–236.96738	–236.98881
2-phenylquinoxaline **(A)**	–649.21024	–649.00667	–649.00095	–649.02883
2-n-butylquinoxaline **(B)**	–575.40101	–575.16529	–575.15883	–575.18838
H_2O	–76.46503	–76.44382	–76.44135	–76.45433
O_2	–150.30980	–150.30610	–150.30393	–150.31757
Nucleophilic Addition				
Add. **1-Aa**	–886.27440	–886.01131	–886.00188	–886.03993
Add. **1-Ba**	–812.46455	–812.16924	–812.15916	–812.19879
TS **1-Aa**	–886.25185	–885.98912	–885.98054	–886.01534
TS **1-Ba**	–812.44180	–812.14656	–812.13748	–812.17296
Int. **1-Aa**	–886.29806	–886.03272	–886.02426	–886.05862
Int. **1-Ba**	–812.48470	–812.18788	–812.17858	–812.21458
Hydrolysis				
Add. **2-Aa**	–962.78243	–962.49233	–962.48233	–962.52008
Add. **2-Ba**	–888.96892	–888.64670	–888.63613	–888.67464
TS **2-Aa**	–962.77558	–962.49009	–962.48041	–962.51758
TS **2-Ba**	–888.96309	–888.64552	–888.63526	–888.67329
Int. **2-Aa**	–962.78655	–962.49670	–962.48645	–962.52493
Int. **2-Ba**	–888.97504	–888.65319	–888.64235	–888.68181
Oxidation				
Prod. **3-Aa**	–1113.21149	–1112.91650	–1112.90452	–1112.94837
Prod. **3-Ba**	–1039.40966	–1039.08209	–1039.05775	–1039.13624
	Change in energy term (kcal/mol)			
	ΔE	ΔE_{ZPVE}	ΔH	ΔG
Nucleophilic Addition				
Add. **1-Aa**	–10.17	–21.11	–21.05	–13.99
Add. **1-Ba**	–9.78	–20.68	–20.68	–13.56
TS **1-Aa**	3.98	–7.18	–7.66	1.44
TS **1-Ba**	4.50	–6.44	–7.07	2.65
Int. **1-Aa**	–25.02	–34.54	–35.10	–25.72
Int. **1-Ba**	–22.42	–32.37	–32.86	–23.47
Hydrolysis				
Add. **2-Aa**	–37.15	–44.45	–45.59	–30.20
Add. **2-Ba**	–34.46	–41.78	–43.03	–27.06
TS **2-Aa**	–32.85	–43.05	–44.38	–28.62
TS **2-Ba**	–30.81	–41.04	–42.48	–26.21
Int. **2-Aa**	–39.74	–47.19	–48.17	–33.24
Int. **2-Ba**	–38.30	–45.86	–46.93	–31.57
Oxidation				
Prod. **3-Aa**	–111.99	–118.54	–119.80	–99.68
Prod. **3-Ba**	–116.63	–122.91	–116.88	–117.44

Table 0.7: Stationary points involved in ONSH reaction. All data result from optimised structures in implicit THF solvent using B3LYP/6-311++G(d, p) at 25 °C

Systems	E	E_{ZPVE}	H	G
	Energy term in a.u.			
Reactants				
Lithiofuran **(a)**	–237.04795	–236.99026	–236.98401	–237.01877
2-phenylquinoxaline **(A)**	–649.21026	–649.00667	–648.99445	–649.04487
2-n-butylquinoxaline **(B)**	–575.40101	–575.16530	–575.15205	–575.20534
H_2O	–76.46503	–76.44382	–76.44004	–76.46147
O_2	–150.30980	–150.30610	–150.30279	–150.32502
Nucleophilic Addition				
Add. **1-Aa**	–886.27440	–886.01131	–885.99201	–886.06209
Add. **1-Ba**	–812.46455	–812.16924	–812.14901	–812.22186
TS **1-Aa**	–886.25185	–885.98912	–885.97104	–886.03569
TS **1-Ba**	–812.44180	–812.14656	–812.12771	–812.19374
Int. **1-Aa**	–886.29580	–886.03042	–886.01244	–886.07630
Int. **1-Ba**	–812.48470	–812.18788	–812.16869	–812.23567
Hydrolysis				
Add. **2-Aa**	–962.78243	–962.49232	–962.47133	–962.54229
Add. **2-Ba**	–888.96892	–888.64670	–888.62483	–888.69735
TS **2-Aa**	–962.77558	–962.49009	–962.46970	–962.53945
TS **2-Ba**	–888.96309	–888.64552	–888.62427	–888.69568
Int. **2-Aa**	–962.78655	–962.49670	–962.47550	–962.54755
Int. **2-Ba**	–888.97504	–888.65319	–888.63108	–888.70503
Oxidation				
Prod. **3-Aa**	–1113.21149	–1112.91650	–1112.89219	–1112.97412
Prod. **3-Ba**	–1039.40966	–1039.08209	–1039.05775	–1039.13623
	Change in energy term (kcal/mol)			
	ΔE	ΔE_{ZPVE}	ΔH	ΔG
Nucleophilic Addition				
Add. **1-Aa**	–10.16	–9.02	–8.50	0.98
Add. **1-Ba**	–9.78	–8.58	–8.13	1.42
TS **1-Aa**	3.99	4.90	4.66	17.54
TS **1-Ba**	4.50	5.65	5.24	19.06
Int. **1-Aa**	–23.59	–21.02	–21.32	–7.94
Int. **1-Ba**	–22.42	–20.28	–20.48	–7.25
Hydrolysis				
Add. **2-Aa**	–37.14	–32.36	–33.15	–10.78
Add. **2-Ba**	–34.46	–29.69	–30.58	–7.38
TS **2-Aa**	–32.84	–30.96	–32.13	–9.00
TS **2-Ba**	–30.81	–28.95	–30.23	–6.33
Int. **2-Aa**	–39.72	–35.10	–35.77	–14.08
Int. **2-Ba**	–38.30	–33.76	–34.50	–12.20
Oxidation				
Prod. **3-Aa**	–111.98	–106.45	–107.24	–77.80
Prod. **3-Ba**	–116.63	–110.82	–112.24	–78.83

Table 0.8: Stationary points involved in the formation of σ^C-adduct (nucleophilic addition reaction) of Li-furan (**a**) with 2-phenylquinoxaline (**A**) at carbon 2. All structures were optimised in implicit THF solvent using B3LYP/6-311++G(d, p) at –78 °C

Systems	*E*	*E*$_{ZPVE}$	*H*	*G*
	Energy term in a.u.			
Reactants				
Lithiofuran (**a**)	–237.04795	–236.97100	–236.96738	–236.98881
2-phenylquinoxaline (**A**)	–649.21024	–649.00667	–649.00095	–649.02883
Nucleophilic Addition				
Add. **1-Aa**$_{C2-C26}$	–886.27440	–886.01131	–886.00188	–886.03993
TS **1-Aa**$_{C2-C26}$	–886.22901	–885.96700	–885.95867	–885.99222
Int. **1-Aa**$_{C2-C26}$	–886.27794	–886.02416	–886.01597	–886.04949
	Change in energy term (kcal/mol)			
	Δ*E*	Δ*E*$_{ZPVE}$	Δ*H*	Δ*G*
Nucleophilic Addition				
Add. **1-Aa**$_{C2-C26}$	–10.17	–21.11	–21.05	–13.99
TS **1-Aa**$_{C2-C26}$	18.31	6.70	6.07	15.95
Int. **1-Aa**$_{C2-C26}$	–12.40	–29.17	–29.90	–19.99

Appendix B

Table 0.1: Stationary points involved in ONSH reaction of **A** with **a** and **b**. All data results from optimised structures in implicit THF solvent using B3LYP/6-311++G(d, p) at 25 °C

Systems	E	E_{ZPVE}	H	G
	Energy term in a.u.			
Reactants				
Lithiofuran **(a)**	–237.04795	–236.99026	–236.98401	–237.01877
2-phenylquinoxaline **(A)**	–649.21026	–649.00667	–648.99445	–649.04487
Lithiothiophene **(b)**	–560.03717	–559.98197	–559.97555	–560.01091
H_2O	–76.46503	–76.44382	–76.44004	–76.46147
O_2	–150.30980	–150.30610	–150.30279	–150.32502
1- Nucleophilic Addition				
Add. **1-Aa**	–886.27440	–886.01131	–885.99201	–886.06209
Add. **1-Ab**	–1209.26371	–1209.00325	–1208.98377	–1209.05388
TS **1-Aa**	–886.25185	–885.98912	–885.97104	–886.03569
TS **1-Ab**	–1209.24176	–1208.98150	–1208.96319	–1209.02770
Int. **1-Aa**	–886.29580	–886.03042	–886.01244	–886.07630
Int. **1-Ab**	–1209.28249	–1209.02027	–1209.00188	–1209.06661
2- Hydrolysis				
Add. **2-Aa**	–962.78243	–962.49232	–962.47133	–962.54229
Add. **2-Ab**	–1285.76250	–1285.47579	–1285.45473	–1285.52534
TS **2-Aa**	–962.77558	–962.49009	–962.46970	–962.53945
TS **2-Ab**	–1285.75808	–1285.47586	–1285.45513	–1285.52491
Int. **2-Aa**	–962.78655	–962.49670	–962.47550	–962.54755
Int. **2-Ab**	–1285.77315	–1285.4862	–1285.46479	–1285.53655
3- Oxidation				
Prod. **3-Aa**	–1113.21149	–1112.91650	–1112.89219	–1112.97412
Prod. **3-Ab**	–1436.19535	–1435.90380	–1435.87891	–1435.96027
	Change in energy term (kcal/mol)			
	ΔE	ΔE_{ZPVE}	ΔH	ΔG
1- Nucleophilic Addition				
Add. **1-Aa**	–10.16	–9.02	–8.50	0.98
Add. **1-Ab**	–10.21	–9.16	–8.64	1.20
TS **1-Aa**	3.99	4.90	4.66	17.54
TS **1-Ab**	3.56	4.48	4.27	17.63
Int. **1-Aa**	–23.59	–21.02	–21.32	–7.94
Int. **1-Ab**	–22.00	–19.85	–20.01	–6.79
2- Hydrolysis				
Add. **2-Aa**	–37.14	–32.36	–33.15	–10.78
Add. **2-Ab**	–31.40	–27.19	–28.04	–5.08
TS **2-Aa**	–32.84	–30.96	–32.13	–9.00
TS **2-Ab**	–28.62	–27.23	–28.30	–4.80
Int. **2-Aa**	–39.72	–35.10	–35.77	–14.08
Int. **2-Ab**	–38.08	–33.72	–34.35	–12.11
3- Oxidation				
Prod. **3-Aa**	–111.98	–106.45	–107.24	–77.80
Prod. **3-Ab**	–108.61	–103.69	–104.22	–74.04

Table 0.2: Stationary points involved in oxidation reaction of 2-phenylquinoxaline (A) with lithiofuran (**a**) and lithiothiophene (**b**). Structures are optimised in implicit THF solvent at –78 °C

Systems	E	E_{ZPVE}	H	G
	Energy term in a.u.			
Reactants				
2-phenylquinoxaline **(A)**	–649.21024	–649.00667	–649.00095	–649.02883
Lithiothiophene **(b)**	–560.03717	–559.98197	–559.97862	–559.99933
Lithiofuran **(a)**	–702.14086	–701.84671	–701.83662	–701.87652
O$_2$	–150.30980	–150.30610	–150.30279	–150.32502
Oxidation Reaction				
Prod. **1-Aa**	–1113.21149	–1112.91650	–1112.90452	–1112.94837
Prod. **1-Ab**	–1436.19535	–1435.90380	–1435.89159	–1435.93479
	Change in energy term (kcal/mol)			
	ΔE	ΔE_{ZPVE}	ΔH	ΔG
Prod. **1-Aa**	–111.99	–118.54	–119.80	–99.68
Prod. **1-Ab**	–108.63	–103.69	–105.35	–79.87

Table 0.3: Stationary points involved in nucleophilic addition reaction of 2-phenylquinoxaline (A) with lithiofuran (**a$_e$**) and lithiothiophene (**b$_e$**). Structures are optimised in implicit THF solvent at -78 °C. The subscript "**e**" indicates two explicit THF solvent molecules

Systems	E	E_{ZPVE}	H	G
	Energy term in a.u.			
Reactants				
2-phenylquinoxaline **(A)**	–649.21024	–649.00667	–649.00095	–649.02883
Lithiofuran **(a)**	–702.14086	–701.84671	–701.83662	–701.87652
Lithiothiophene **(b$_e$)**	–1025.13113	–1024.83943	–1024.82948	–1024.86810
Nucleophilic Addition Reaction				
Add. **1-Aa$_e$**	–1351.37163	–1350.87185	–1350.85584	–1350.90947
Add. **1-Ab$_e$**	–1674.36357	–1673.86642	–1673.85046	–1673.90346
TS **1-Aa$_e$**	–1351.35611	–1350.85544	–1350.84076	–1350.88924
TS **1- Ab$_e$**	–1674.34392	–1673.84698	–1673.83184	–1673.88226
Int. **1-Aa$_e$**	–1351.40284	–1350.90060	–1350.88558	–1350.93578
Int. **1- Ab$_e$**	–1674.38486	–1673.88574	–1673.87053	–1673.92124
	Change in energy term (kcal/mol)			
	ΔE	ΔE_{ZPVE}	ΔH	ΔG
Add. **1-Aa$_e$**	–12.88	–11.59	–11.46	–2.58
Add. **1-Ab$_e$**	–13.94	–12.75	–12.57	–4.09
TS **1-Aa$_e$**	–3.14	–1.29	–2.00	10.11
TS **1- Ab$_e$**	–1.60	–0.56	–0.88	9.20
Int. **1-Aa$_e$**	–32.47	–29.63	–30.12	–19.09
Int. **1- Ab$_e$**	–27.29	–24.88	–25.17	–15.25

Appendix C

Table 0.1: Adducts formed from reactants lithiofuran (**a**) and 6-nitro-2-phenylquinoxaline (**C**) at various positions to one another. All reported structures are optimised in implicit THF solvent at -78 °C. the energies are measured relative to the reactants **C** and **a**

Systems	E	E_{ZPVE}	H	G
	Energy term in a.u.			
Reactants				
Lithiofuran (**a**)	–237.04795	–236.97100	–236.96738	–236.98881
6-nitro-2-phenylquinoxaline (**C**)	–853.77554	–853.57287	–853.56576	–853.59737
Nucleophilic Addition Reaction				
Add. **1-Ca**$_{C3-C26}$	–1090.84100	–1090.57581	–1090.56514	–1090.60620
Add. **1-Ca**$_{C5-C26}$	–1090.83910	–1090.57399	–1090.56358	–1090.60279
Add. **1-Ca**$_{C7-C26}$	–1090.83910	–1090.57399	–1090.56358	–1090.60280
Add. **1-Ca**$_{c1}$	–1090.83604	–1090.57108	–1090.56036	–1090.60168
Add. **1-Ca**$_{c2}$	–1090.83608	–1090.57125	–1090.56050	–1090.60184
Add. **1-Ca**$_{c3}$	–1090.83935	–1090.57427	–1090.56352	–1090.60490
Add. **1-Ca**$_{c4}$	–1090.83815	–1090.57350	–1090.56285	–1090.60282
Add. **1-Ca**$_{c5}$	–1090.83515	–1090.57008	–1090.55959	–1090.59926
Add. **1-Ca**$_{c6}$	–1090.83815	–1090.57343	–1090.56338	–1090.60154
Add. **1-Ca**$_{c7}$	–1090.84166	–1090.57633	–1090.56564	–1090.60673
Add. **1-Ca**$_{c8}$	–1090.83911	–1090.57393	–1090.56355	–1090.60263
Add. **1-Ca**$_{c9}$	–1090.83515	–1090.57008	–1090.55959	–1090.59926
	Change in energy term (kcal/mol)			
	ΔE	ΔE_{ZPVE}	ΔH	ΔG
Add. **1-Ca**$_{C3-C26}$	–10.99	–20.04	–20.07	–12.56
Add. **1-Ca**$_{C5-C26}$	–9.80	–18.90	–19.10	–10.42
Add. **1-Ca**$_{C7-C26}$	–9.80	–18.90	–19.10	–10.43
Add. **1-Ca**$_{c1}$	–7.87	–17.07	–17.08	–9.73
Add. **1-Ca**$_{c2}$	–7.90	–17.18	–17.16	–9.83
Add. **1-Ca**$_{c3}$	–9.95	–19.07	–19.06	–11.75
Add. **1-Ca**$_{c4}$	–9.20	–18.59	–18.64	–10.44
Add. **1-Ca**$_{c5}$	–7.32	–16.45	–16.59	–8.21
Add. **1-Ca**$_{c6}$	–9.20	–18.55	–18.97	–9.64
Add. **1-Ca**$_{c7}$	–11.40	–20.37	–20.39	–12.90
Add. **1-Ca**$_{c8}$	–9.81	–18.86	–19.08	–10.32
Add. **1-Ca**$_{c9}$	–7.32	–16.45	–16.59	–8.21

Table 0.2: Adducts formed from reactants lithiofuran (**a**) and 6-nitro-2-phenylquinoxaline (**C**) at various positions to one another. All reported structures are optimised in implicit THF solvent at -78 °C. The energies are measured relative to the reactants **C** and **a**

Add. **1-Ca$_{c4}$**

Add. **1-Ca$_{c9}$**

Add. **1-Ca$_{c5}$**

.

14

Table 0.3: Stationary points involved in nucleophilic addition reaction of 2-phenylquinoxaline (**A**)/6-nitro-2-phenylquinoxaline (**C**) and with lithiofuran (**a**) at C3 electrophilic sites. Structures are optimised in implicit THF solvent at –78 °C. Change in energies is measured relative to separate reactants

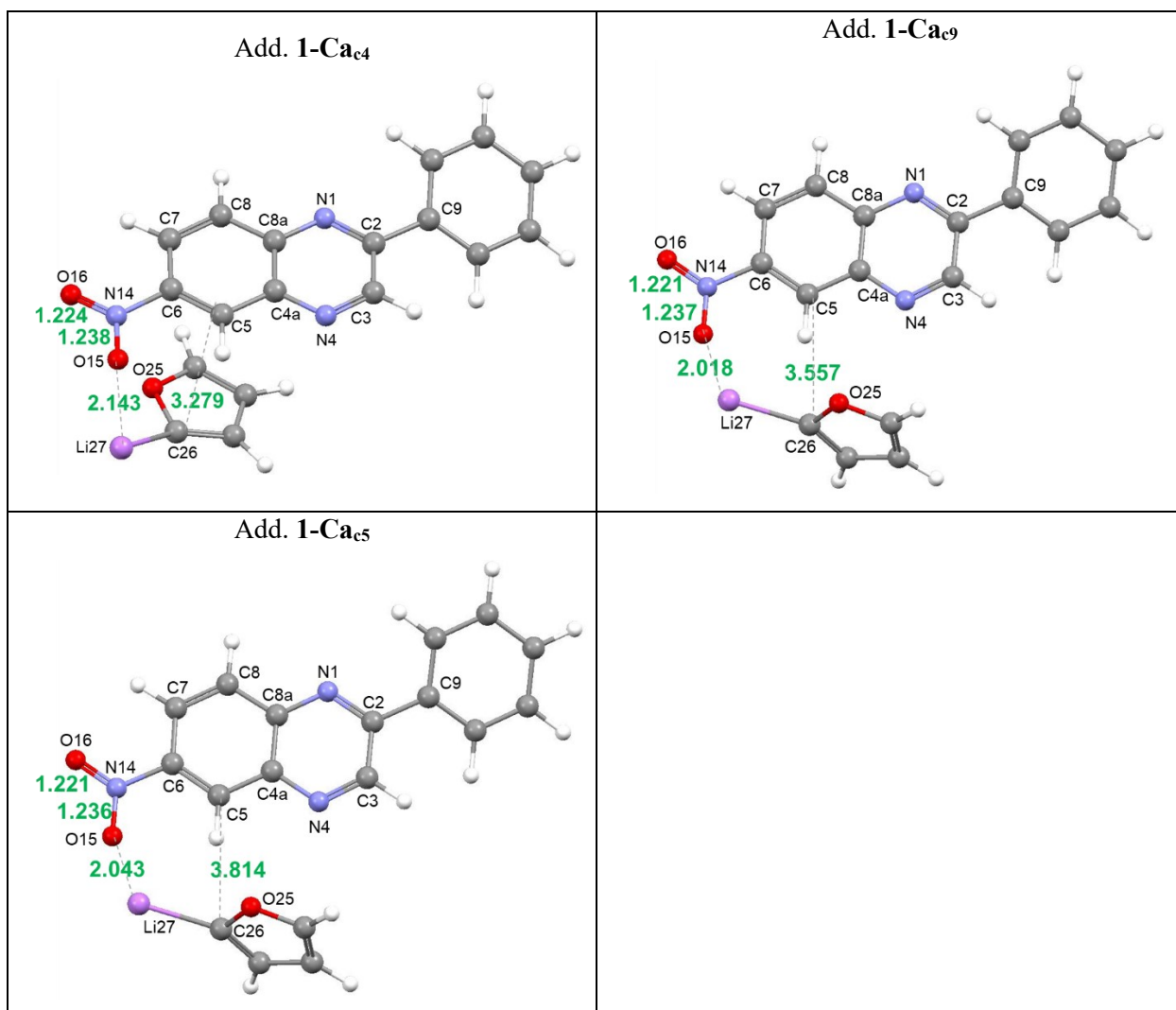| Systems	E	E_{ZPVE}	H	G
	Energy term in a.u.			
Reactants				
Lithiofuran (**a**)	–237.04795	–236.97100	–236.96738	–236.98881
2-phenylquinoxaline (**A**)	–649.21024	–649.00667	–649.00095	–649.02883
6-nitro-2-phenylquinoxaline (**C**)	–853.77554	–853.57287	–853.56576	–853.59737
Nucleophilic Addition Reaction				
Add. **1-Aa**	–886.27440	–886.01131	–886.00188	–886.03993
Add. **1-Ca**$_{C3-C26}$	–1090.84100	–1090.57581	–1090.56514	–1090.60620
TS **1-Aa**	–886.25185	–885.98912	–885.98054	–886.01534
TS **1-Ca**$_{C3-C26}$	–1090.82591	–1090.56099	–1090.55104	–1090.58939
Int. **1-Aa**	–886.29806	–886.03272	–886.02426	–886.05862
Int. **1-Ca**$_{C3-C26}$	–1090.87791	–1090.61051	–1090.60060	–1090.63889
	Change in energy term (kcal/mol)			
	ΔE	ΔE_{ZPVE}	ΔH	ΔG
Add. **1-Aa**	–10.17	–21.11	–21.05	–13.99
Add. **1-Ca**$_{C3-C26}$	–10.99	–20.04	–20.07	–12.56
TS **1-Aa**	3.98	–7.18	–7.66	1.44
TS **1-Ca**$_{C3-C26}$	–1.52	–10.74	–11.23	–2.01
Int. **1-Aa**	–25.02	–34.54	–35.10	–25.72
Int. **1-Ca**$_{C3-C26}$	–34.15	–41.82	–42.33	–33.08

15

Table 0.4: Geometrically optimised stationary points involved in the nucleophilic addition reaction of 2-phenylquinoxaline (**A**)/6-nitro-2-phenylquinoxaline (**C**) and with lithiofuran (**a**) at C3 electrophilic sites. All structures were optimised in implicit THF solvent using B3LYP/6-311++G(d,p) at –78 °C (energies in kcal/mol)

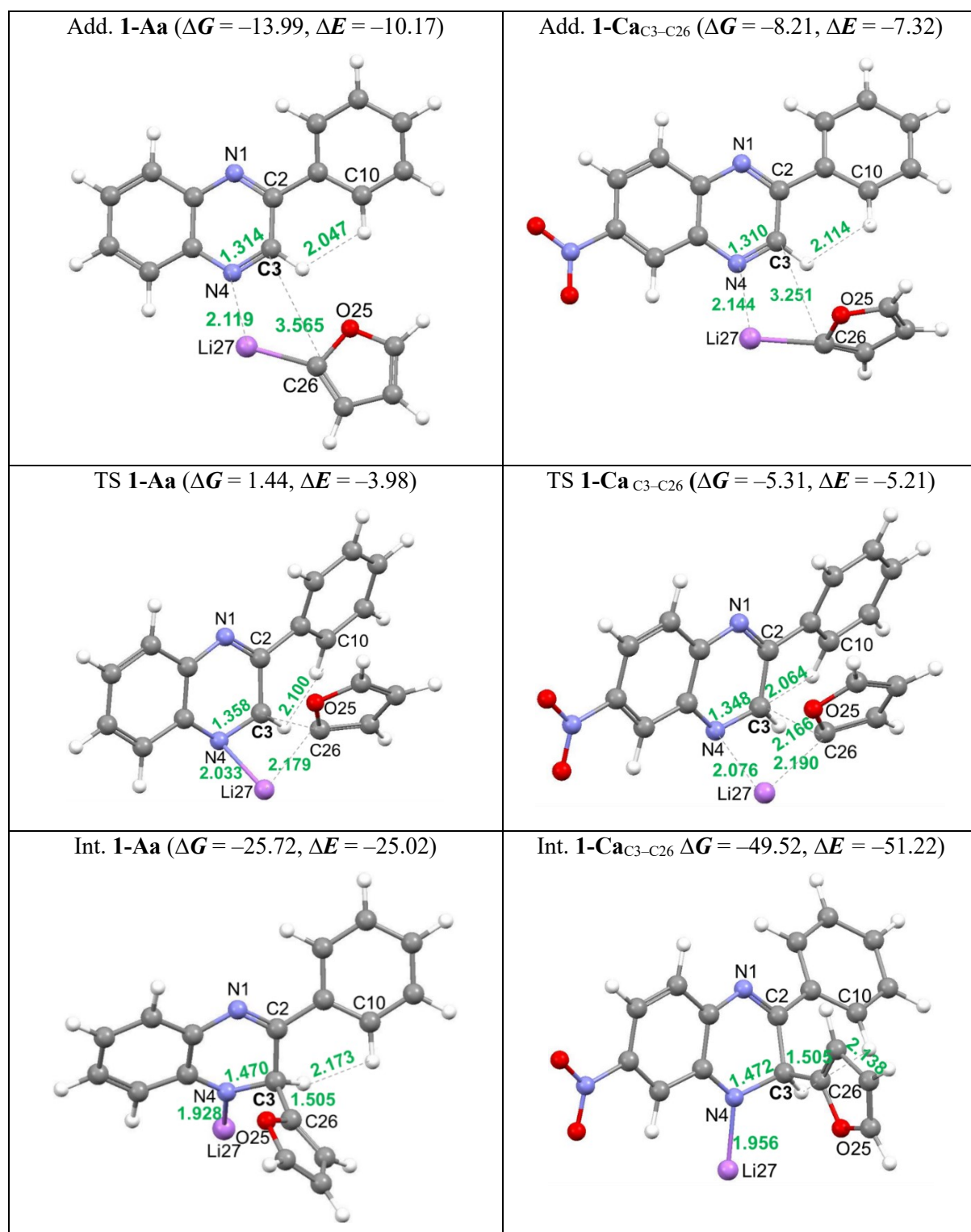| Add. **1-Aa** (ΔG = –13.99, ΔE = –10.17)	Add. **1-Ca**$_{C3–C26}$ (ΔG = –8.21, ΔE = –7.32)
TS **1-Aa** (ΔG = 1.44, ΔE = –3.98)	TS **1-Ca** $_{C3–C26}$ (ΔG = –5.31, ΔE = –5.21)
Int. **1-Aa** (ΔG = –25.72, ΔE = –25.02)	Int. **1-Ca**$_{C3–C26}$ ΔG = –49.52, ΔE = –51.22)

Table 0.5: *Stationary points involved in nucleophilic addition reaction of 2-*n*-butylquinoxaline (B)/6-nitro-2-phenylquinoxaline (C) and with lithiofuran (a) at C3 electrophilic sites. Structures are optimised in implicit THF solvent at –78 °C. Changes in energies are measured relative to separate reactants*

Systems	E	E_{ZPVE}	H	G
	Energy term in a.u.			
Reactants				
Lithiofuran (**a**)	–237.04795	–236.97100	–236.96738	–236.98881
2-n-butylquinoxaline (**B**)	–575.40101	–575.16529	–575.15883	–575.18838
6-nitro-2-phenylquinoxaline (**C**)	–853.77554	–853.57287	–853.56576	–853.59737
Nucleophilic Addition Reaction				
Add. **1-Ba**	–812.46455	–812.16924	–812.15916	–812.19879
Add. **1-Ca**$_{C3-C26}$	–1090.84100	–1090.57581	–1090.56514	–1090.60620
TS **1-Ba**	–812.44180	–812.14656	–812.13748	–812.17296
TS **1-Ca**$_{C3-C26}$	–1090.82591	–1090.56099	–1090.55104	–1090.58939
Int. **1-Ba**	–812.48470	–812.18788	–812.17858	–812.21458
Int. **1-Ca**$_{C3-C26}$	–1090.87791	–1090.61051	–1090.60060	–1090.63889
	Change in energy term (kcal/mol)			
	ΔE	ΔE_{ZPVE}	ΔH	ΔG
Add. **1-Ba**	–9.78	–20.68	–20.68	–13.56
Add. **1-Ca**$_{C3-C26}$	–10.99	–20.04	–20.07	–12.56
TS **1-Ba**	4.50	–6.44	–7.07	2.65
TS **1-Ca**$_{C3-C26}$	–1.52	–10.74	–11.23	–2.01
Int. **1-Ba**	–22.42	–32.37	–32.86	–23.47
Int. **1-Ca**$_{C3-C26}$	–34.15	–41.82	–42.33	–33.08

17

Table 0.6: Conformational adducts of c3, c4, c5 and c7 involved in the nucleophilic addition reaction of 6-nitro-2-phenylquinoxaline (**C**) with lithiofuran (**a**) at C7 electrophilic site

Systems	E	E_{ZPVE}	H	G
	Energy term in a.u.			
Reactants				
Lithiofuran (**a**)	–237.04795	–236.97100	–236.96738	–236.98881
6-nitro-2-phenylquinoxaline (**C**)	–853.77554	–853.57287	–853.56576	–853.59737
Nucleophilic Addition Reaction				
Add. **1-Aa**$_{c3}$	–1090.83515	–1090.57008	–1090.55959	–1090.59926
Add. **1-Ca**$_{c3a}$	–1090.83815	–1090.57350	–1090.56285	–1090.60282
Add. **1-Aa**$_{c4}$	–1090.83935	–1090.57427	–1090.56352	–1090.60490
Add. **1-Ca**$_{c5}$	–1090.84166	–1090.57633	–1090.56564	–1090.60673
Add. **1-Ca**$_{c7}$	–1090.83935	–1090.57427	–1090.56352	–1090.60490
TS **1-Aa**$_{c3}$	–1090.83179	–1090.56698	–1090.55724	–1090.59464
TS **1-Ca**$_{c3a}$	–1090.83385	–1090.56869	–1090.55903	–1090.59628
TS **1-Aa**$_{c4}$	–1090.82841	–1090.56356	–1090.55384	–1090.59110
TS **1-Ca**$_{c5}$	–1090.82571	–1090.56070	–1090.55084	–1090.58884
TS **1-Ca**$_{c7}$	–1090.82591	–1090.56100	–1090.55105	–1090.58939
Int. **1-Aa**$_{c3}$	–1090.90511	–1090.63726	–1090.62755	–1090.66510
Int. **1-Ca**$_{c3a}$	–1090.90509	–1090.63733	–1090.62759	–1090.66514
Int. **1-Aa**$_{c4}$	–1090.88835	–1090.61978	–1090.61034	–1090.64680
Int. **1-Ca**$_{c5}$	–1090.87791	–1090.61052	–1090.60060	–1090.63891
Int. **1-Ca**$_{c7}$	–1090.87791	–1090.61051	–1090.60060	–1090.63889
	Change in energy term (kcal/mol)			
	ΔE	ΔE_{ZPVE}	ΔH	ΔG
Add. **1-Aa**$_{c3}$	–7.32	–16.45	–16.59	–8.21
Add. **1-Ca**$_{c3a}$	–9.20	–18.59	–18.64	–10.44
Add. **1-Aa**$_{c4}$	–9.95	–19.07	–19.06	–11.75
Add. **1-Ca**$_{c5}$	–11.40	–20.37	–20.39	–12.90
Add. **1-Ca**$_{c7}$	–9.95	–19.07	–19.06	–11.75
TS **1-Aa**$_{c3}$	–5.21	–14.50	–15.12	–5.31
TS **1-Ca**$_{c3a}$	–6.51	–15.58	–16.24	–6.34
TS **1-Aa**$_{c4}$	–3.09	–12.35	–12.98	–3.09
TS **1-Ca**$_{c5}$	–1.39	–10.56	–11.10	–1.67
TS **1-Ca**$_{c7}$	–1.52	–10.75	–11.23	–2.02
Int. **1-Aa**$_{c3}$	–51.22	–58.60	–59.24	–49.52
Int. **1-Ca**$_{c3a}$	–51.21	–58.65	–59.27	–49.55
Int. **1-Aa**$_{c4}$	–40.70	–47.64	–48.44	–38.04
Int. **1-Ca**$_{c5}$	–34.15	–41.82	–42.33	–33.09
Int. **1-Ca**$_{c7}$	–34.15	–41.82	–42.33	–33.08

Table 0.7: Conformational adducts of c4 and c5 involved in the nucleophilic addition reaction of 6-nitro-2-phenylquinoxaline (**C**) with lithiofuran (**a**) at C7 electrophilic site

| Systems	E	E_{ZPVE}	H	G
	Energy term in a.u.			
Reactants				
Lithiofuran (**a**)	–237.04795	–236.97100	–236.96738	–236.98881
6-nitro-2-phenylquinoxaline (**C**)	–853.77554	–853.57287	–853.56576	–853.59737
Nucleophilic Addition Reaction				
Add. **1-Aa$_{c4}$**	–1090.83515	–1090.57008	–1090.55959	–1090.59926
Add. **1-Ca$_{c5}$**	–1090.83815	–1090.57350	–1090.56285	–1090.60282
TS **1-Ca$_{c4}$**	–1090.80563	–1090.54150	–1090.53159	–1090.56964
TS **1-Ca$_{c5}$**	–1090.81849	–1090.55410	–1090.54424	–1090.58242
Int. **1-Aa$_{c4}$**	–1090.85800	–1090.59151	–1090.58181	–1090.61914
Int. **1-Ca$_{c5}$**	–1090.87340	–1090.60680	–1090.59692	–1090.63509
	Change in energy term (kcal/mol)			
	ΔE	ΔE_{ZPVE}	ΔH	ΔG
Add. **1-Aa$_{c4}$**	–7.32	–16.45	–16.59	–8.21
Add. **1-Ca$_{c5}$**	–9.20	–18.59	–18.64	–10.44
TS **1-Ca$_{c4}$**	11.20	1.49	0.98	10.38
TS **1-Ca$_{c5}$**	3.14	–6.42	–6.96	2.36
Int. **1-Aa$_{c4}$**	–21.66	–29.90	–30.54	–20.69
Int. **1-Ca$_{c5}$**	–31.32	–39.49	–40.02	–30.69
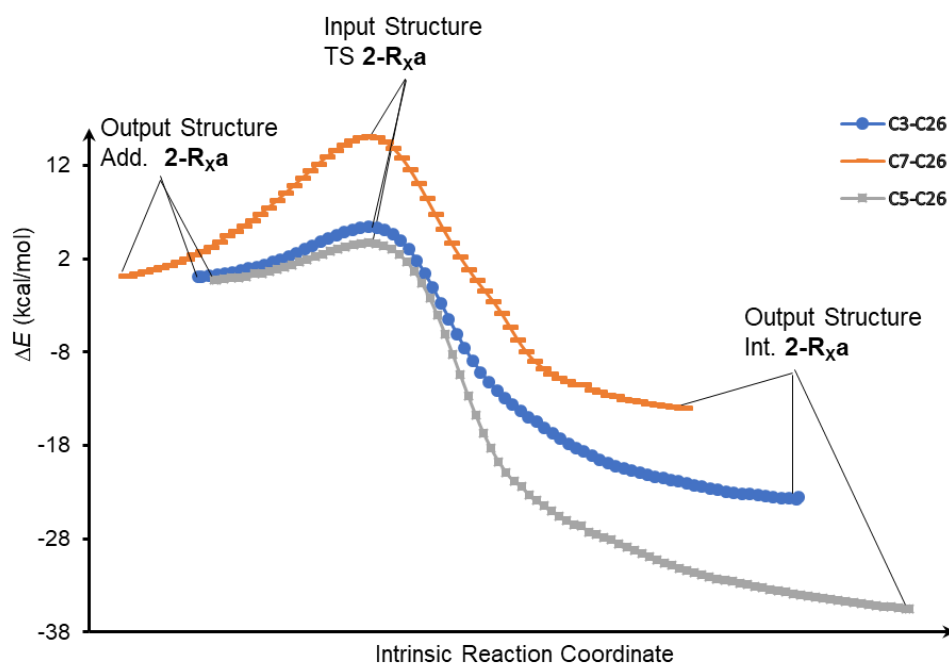
Figure 0.1: IRC profile for the nucleophilic addition of lithiofuran at different electrophilic sites (C3, C5 and C7) of 6-nitro-2-phenylquinoxaline
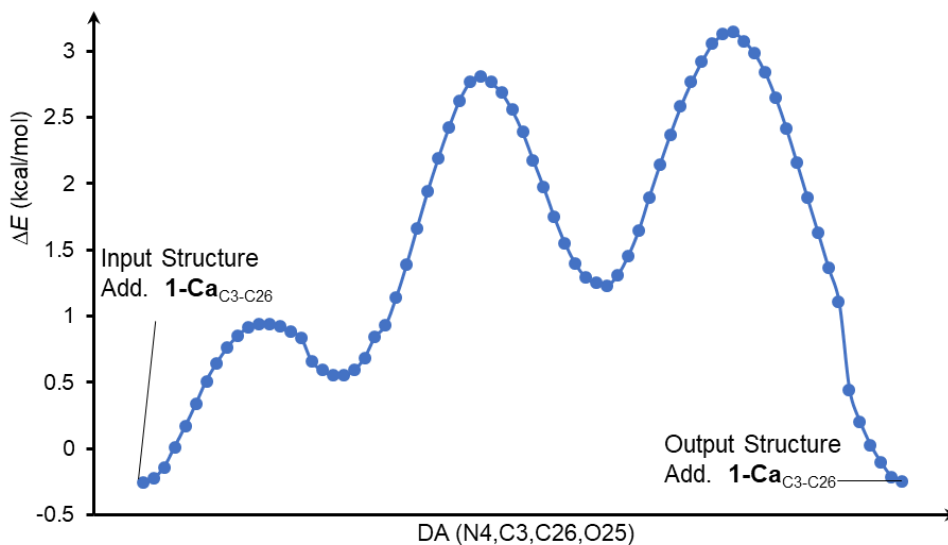
19

Figure 0.2: Dihedral angular profile for the nucleophilic addition of lithiofuran (**a**) at one of the electrophilic reactive sites (C3,) of 6-nitro-2-phenylquinoxaline (**C**)
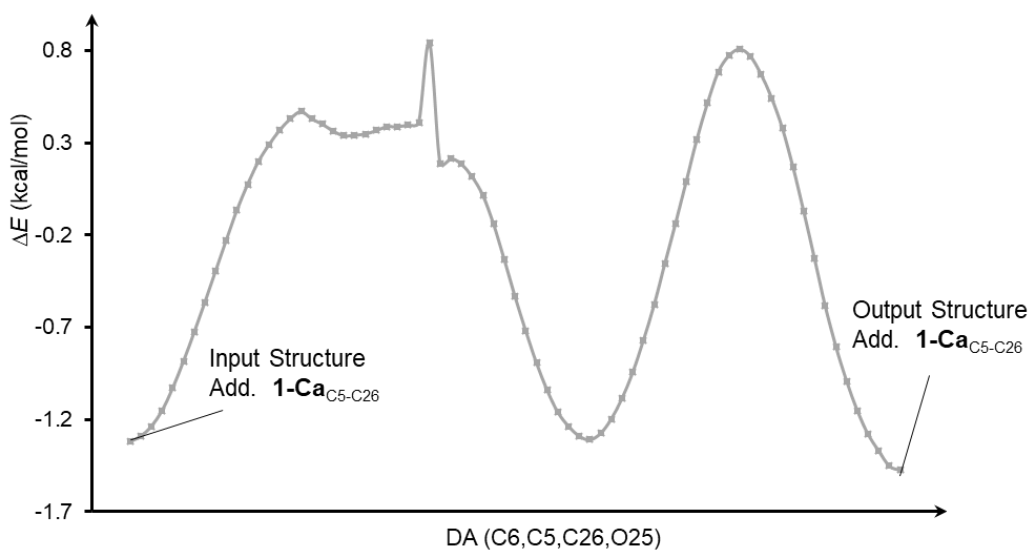

Figure 0.3: Dihedral angular profile for the nucleophilic addition of lithiofuran (**a**) at one of the activated electrophilic sites of the nitro group (C5,) 6-nitro-2-phenylquinoxaline (**C**)